NASA/TM—2016-219130

Analysis of 2015 Winter In-Flight Icing Case Studies With Ground-Based Remote Sensing Systems Compared to In-Situ SLW-Sondes

David J. Serke
National Center for Atmospheric Research, Boulder, Colorado

Michael C. King
Glenn Research Center, Cleveland, Ohio

Reid Hansen
National Center for Atmospheric Research, Boulder, Colorado

Andrew L. Reehorst
Glenn Research Center, Cleveland, Ohio

October 2016

NASA STI Program . . . in Profile

Since its founding, NASA has been dedicated to the advancement of aeronautics and space science. The NASA Scientific and Technical Information (STI) Program plays a key part in helping NASA maintain this important role.

The NASA STI Program operates under the auspices of the Agency Chief Information Officer. It collects, organizes, provides for archiving, and disseminates NASA's STI. The NASA STI Program provides access to the NASA Technical Report Server—Registered (NTRS Reg) and NASA Technical Report Server—Public (NTRS) thus providing one of the largest collections of aeronautical and space science STI in the world. Results are published in both non-NASA channels and by NASA in the NASA STI Report Series, which includes the following report types:

- TECHNICAL PUBLICATION. Reports of completed research or a major significant phase of research that present the results of NASA programs and include extensive data or theoretical analysis. Includes compilations of significant scientific and technical data and information deemed to be of continuing reference value. NASA counter-part of peer-reviewed formal professional papers, but has less stringent limitations on manuscript length and extent of graphic presentations.

- TECHNICAL MEMORANDUM. Scientific and technical findings that are preliminary or of specialized interest, e.g., "quick-release" reports, working papers, and bibliographies that contain minimal annotation. Does not contain extensive analysis.

- CONTRACTOR REPORT. Scientific and technical findings by NASA-sponsored contractors and grantees.

- CONFERENCE PUBLICATION. Collected papers from scientific and technical conferences, symposia, seminars, or other meetings sponsored or co-sponsored by NASA.

- SPECIAL PUBLICATION. Scientific, technical, or historical information from NASA programs, projects, and missions, often concerned with subjects having substantial public interest.

- TECHNICAL TRANSLATION. English-language translations of foreign scientific and technical material pertinent to NASA's mission.

For more information about the NASA STI program, see the following:

- Access the NASA STI program home page at http://www.sti.nasa.gov

- E-mail your question to help@sti.nasa.gov

- Fax your question to the NASA STI Information Desk at 757-864-6500

- Telephone the NASA STI Information Desk at 757-864-9658

- Write to:
  NASA STI Program
  Mail Stop 148
  NASA Langley Research Center
  Hampton, VA 23681-2199

NASA/TM—2016-219130

Analysis of 2015 Winter In-Flight Icing Case Studies With Ground-Based Remote Sensing Systems Compared to In-Situ SLW-Sondes

David J. Serke
National Center for Atmospheric Research, Boulder, Colorado

Michael C. King
Glenn Research Center, Cleveland, Ohio

Reid Hansen
National Center for Atmospheric Research, Boulder, Colorado

Andrew L. Reehorst
Glenn Research Center, Cleveland, Ohio

National Aeronautics and
Space Administration

Glenn Research Center
Cleveland, Ohio 44135

October 2016

Acknowledgments

The authors would like to thank the NASA Glenn Research Center Aircraft Operations Office and the Cleveland Hopkins Airport Air Traffic Control for their support and cooperation for all balloon operations. This work was funded under the NASA Convergent Aeronautics Solutions Project of the Transformative Aeronautics Concepts Program. The National Center for Atmospheric Research is sponsored by the National Science Foundation.

Level of Review: This material has been technically reviewed by technical management.

Available from

NASA STI Program
Mail Stop 148
NASA Langley Research Center
Hampton, VA 23681-2199

National Technical Information Service
5285 Port Royal Road
Springfield, VA 22161
703-605-6000

This report is available in electronic form at http://www.sti.nasa.gov/ and http://ntrs.nasa.gov/

Analysis of 2015 Winter In-Flight Icing Case Studies With Ground-Based Remote Sensing Systems Compared to In-Situ SLW-Sondes

David J. Serke
National Center for Atmospheric Research
Boulder, Colorado 80301

Michael C. King
National Aeronautics and Space Administration
Glenn Research Center
Cleveland, Ohio 44135

Reid Hansen
National Center for Atmospheric Research
Boulder, Colorado 80301

Andrew L. Reehorst
National Aeronautics and Space Administration
Glenn Research Center
Cleveland, Ohio 44135

Abstract

National Aeronautics and Space Administration (NASA) and the National Center for Atmospheric Research (NCAR) have developed an icing remote sensing technology that has demonstrated skill at detecting and classifying icing hazards in a vertical column above an instrumented ground station. This technology has recently been extended to provide volumetric coverage surrounding an airport. Building on the existing vertical pointing system, the new method for providing volumetric coverage utilizes a vertical pointing cloud radar, a multifrequency microwave radiometer with azimuth and elevation pointing, and a NEXRAD radar. The new terminal area icing remote sensing system processes the data streams from these instruments to derive temperature, liquid water content, and cloud droplet size for each examined point in space. These data are then combined to ultimately provide icing hazard classification along defined approach paths into an airport.

To date, statistical comparisons of the vertical profiling technology have been made to Pilot Reports and Icing Forecast Products. With the extension into relatively large area coverage and the output of microphysical properties in addition to icing severity, the use of these comparators is not appropriate and a more rigorous assessment is required. NASA conducted a field campaign during the early months of 2015 to develop a database to enable the assessment of the new terminal area icing remote sensing system and further refinement of terminal area icing weather information technologies in general. In addition to the ground-based remote sensors listed earlier, in-situ icing environment measurements by weather balloons were performed to produce a comprehensive comparison database. Balloon data gathered consisted of temperature, humidity, pressure, supercooled liquid water content, and 3-D position with time.

Comparison data plots of weather balloon and remote measurements, weather balloon flight paths, bulk comparisons of integrated liquid water content and icing cloud extent agreement, and terminal-area hazard displays are presented. Discussions of agreement quality and paths for future development are also included.

1.0 Introduction

Aircraft icing continues to be a major issue for the aircraft community. Despite advances in all aspects of icing related technologies, icing accidents still occur and aircraft winter operations are negatively impacted. Part of the challenge of dealing with icing conditions is the significant spatial and temporal variability of icing severity. It is not unusual for a series of aircraft on a landing approach to experience different levels of icing severity over a relatively short period of time. This variability makes the accurate prediction of icing conditions very difficult. While weather models and their predictions of icing have improved dramatically, the need for the direct detection and measurement of hazardous icing conditions aloft is still great.

Ideally, all aircraft would have onboard systems to indicate icing conditions in their flight path, analogous to thunderstorm detection with airborne radar. However even if these systems were developed, and became practical and affordable, the likelihood of all aircraft being adequately equipped is low. Therefore a more practical approach is to provide coverage to indicate icing conditions in areas of greatest traffic volume and flight risk: the terminal area.

Development of a ground-based hazard detection algorithm test bed, the NASA icing Remote Sensing System (NIRSS), began in 1997 (Ref. 1). NIRSS consists of three vertically pointed instruments: a Metek Ka-band cloud radar (Ref. 2), a Radiometrics Corporation multifrequency microwave radiometer (Ref. 3), and a Vaisala laser ceilometer. NIRSS's hardware components are shown in Figure 1.

An acknowledged shortcoming of the NIRSS technology has been that it only provides a vertical profile of icing condition severity. To help fully protect a terminal area and provide information that accounts for the temporal and spatial variability of icing conditions, a volumetric remote measurement capability is required. To provide the most utility to the widest range of aircraft, a ground-based icing remote sensing system with airport terminal volume coverage is envisioned (Ref. 4) which is shown notionally in Figure 2.

A terminal icing remote sensing system needs to provide reliable and timely information to operators and traffic managers. The volume of coverage needs to be of a reasonable range and altitude, allowing for routing flexibility to avoid hazardous conditions for both arriving and departing traffic. Such a system has been developed and was fielded during the winter of 2015 in the Cleveland Hopkins Airport area. A field campaign was conducted that gathered the remote sensor data in addition to specially instrumented weather balloon in-situ data.

The campaign tested several prototype algorithms meant to detect the location and severity of in-flight icing (or icing aloft, as opposed to ground icing) within the terminal airspace. Terminal airspace for this project was defined as within 25 km horizontal distance of the terminal, which in this instance was Hopkins International Airport in Cleveland, Ohio.

In addition to NIRSS, in-situ icing measurements of the profiles of supercooled liquid water content (SLWC) were collected with vibrating wire sensors attached to weather balloons (Ref. 5) which provided a comprehensive database for comparison. Key fields from the SLWC-sensors included air temperature, humidity and supercooled liquid water content, cataloged by time and 3-D location.

The goal of the reported effort was to develop a comparison database to allow the assessment of terminal area icing remote sensing technologies. This paper gives an overview of the vertically pointing and terminal area NIRSS algorithms, the in-situ weather balloon systems, and a detailed review of the case studies in which the results from NIRSS are compared to the in-situ measurements.

2.0 In-Flight Icing Background

When subfreezing air becomes supersaturated with respect to water and ice, ice crystals begin to grow on freezing nuclei such as mineral dust, aerosols, other pollution particles or existing ice crystals by the process of diffusion (Ref. 6). In the absence of significant populations of such ice nuclei, liquid water drops begin to condense out of the air from the water vapor. In these situations, supercooled liquid water (SLW) drops can form. In-flight icing occurs when an aircraft impacts with these SLW drops, which very

quickly freeze to the airframe surface and begin to accrete. The resulting ice accretion typically builds up on the leading edges of the airframe's surfaces. Ice accretion while in flight acts to increase drag and reduce the lift. Significant ice accretion can degrade an aircraft's flight characteristics enough to be a significant safety hazard, which has been recognized as a contributing factor to many crashes with resulting loss of life.

No single instrument has yet been developed which can unambiguously detect in-flight icing conditions remotely. For this reason, combinations of sensors have been under development for some time to detect in-flight icing (Refs. 7 and 8). This study has focused on methods to utilize two ground-based remote sensing platforms with the purpose of providing accurate and timely warnings on in-flight icing hazard.

3.0 Data Sources

For this analysis, the following sources for comparison data were used: Pilot Reports (PIREPs), Radiosondes, and the NIRSS. These data sources are described in the below paragraphs along with their relative geometric location to each other.

3.1 PIREPs

PIREPs are voluntary reports made by pilots of the time and location of meteorological conditions that their aircraft has encountered. In-flight icing is one of many possible conditions that can be reported. Icing is reported by type and the intensity or rate of accretion. The type of ice is reported as "CLR" (clear), "RIME," or "MXD" (mixed). The intensity is reported as "TR" (trace), "LGT" (light), "MDT" (moderate), and "SVR" (severe). The authors converted these qualitative conventions to a 0 to 8 scale of severity for quantitative comparisons. Any icing PIREPs within 50 km of Cleveland-Hopkins Airport were used as a qualitative comparison to the existence of icing for the two ground-based algorithms.

3.2 Radiosondes

The main source of comparison data for the NIRSS algorithms was collected via radiosondes carried by weather balloons. The following paragraphs describe the radiosonde system and how SLWC was calculated from the measured parameters.

3.2.1 Sounding Systems

International Met Systems, Inc. (InterMet) sounding systems were used for the field campaign. A mobile ground station, the iMet-3150 403 MHz Sounding System, was used between January 22, 2015 and February 11, 2015. This system utilizes the iMet-1-RSB Radiosonde. An iMet-3200A 403 MHz Sounding System was used between March 11, 2015 and April 23, 2015. This ground system is a fixed-installation system that has improved reception over the mobile system and utilizes the iMet-1-RSBN Radiosonde, which operates on a narrower band than the iMet-1-RSB Radiosonde. Both the iMet-3150 and iMet-3200A are automated sounding systems that acquire and store data without need for user input after balloon release.

3.2.2 Balloon-Borne Vibrating-Wire Supercooled Liquid Water Content Sensors

Each weather balloon instrument package included a specialized sensor used to obtain in-situ information of icing conditions aloft. These sensors measure the natural frequency of a vibrating wire, allowing the user to calculate the SLWC profile along the path of the weather balloon. The principle behind the vibrating wire sensor is the change in natural frequency of a wire due to ice accretion along the wire. The natural frequency of the wire decreases as ice accretes. Profiles of SLWC can be derived from the time history of the measured wire vibration frequency (Ref. 9).

The SLWC-sensors included in the instrument packages used during the 2015 winter campaign were developed by Anasphere, Inc., based on the original concept published in References 9 and 10. Serke et al., (Ref. 5) describes the first generation of the Anasphere, Inc. SLWC-sensor in greater detail. Generation 2 versions of the Anasphere, Inc. SLWC sensor were used for several releases from the NASA Glenn Research Center and Oswego, New York during the winter of 2014 (Ref. 11). For this field campaign, Generation 2 versions of the sensor were used between January 22, 2015 and February 11, 2015. When a Generation 3 version of the sensor, shown in Figure 3, that included improvements identified during check out tests in 2014 (Ref. 12), were utilized between March 11, 2015 and April 23, 2015. At the time of the field campaign, these sensors had undergone basic bench calibrations. A full icing wind tunnel calibration was initiated in late 2015 but was not available for the data analysis presented here.

3.2.3 Calculation of Supercooled Liquid Water Content Profile

The SLWC profiles for each sounding are derived from the time history of the frequency profiles, the balloon ascent rate and an assumed drop median volumetric diameter. Equation (1) shows the general form of the equation originally derived in Reference 10 and later re-examined in Reference 12. The terms ε, D and ω are the collection efficiency of the wire, the wire diameter and the ascent rate, respectively. The assumed drop size in all cases was 15 μm unless there was observational evidence of drizzle-sized drops. The term C is model assumption specific, as shown in Reference 12, and df/dt is the frequency time derivative, obtained using a generalized central differencing method. Outliers were removed prior to processing, and the frequency profiles were smoothed using a robust local regression using weighted linear least squares and a second-degree polynomial.

$$\mathrm{SLWC} = \frac{c}{\varepsilon D \omega} \frac{df}{dt} \tag{1}$$

3.3 NIRSS

The NIRSS was operated during the entire field campaign. The below sections describe the NIRSS capability with respect to vertical and volumetric measurements along with how the NIRSS is used to determine icing severity aloft in each case.

3.3.1 Vertically Pointing

From 2003 until 2014, NIRSS output icing severity warnings for the vertical profile above the instrumentation. As noted earlier, NIRSS consists of three vertically pointed instruments: a Metek MIRA-36 Ka-band cloud radar, a Radiometrics Corporation TP/WVP-3000 multifrequency microwave radiometer, and a Vaisala CT-25K laser ceilometer.

The radar provides cloud base, tops and particle density distribution information, the radiometer provides temperature, humidity profiles and integrated liquid water (ILW) measurements, and the ceilometer provides refined cloud base measurements that are relatively insensitive to precipitation. The NIRSS algorithm combines these measurements to determine the presence of icing conditions aloft and assigns a severity based on the calculated local liquid water content (LWC) intensity. This severity index is output as a profile above the NIRSS ground location.

The system employs an elevation scanning multichannel radiometer, built by Radiometrics Corporation, which passively collects incoming microwave radiation at a number of channels in the K and V-bands of the electromagnetic spectrum (Refs. 13 and 14). The K-band lies within an atmospheric water vapor resonance feature and thus variations at specific frequencies within the band are primarily caused by variations in the amount of liquid and gaseous water. The V-band is on the shoulder of an atmospheric oxygen resonance frequency (60 GHz). As the frequency is varied away from this peak of the absorption feature, this yields information on the atmospheric temperature farther and farther from the radiometer (in range).

The radiometer software utilizes neural networks that have been trained using large historical archives of integrated water vapor (IWV), temperature, humidity, and calculated ILW profiles combined with the measured radiometric brightness temperatures to generate real-time ILW, IWV, and profiles of temperature and humidity. NIRSS ingests the radiometer profiles, a Ka-band cloud radar profile and a cloudbase height measurement from a laser ceilometer into a "fusion" machine, and combines the instrument fields into an in-flight icing product. The height range of the 0 and –20 °C isotherms are targeted as the area where in-flight icing is most likely to exist, based on experience gained from previous research flight campaigns (Refs. 7 and 15). The vertical extent of cloud boundaries are provided by the ceilometer and K-band cloud radar. If cloud exists within the height range where icing temperatures exist, any liquid sensed by the radiometer is then distributed vertically with fuzzy logic (Ref. 16). A statistical analysis examining the agreement of NIRSS and the Current Icing Product (CIP) with PIREPs found that NIRSS performed well with an 80 percent probability of detecting positive PIREPs, and a 70 percent probability of detecting negative PIREPs (Ref. 17).

3.3.2 Volumetric

In 2014, a version of NIRSS that could provide in-flight icing hazard warnings for an airport terminal airspace volume was introduced (Ref. 4). The development of a terminal area icing remote sensing capability requires the coverage of critical terminal airspace while residing within current hardware technology cost constraints, thus a dedicated scanning cloud radar was not sought. Rather, the vertical cloud profile was assumed to apply to the entire terminal volume. This is a reasonable assumption since the vertical extent of radar reflectivity features often do not vary significantly within 50 horizontal kilometers of the terminal area in wintertime stratiform events, when dealing with 1 to 5 min time resolution. This assumption is made based on years of the authors observing the correlation between 3-D radar reflectivity within the terminal area and the temporal evolution of synoptic-scale meteorological phenomena. One notable exception to this assumption is strong cold-frontal passages.

The terminal area icing remote sensing system uses the NIRSS measurements and adds measurements from a Radiometrics MP-3000A (the current version of the older TP/WVP-3000) and the National Oceanic and Atmospheric Administration KCLE NEXRAD weather radar. Both of these instruments add scanning capability to the measurements of NIRSS in order to expand the capability from a vertical profile to a volume surrounding the airport. The MP-3000A used for this field campaign utilized an azimuth drive in addition to the instrument's internal elevation scanning mechanism. Since the radiometer can be azimuthally positioned to allow measurements at multiple discrete headings within each 5 min time period, slant-angle radiometer ILW and temperature profile can be collected along all of the airport approach azimuths. Having a radiometer that can scan along each respective approach runway at multiple elevations can provide individualized runway approach vector icing severity warning values. Previous research shows that slant angle products from the radiometer have improved vertical resolution in the lowest few kilometers and thus higher overall accuracy compared to vertically profiled values (Ref. 18). The radiometer was programmed to acquire radiometric measurements at 10°, 15°, 20°, and 25° of elevation at the azimuth headings of the Cleveland Hopkins Airport runways. Custom Neural Nets were utilized by this instrument to output derived temperature and humidity profiles and integrated liquid water path outputs for these non-zenith elevations.

The domain of concern for the software is the total volume of airspace within 25 horizontal kilometers of an airport. The software ingests slant elevation ILW fields at various azimuths along with all of the vertically pointing NIRSS fields (temperature, ILW, LWC, droplet size, cloud base, cloud top, number of layers, etc.), packages these profiled fields into data "packets," and uses a method to advect the data packets into the 3-D airport terminal environment. This is done every 5 min, which is the temporal resolution of the 3-D radar mosaic product. Several packets of various ages are located within the terminal domain at any given time—each containing all of the relevant meteorological fields for in-flight icing diagnosis. The advection method ingests NEXRAD reflectivity data and runs it through previously existing pattern recognition and tracking software (Ref. 19). This code is setup to output East-West and

North-South vector components of the horizontal advection as it follows the 0 dBZ reflectivity contour in time at the 1 km above-ground-level (AGL) height level. In this manner, patterns in NEXRAD reflectivity or surface wind speed and direction are used to advect packets of profiled input and derived output fields within the airport domain.

Aircraft are most vulnerable to in-flight icing during approach, flying at lower speeds with low engine power and high drag configuration while at near-constant altitudes for a prolonged period of time. Each airport has predetermined approach routes for aircraft, with rules that define the aircraft altitude at given distances for each different runway heading. The software needs to model these approach vectors by inflating the 2-D centerline, as defined by FAA approach plates, into a 3-D volume to represent the air volume that an aircraft could be affected by during approach. This volume is defined by centering a box of 0.25 km (~1000 ft) vertical by 2 km (~6500 ft) horizontal on the vector. The lateral size of the boxes are doubled at the outer portions of the approach path to accommodate defined holding areas when needed. The resulting approach volumes are then sectioned horizontally into 9 zones based on runway heading and radial distance from the tarmac: Zone (1) contains all of the approach volume within a 5×5 km box centered over the airport is defined in one volume zone; Zones (2) through (5) contain 4 volume zones along the runway headings outside the center box and inside a 25×25 km box and; Zones (6) through (9) contain four more volume zones extending from the middle box out to the outer 50×50 km box. Figure 4 is a top-view, 2-D representation of all the approach zones for the prototype system at Cleveland Hopkins Airport and Figure 5 shows an isometric view with more details of Zones (1) through (9) for one approach path. The most recent icing severity output profile that is determined by the software to be located within a given volume zone is applied to that zone at 5 min intervals. The highest icing severity level designation (“none,” “trace,” “light,” “moderate,” and “severe”) that exists within the defined vertical bounds of the given volume zone is assigned as that zone’s in-flight icing severity value at a given time. This effort is at a proof-of-concept stage of development. Further refinements, such as plotting of maximum SLWC instead of qualitative icing severity classifications might be more appropriate for operational use.

3.4 Measurement Geometry

Positions of the respective instrumentation for this field campaign are shown in Figure 6. The field instrumentation were all located within 200 m of each other. The radiometer scan volume includes zenith and 10°, 15°, 20° and 25° elevation scans along the four runway headings at 58°, 101°, 238° and 281° azimuth. These five views were repeatedly collected every 5 min. Over the course of the initial analyses for each case, it was found that on average the ILW from the 15° elevation scan in the closest azimuthal direction to the sensor track corresponded closest in magnitude to the sensor ILW. For this report, all sensors were compared to the zenith radiometer profiles.

4.0 Results and Discussion

4.1 Case Studies

The authors operated NIRSS at the NASA Glenn Research Center in Cleveland, Ohio throughout the winter of 2015. The presence of in-flight icing was provided by PIREPs and by the balloon-borne SLWC-sensors. Daily in-flight icing forecast meetings were conducted at NCAR, and the resulting decision to release radiosondes for the following 24-hour period was relayed to NASA GRC. The researchers at NASA GRC issued a “Notice to Airmen” (NOTAM) for the defined forecast period upon receiving a positive icing forecast from NCAR. Researchers coordinated with NASA GRC hangar personnel and Cleveland-Hopkins Airport air traffic control to ensure sate, minimally obtrusive operations in Class B airspace. NCAR provided now-casting during the forecast period, and the researchers based the final decision to release an instrumented weather balloon on the current radiometer-derived integrated liquid water value. Twenty-three weather balloon releases were conducted over the course of ten case dates from

January to April, 2015 (Table 1) and are analyzed individually in detail below. PIREP times and icing severities were used only as an indicator of the presence of in-flight icing conditions within the study area, not as a quantitative icing comparison.

4.1.1 January 22, 2015

On January 22, 2015, a short-wave trough moved through the Cleveland area. The short wave was associated with a persistent low pressure system located over the Hudson Bay region (Fig. 7). The local surface temperatures were –4.4 °C with dewpoint temperatures around –6.6 °C. Winds were around 2 ms^{-1} from the northwest, shifting to the southwest at the time of the sensor release. The local automated weather reported station was reporting light snow, fog and mist changing to light snow at the surface at the time of the sensor release. Several positive icing PIREPs were reported in the Cleveland terminal airspace from 13:14 to 15:15 UTC on this date, including two “moderate” icing severities. The PIREPs around the time of the sensor indicated icing between 670 and 2100 m AGL.

A SLWC-sensor was released from the NASA Glenn Research Center grounds at 14:17 UTC. Figure 8 shows the sensor travelled in an easterly direction (red) up through the maximum height that SLWC was recorded at 2.5 km altitude. The thermodynamic profile (Fig. 9, left) shows a complex cloud that is formed from multiple layers merging to create one continuous cloud from 0.2 to 2.3 km above ground level (AGL), with temperatures in the prime in-flight icing range of –6 °C near cloud base to –12 °C at cloud top. The vibrational frequency of the wire (center) is seen to start decreasing from a starting value near 44.5 Hz as it gets into the cloud layer and levels out near cloud top at a value near 43.5 Hz. The total decrease in frequency through the cloud layer was approximately 1 Hz. SLWC results are estimated from the change in frequency per unit height per unit time (Ref. 5) and the derived profile is shown in Figure 6, right panel. Temperature inversions in a saturated environment at 0.8 and 1.4 km AGL are colocated with relative or absolute maximums in SLWC. The temperature inversion at 2.3 km corresponds with the height of cloud top and sensor SLWC extinction. The presence of these temperature inversions within the cloud layer, even very small ones, indicate the presence of atmospheric lifting and subsequent saturation of discrete layers within the cloud depth. Maximum SLWC of 0.35 gm^{-3} occurs at 0.8 km AGL and then rapidly reduces to near zero at 1 km AGL. The top half of the cloud has a relative maximum of 0.15 gm^{-3} just above 1.2 km AGL before the SLWC gradually is reduced back to zero by the cloud top height of 2.3 km. The derived SLWC slant profile from the sensor (blue line) and the derived SLWC profile from the colocated NIRSS platform (black line) are also shown on Figure 9. The sensor values are not really from a vertical profile, rather they are a slant path defined by the ascent rate and horizontal winds experienced by the balloon. Significant differences exist in these two estimated SLWC profiles, such as the height of the absolute maximum in SLWC. This is due to NIRSS having a more wedge-shaped output due to the dominant weighting of an idealized wedge-shaped profile in the NIRSS logic. The overall magnitude and height bounds of the NIRSS-derived SLWC is comparable to that derived from the sensor. Differences in these two SLWC products can be partially attributed to the radiometer channels sampling 4° to 6° angle viewing cones (Ref. 10) whereas the sensors are essentially time-varying point measurements (Ref. 5).

The terminal area NIRSS product, shown in Figure 10, is the result of the recent development effort to add volumetric capability and extend the ground-based remote sensing aviation hazard detection to the runway approach vectors. In this plot, the maximum NIRSS icing severity values within the range-segmented, FAA-defined glide paths for commercial aircraft operating in the Cleveland airspace are color-coded for “none,” “trace,” “light,” “light/moderate,” “moderate,” “moderate/heavy,” and “heavy” icing severity categories. The box which includes the immediate terminal area is assigned the maximum hazard level given in the profile as determined by the vertically pointing NIRSS (In this case “heavy” severity, colored red). The hazard value for the four boxes along each runway heading within 12.5 km (6.7 nautical miles) of the terminal are assigned the maximum NIRSS hazard within each box volume defined by the 15° slant angle radiometer ILW distributed over the given vertical cloud profile. Finally, the hazard value for boxes along each runway heading between 12.5 and 25 km (6.7 and 13.5 nautical

miles) distance from the ground-based instrumentation are assigned the maximum NIRSS hazard within each box volume as defined by the closest slant angle NIRSS hazard profile as advected by radar detected features. The magnitude of the resulting NIRSS volumetric icing in each approach volume seems high based on a maximum SLWC in the profile of about 0.3 gm^{-3}.

4.1.2 January 29, 2015

On January 29, 2015, a mature low pressure system was set up over Southern Ontario, Canada, with an occluded front south through the Cleveland area (Fig. 11). ASOS reported cloud base height at 3000 ft (1 km) and the surface winds were out of the south. There were no lake-effect enhancements for this case due to the southerly wind direction in the boundary layer. Cleveland's ASOS reported "light snow" at 19:00 UTC and "light drizzle" at 20:00 UTC, which meant that a switch in the phase of surface precipitation occurred sometime near the time of the two sensor releases. There were four "light rime icing" and one "moderate mixed icing" PIREP around the sensor release times.

Two SLWC sensors were released on this date, the first of which was released at 19:25 UTC. Figure 12 shows the sensor travelled in a north-easterly direction (red) up through the maximum height that SLWC was recorded at 2.8 km altitude. The thermodynamic profile (Fig. 13, left panel) is unsaturated from the surface up to 1.0 km, and remains saturated from that height through the maximum height of the sensor at 7.2 km. The profile is sub-freezing from cloudbase up through 7.2 km. Frequency (center panel) is steady at about 45.2 Hz from the surface up to about 1.2 km, where it decreases steadily up to 1.7 km. The frequency recovers slightly and stabilizes from 1.7 km up to 2.5 km, where the values begin a steeper decrease to an absolute minimum at 3.6 km. From this altitude, a slow increase in frequency begins which only recovers 0.6 Hz of the 1.8 Hz decrease since the initial release frequency. The derived SLWC profile (right panel) has a relative maximum of 0.3 gm^{-3} centered at 1.5 km, and a discrete wedge-shaped SLWC absolute maxima feature with a value of 0.5 gm^{-3} at 3.4 km altitude. NIRSS has SLWC base and top at reasonable heights compared to the sensor. NIRSS misses the concentration of SLWC in discrete spikes due to the differences in techniques employed to measure the liquid. The terminal area NIRSS product, shown in Figure 14, has moderate to severe icing in almost all of the runway approach volumes. This result seems reasonable based on the magnitude and altitude of in-situ SLWC.

The second SLWC-sensor was released at 20:06 UTC. Figure 15 shows the sensor travelled in a north-easterly direction (red) up through the maximum height that SLWC was recorded at 7.9 km altitude. The thermodynamic profile (Fig. 16, left panel) is unsaturated from the surface up to about 1.0 km, then is saturated from 1.0 up to at least 3.2 km. Above this height, the profile is either saturated or nearly saturated through to the highest levels that the sensor recorded data. The sounding is above freezing from the surface to the cloudbase height of 1.0 km and is subfreezing for the remainder of the flight. The pre-release wire frequency (center) starts at 44.8 Hz and is steady until about 1.2 km. At this height, a rapid decrease is observed which levels off at around 44.5 Hz at 1.5 km altitude. Frequency begins a slow increase above 2.3 km. There are many missing frequency data points during this flight, especially around 1.9 km and above 3.6 km in altitude. The cause of these outages is currently unknown, possibly due to interference from surrounding radio sources or shortcomings in the sensor/antenna geometry. SLWC derived from frequency (right panel, blue line) shows a spike from 1.1 up to 1.6 km, with a maximum of 0.35 gm^{-3} centered on 1.3 km. NIRSS SLWC below 1.5 km matches up reasonably well with the sensor base and top heights. NIRSS detects significant SLWC above 2.5 km, whereas the sensor profile is suspect at these heights due to the aforementioned missing data issue.

NIRSS volumetric product (Fig. 17) has moderate to heavy severity icing in nearly all approach volumes. This result seems reasonable considering the lower level spike in SLWC detected by the sensor at this time.

4.1.3 February 4, 2015

On February 4, 2015, Cleveland had significant in-flight icing associated with the passage of a cold front (Fig. 18). The front was associated with a surface low pressure system over Southern Ontario, Canada. Surface temperatures were –1 °C with a dew-point was –4 °C at 13:30 UTC. Winds were out of the south at 2.5 ms^{-1}, switching to southwesterly flow at 4.5 ms^{-1} at the time of the two sensor releases. Cleveland's ASOS reported "light snow" before, and "heavy snow" after the second release. Throughout the event, there were three reports of "trace icing", ten reports of "light icing", and three reports of "moderate icing".

The first sensor release was at 13:42 UTC. Data from the sensor was not received by the ground acquisition station above the 680 mb, or 3.2 km altitude level. This was most likely due to issues the scientists were having with the receiver antenna during the first few cases of the season and the relative orientation of the sensor flight to the ground receiver antenna which caused partial signal blockage. The mean wind direction that influenced the sensor up to the highest altitude that had SLWC at 2.5 km was 245°, or from the west-southwest (Fig. 19). The temperature profile (Fig. 20, left panel) was sub-freezing for the duration of recorded flight, with surface temperatures near 0 °C. Saturated conditions exist in a thin layer between 1.1 and 1.2 km and again from 1.6 up to 2.5 km. Above 2.5 km, a much drier airmass exists, as witnessed by the rapid decrease in dewpoint temperature. The pre-release frequency (center) is around 44.3 Hz, and remains near that value until 1.9 km. This case exhibited the noisiest frequency trace through non-saturated heights of any of the cases for some unknown reason. At 1.8 km, a rapid and linear decrease in frequency begins until 2.5 km, where frequency reaches a minimum of 43.9 Hz. Above 2.5 km, frequency increases rapidly toward the pre-release frequency value as the accreted ice sublimates in the unsaturated air mass above the cloud top height. The frequency plot shows how several outliers were identified and removed below 1.3 km, but several excursions from the baseline are observed, which translate into false positive SLWC identification in the unsaturated atmosphere below 1 km. It is observed that all of the outliers seem to be on the higher frequency side of the baseline frequency trace. A SLWC layer (right panel, blue line) from 1.8 to 2.5 km maximizes at 0.25 gm^{-3} at 2.0 km. NIRSS SLWC (black line) is concentrated in a spike with magnitude over 0.8 gm^{-3} at 0.4 km in height. NIRSS volumetric product (Fig. 21) has heavy severity icing at the lowest and closest approach boxes in all four runway headings due to the spike in SLWC discussed previously. This result is consistent with the vertically pointing output, but output from NIRSS for this case needs to be explored in greater detail at a later time.

The second sensor release was at 17:07 UTC. Data from the sensor was not received by the ground acquisition station above the 620 mb, or 3.9 km altitude level. This was most likely due to the same reasons as described for the first sensor release. The mean wind direction that influenced the sensor up to the highest altitude that had SLWC at 1.8 km was 250°, or from the west-southwest (Fig. 22). The temperature profile (Fig. 23, left panel) was subfreezing, except for the lowest 0.1 km. Surface temperature was +1.9 °C. The profile was saturated from 0.9 up to 1.8 km and this cloud layer had a mean temperature of about –5 °C. The pre-release frequency (center) is 44.3 Hz. An upward frequency drift is observed in this sensor profile. Many outliers are apparent throughout this profile. All of the outliers (red circles) seem to be on the higher frequency side of the baseline frequency trace. Many of these outliers were identified in the quality control software and removed. A significant decrease in frequency is observed from 1.6 to 1.8 km. Above 1.8 km, the frequency rapidly returns to and exceeds the pre-release value. The only SLWC values above the accepted noise threshold (right panel, blue line, less than or equal to 0.05 gm^{-3}) occur in a layer from 1.6 to 1.8 km and reach a maximum value of 0.2 gm^{-3}. NIRSS (black line) did not detect SLWC below 2 km as the sensor did. NIRSS detected liquid from 2 to 4 km where the sensor frequency trace was exceptionally noisy. While NIRSS SLWC heights do not match the sensor, the maximum SLWC (~0.2 gm^{-3}) and ILW magnitude match well.

NIRSS volumetric product (Fig. 24) shows "heavy" severity icing in the column directly above the ground-based instrumentation (center box) and "heavy" severity to the west at 20 km distance. The volumetric product for this case needs to be examined in greater detail for accuracy at a later time.

4.1.4 February 11, 2015

On February 11, 2015, a cold front pushed through the Cleveland area just south of a triple point (the intersection of a cold, warm and occluded fronts, Fig. 25). These frontal features were associated with a low positioned just North of Lake Erie in Ontario, Canada. Two launches took place from NASA Glenn Research Center at 20:00 UTC and 21:10 UTC. Surface temperatures were around –1 °C with dew-points at –3 °C. Surface winds were out of the southwest at 5 ms^{-1} at the time of the first launch, switching to west at 6 ms^{-1} at the time of the second launch. The ASOS in Cleveland was reporting "fog," "mist," and "light drizzle".

In between the two launches were two reports of "light rime icing" and one report of "moderate rime icing". There were a total of five reports of "light rime icing", seven reports of "moderate rime icing" and one case of "severe rime icing" within 100 km of KCLE within an hour of the launches. The moderate or greater PIREPs were reported from 20:30 UTC on the 11th until 2:15 UTC on the 12th.

The mean wind direction that influenced the sensor up to the highest altitude that had SLWC was 255°, or from the west-southwest (Fig. 26). The 20:00 UTC sensor release (Fig. 27, left panel) show mostly unsaturated conditions up to about 2.2 km MSL with a deep temperature inversion beginning at 1.9 km. The entire profile is subfreezing, except for perhaps the lowest tens of meters. Above this 2.2 km, the sounding is approximately saturated up to about 3.0 km MSL and falls within a temperature range of –5 to –9 °C. The sensor frequency (center) is noisy but nearly constant up to 2.2 km, then decreases steadily from the initial un-iced frequency of 44.2 to 43.1 Hz at 3.0 km MSL. The resulting SLWC (right panel, blue line) has several pockets of SLWC that do not register up to 0.1 gm^{-3} centered at 0.9, 1.5, and 3.8 km MSL, respectively, and two significant SLWC maximums of 0.45 gm^{-3} between 2.4 and 2.8 km MSL. NIRSS SLWC (black line) has the SLWC base too low and the top too high, when compared to the sensor. NIRSS misses the main concentration of sensor SLWC in the two spikes between 2 and 3 km in altitude due to the manner in which NIRSS distributes the ILW as detected by the radiometer. The NIRSS volumetric product is unavailable for this sensor release because NEXRAD Level 2 mosaic data were missing.

The sensor released at 21:10 UTC measured a thermodynamic profile (Fig. 28, left panel) that was subfreezing except for the lowest tens of meters near the surface. No map of the balloon path is provided, since the GPS position was not recorded for this flight due to system malfunction. Saturated conditions now exist from 0.3 to 4.1 km MSL, covering a range of temperatures from –3 °C at cloud base to –15 °C at cloud top. A saturated inversion layer existed between 2.4 and 2.6 km MSL and another weaker saturated inversion layer is evident at 3.6 km MSL. The sensor detected cloud top height is about 4.2 km MSL. The release frequency (center) of 43.9 Hz was reported up to the cloud condensation level at 0.3 km MSL, then the frequency decreased steadily up to the base of the first saturated inversion height at 2.6 km MSL. Above the first saturated inversion, the frequency is steady state up to 3.0 km MSL, then resumes the steady rate of decrease up to the height of the second weaker saturated inversion at 3.4 km MSL. A slow increase in sensor frequency is registered above the second weaker saturated inversion, and then a steeper, steady increase in frequency is recorded above the cloud top height as ice begins to sublimate off of the wire due to subsaturated conditions and exposure to the sun's radiation. The derived SLWC profile (right panel, blue line) begins at roughly the cloud condensation level (CCL) at 0.3 km MSL and increases up to a maximum of 0.8 gm^{-3} at 2.3 km MSL, just below the strongest saturated inversion layer. Above 2.3 km, SLWC drops rapidly to zero just above the top of the inversion at 2.8 km MSL. From here the SLWC increases rapidly to another maximum of 0.8 gm^{-3} just below the second weaker saturated inversion at 3.3 km MSL before rapidly decreasing to zero again at the height of the weaker inversion at 3.6 km MSL. NIRSS SLWC (black line) base at 0.3 km matches with the sensor, but NIRSS SLWC ends too low at 2 km. Differences in SLWC tops are likely due to the differences in measuring techniques (in-situ point measurement versus remote 5° viewing angle). The magnitude of maximum SLWC for NIRSS (0.7 gm^{-3}) versus sensor (0.8 gm^{-3}) and the magnitude of ILWs were fairly decent. NIRSS volumetric product is unavailable for this sensor release because NEXRAD Level 2 mosaic data were missing.

4.1.5 March 13, 2015

During this event, Cleveland was being effected by an approaching warm front that was associated with a surface low pressure system stationed over Arkansas (Fig. 29). Looking on radar composite (not shown), a Mesoscale Convective System appears to be moving towards the Cleveland area. This case had rather warm surface temperatures compared to the previous wintery cases. At the time of the sensor releases, NASA Glenn reported +10 °C with dew-points around +5 °C. Winds were out of the south at 2.5 to 4 ms^{-1} at the time of the second sensor launch. Cloud bases reported by ASOS were 670 m. ASOS reported "light rain" throughout the duration of the sensor releases. There was only one PIREP that mentioned icing throughout the day, and it was recorded at 15:53 UTC.

Three SLWC-sensors were released during this case. The mean wind direction that influenced the first sensor up to the highest altitude that had SLWC was 230°, or from the southwest (Fig. 30). The sensor released at 20:43 UTC measured a thermodynamic profile (Fig. 31, left panel) that was non-freezing up to 2.5 km. Saturated conditions existed above 0.7 km MSL. The frequency (center) has few significant decreases in magnitude during this release. The derived SLWC profile (right panel, blue line) has a maximum of 0.15 gm^{-3} at 0.9 km MSL and has a few other lesser spikes to 0.1 gm^{-3}. NIRSS SLWC (black line) bounds the various low-magnitude spikes in SLWC derived from the sensor quite well, but NIRSS has a significantly higher ILW than the sensor does for this case.

NIRSS volumetric product (Fig. 32) has "heavy" severity icing in the column directly above the ground-based instrumentation (center box) and "heavy" severity generally out to 25 km distance, with lesser severity values at further ranges and higher altitudes. These severity magnitudes seem somewhat high based on the height and magnitude of detected liquid by the sensor. Further assessment is needed on this result.

The mean wind direction that influenced the second sensor up to the highest altitude that had SLWC at 3.1 km was 250°, or from the west-southwest (Fig. 33). The sensor released at 21:59 UTC measured a thermodynamic profile (Fig. 34, left panel) that was non-freezing up to 2.5 km. Saturated conditions existed above 0.9 km MSL. The frequency (center) has few significant decreases in magnitude during this release. The derived SLWC profile (right panel, blue line) has a maximum of 0.2 gm^{-3} at 0.9 km MSL and has a few other lesser spikes to 0.1 gm^{-3}. NIRSS SLWC (black line) bounds the various low-magnitude spikes in SLWC derived from the sensor quite well, but NIRSS has a significantly higher ILW than the sensor does for this case.

NIRSS volumetric product (Fig. 35) has "heavy" severity icing in the column directly above the ground-based instrumentation (center box) and "heavy" severity generally out to 25 km distance, with lesser severity values at further ranges and higher altitudes. These severity magnitudes seem somewhat high based on the height and magnitude of detected liquid by the sensor. Further assessment is needed on this result.

The mean wind direction that influenced the third sensor up to the highest altitude that had SLWC at 4.2 km was 260°, or from the west-southwest (Fig. 36). The sensor released at 23:38 UTC measured a thermodynamic profile (Fig. 37, left panel) that was non-freezing up to 2.6 km. Saturated conditions existed above 0.4 km MSL. The frequency (center) has several discrete decreases in magnitude during this release, most notably between 0.8 and 1.5 km, from 1.8 to 2.1 km and 2.8 to 4.2 km. The derived SLWC profile (right panel, blue line) has a maximum of 0.2 gm^{-3} at several of these frequency depressions and has a few other lesser spikes to 0.1 gm^{-3}. NIRSS SLWC (black line) bounds the various low-magnitude spikes in SLWC derived from the sensor quite well, but NIRSS has a significantly higher ILW and higher maximum SLWC value than the sensor does for this case.

NIRSS volumetric product (Fig. 38) has "heavy" severity icing in the column directly above the ground-based instrumentation (center box) and "heavy" severity generally out to 25 km distance, with lesser severity values at further ranges and higher altitudes. These severity magnitudes seem somewhat high based on the height and magnitude of detected liquid by the sensor. Further assessment is needed on this result.

4.1.6 March 17, 2015

On March 17, 2015, a relatively strong cold front passed through the Cleveland area (Fig. 39). This frontal feature was associated with a triple point sitting over Southern Quebec. Surface temperatures were 1 °C with dew-points at –2.7 °C. Surface winds were out of the north-northwest at 8 ms^{-1} at the time of the first launch, switching to a northerly flow of 9 ms^{-1} at the time of the second launch. Cleveland ASOS did not report any precipitation reaching the surface during the event. There were five "light rime icing" PIREPs around the sensor release times and one report of "moderate rime icing" within the 150 km radius region around Cleveland. PIREPs were concentrated over the area south of the Cleveland Metro area.

Two SLWC-sensors were released during this case. The first sensor was released at 13:54 UTC. This sensor drifted only slightly to the south by the time it rose through the highest SLWC level (Fig. 40). The temperature and dewpoint instruments on the sensor (Fig. 41, left panel) had unrealistically high values up to 0.6 km. This was later determined to be caused by a typo in the radiosonde system configuration file for this flight. The erroneous temperature data was removed from the plot. ASOS is reporting a surface temperature of +2.5 °C with no precipitation. From 0.6 to 1.25 km the sounding is saturated and is in the temperature range of –3 to –7 °C. From 1.25 to 1.8 km the sounding is nearly saturated. Above 1.8 km, the sounding is unsaturated. Between 0.6 and 0.8 km, the frequency values (center) experience and unknown high anomaly. The values at these heights are identified and filtered out (red circles) by the automated quality control software. Just above this height, the frequency is seen to fall to a minimum at 1.25 km. In the nearly saturated layer from 1.25 to 1.8 km, frequency hovers around 44 Hz. At the top of the cloud, frequency rises uniformly back to just above the initial release frequency of 44.4 Hz as the ice sublimates away to bare wire. Once all the ice is gone (at 2.0 km), the frequency is seen to continue a gradual increase.

The frequency profiles from several Generation 3 SLWC-sensors used during this test period demonstrated upward drift with increasing altitude. This behavior is most apparent in cases where the balloon did not pass through supercooled liquid water, but likely exists in all soundings using the Generation 3 SLWC-sensors. The apparent, upward drift is gradual, and has been identified as a thermal effect caused by cooling of the sensor package at higher altitudes. Further examination of the data is expected to lead to a correlation between the upward drift and ambient conditions, allowing for a correction to be developed for SLWC profiles.

The SLWC profile (right panel, blue line) has a maximum of 0.3 gm^{-3} centered on 1.0 km. This is at the top of the saturated layer and just below the overlying nearly saturated cloud layer. NIRSS ILW, maximum SLWC, base of SLWC and SLWC top match very well with the sensor in the SLWC layer that exists between 0.5 and 1.5 km. The NIRSS Ka-band radar detects a weak cloud from 4.4 to 5.7 km, whose temperature is seen to be greater than –20 °C, so NIRSS distributes liquid to it. No liquid is observed in the sensor at these levels.

NIRSS volumetric product (Fig. 42) shows "heavy" severity icing in the column directly above the ground-based instrumentation (center box) and "heavy" severity to the west and southwest at 20 to 25 km distance. This result seems reasonable based on the height and magnitude of detected liquid by the sensor.

The second sensor was released at 14:47 UTC. Figure 43 shows the sensor drifted in a southerly direction from release time until it exited cloud top. The profile first becomes saturated (Fig. 44, left panel) at 0.9 km, is clearly saturated up to 1.2 km and is nearly saturated up to 1.8 km. At 1.8 km, a strong capping inversion exists, and the remainder of the profile above this height is unsaturated. The lowest 8 to 10 ranged frequency values (center) are very noisy for an unknown reason, and are removed by the automated QC system. Starting at 1 km, the frequency is observed to gradually and then rapidly decrease to a minimum at 1.8 km. At this height, frequency reverses and rapidly increases back to the initial release frequency near 3.0 km as the accreted ice sublimates. In the dry air above 3.0 km, frequency is seen to slightly and linearly drift higher. The resulting SLWC profile (right panel, blue line) has a wedge-shape which maximizes at 1.4 gm^{-3} in the nearly saturated layer at 1.5 km altitude. This magnitude of SLWC is observed to be superadiabatic, so further analysis of this case is required. Sporadic blips of SLWC exist above the cloud top level at 3.5 km due to noise in the frequency measurements.

The resulting SLWC values are considered below the noise threshold of the sensor. The SLWC top from NIRSS (black line) matches well with the sensor value, and the SLWC base from NIRSS is 0.3 km lower than that detected from the sensor. NIRSS had a maximum SLWC value of 0.7 gm^{-3} at 1.7 km, compared to the sensor's value of 1.4 gm^{-3} at 1.5 km. The ILW was roughly the same for NIRSS and sensor.

NIRSS volumetric product (Fig. 45) shows "heavy" severity in the vertical profile, and "heavy" severity in the furthest approach volumes to the west and southwest due to the significant SLWC detected by the sensor. The NIRSS volumetric output for this case is very reasonable given the in-situ measurements.

4.1.7 March 20, 2015

On March 20, 2015 at 15:00 UTC, a weak surface low pressure was located over West Virginia with a surface trough extending northward through the Cleveland area (Fig. 46). Cleveland surface temperature was +3 °C, with the dew-point at –5.5 °C. By the second release, the temperature had climbed to +5.5 °C, with a dew-point of –2.2 °C. Surface pressure was dropping as the trough and associated instability passed through the region. Surface winds were sporadic throughout the day, settling on westerly flow at 2.5 ms^{-1} at the time of the launches. There were eight "light rime icing" PIREPs within 150 km of the Cleveland Hopkins Airport, one of which was a "moderate icing" report.

Two SLWC-sensors were released during this case. The first sensor was released at 15:00 UTC and it ascended nearly vertically through all SLWC up to 2.9 km, with a slight drift to the east (Fig. 47). Above freezing temperatures existed from the surface up to 0.9 km in the sensor profile (Fig. 48, left panel), and the remainder of the profile was sub-freezing. A saturated layer exists from 2.1 up to 3.7 km, with a 3 °C saturated temperature inversion beginning at 2.9 km. Frequency (center) exhibits a slow and steady upward drift from the surface up to 2.2 km. At this height, values decrease by 1 Hz up to the saturated inversion at 3.0 km. Through the remainder of the cloud layer, values increase at twice the rate of the clear air upward drift. From the top of the cloud at 3.7 km up until 5.0 km, an even higher rate of frequency increase is observed as drier air and solar insolation cause the accreted ice to sublimate. Above 5.0 km, the wire is free of ice and the wire resumes a slow, linear rate of frequency increase due to drift. The SLWC profile (right panel, blue line) has a steady increase from the cloudbase at 2.1 km up to a maximum at the base of the saturated inversion at 2.9 km of 0.5 gm^{-3}. The SLWC is a true wedge-shaped profile, similar to many research flights from previous flight campaigns. NIRSS had a SLWC (black line) base at 1.0 km, significantly lower than the sensor's 2.0 km base. NIRSS SLWC topped out at 2.9 km, which was very similar to the sensor SLWC top at 3.0 km. The maximum NIRSS SLWC was 0.25 gm^{-3} near cloudtop, which was roughly half of the maximum sensor SLWC, located at the same height.

The NIRSS volumetric product (Fig. 49) shows "heavy" severity in the vertical profile, and "trace" severity in the furthest approach volumes to the west and southwest which correspond to the heights of the lowest detected NIRSS SLWC. The NIRSS volumetric output for this case is reasonable given the vertical NIRSS profile and in-situ measurements.

The second sensor was released at 15:49 UTC and it ascended nearly vertically through SLWC up to 2.7 km, with a slight drift to the east (Fig. 50). Temperatures in the profile (Fig. 51, left panel) are above freezing from the surface to 0.9 km and sub-freezing through the remainder of the flight. There are no obvious completely saturated levels, according to the sensor, but from 2.1 to an inversion around 2.7 km, the profile is above 90 percent relative humidity. The frequency profile (center) exhibits a monotone, linear upward drift in frequency, except for from the base of the nearly saturated layer at 2.1 km up to the top at 2.7 km. The frequency decrease in this height range corresponds to a peak in SLWC of 0.25 gm^{-3} (right panel, blue line). Other sporadic blips of SLWC exist below 0.05 gm^{-3} associated with the noise in the frequency measurements. NIRSS SLWC (black line) has a base at 1.5 km and a top in the first cloud layer at 2.7 km. The maximum SLWC in this first layer is 0.20 gm^{-3}. NIRSS also has a thin second SLWC layer just above the first layer that the sensor does not detect. The second NIRSS layer is at the top of and within the nearly saturated cloud layer, so the difference in measurement methods could account for the difference in detection of this second liquid layer.

The NIRSS volumetric product (Fig. 52) shows “heavy” severity in the vertical profile, and “trace” severity in the furthest approach volumes to at further ranges along all four runway approaches. The NIRSS volumetric output for this case is reasonable given the vertical NIRSS profile and in-situ measurements.

4.1.8 March 25, 2015

On March 25, 2015 a triple point was approaching the Cleveland area from the West. (A triple point is the intersection of a warm, cold, and occluded front, Fig. 53). The triple point was associated with a surface low pressure system located over Lake Michigan. Superimposed on the triple point was also a shortwave associated with the same low pressure system. Surface temperatures at NASA Glenn were +4.5 °C with dewpoints at 3 °C for the first two launches. The third launch reported temperatures of +8 °C, with dewpoints of +5.5 °C. Winds were predominantly out of the southeast with velocities ranging from 2 to 4 ms^{-1} during the launches. Cleveland’s ASOS recorded “light rain” during the first two launches. There were eight “light rime icing” PIREPs during the event.

Three SLWC-sensors were released during this case. The mean wind direction that influenced the first sensor up to the highest altitude that had SLWC was 205°, or from the south-southwest (Fig. 54). The sensor released at 12:22 UTC measured a thermodynamic profile (Fig. 55, left panel) that was non-freezing up to 2.3 km. Saturated conditions existed above 1.7 km MSL. The frequency (center) has one obvious period of decreases in magnitude during this release, from 3.8 to 4.3 km in altitude. The derived SLWC profile (right panel, blue line) has a maximum of 0.15 gm^{-3} at 3.8 km MSL and has a few other lesser spikes to 0.1 gm^{-3}. NIRSS SLWC (black line) bounds the various low-magnitude spikes in SLWC derived from the sensor quite well. NIRSS has a somewhat higher ILW than the sensor does for this case.

NIRSS volumetric product (Fig. 56) has “heavy” severity icing in the column directly above the ground-based instrumentation (center box) and “light” severities generally out to 25 km distance to the west, with lesser severity values at further ranges for all four runway approaches. These severity magnitudes are very reasonable based on the height and magnitude of detected liquid by the sensor.

The second sensor was released at 14:16 UTC and the mean wind direction up to the highest altitude that had SLWC was from 205°, or from the south-southwest (Fig. 57). The profile is above freezing up until 2.2 km (Fig. 58, left panel) and exhibits near saturation from the surface up to 1.9 km. A fully saturated layer exists from 1.9 to 2.5 km. From 2.5 km up to 3.4 km, there are several thin saturated layers surrounded in height by nearly saturated conditions. Above 3.4 km, there are some higher humidity layers but no heights are close to saturation. The frequency plot (center) shows decreases from 2.1 up to 2.5 km and again from 2.9 up to 3.3 km. These frequency depressions translate to SLWC maxima of 0.17 gm^{-3} centered on 2.3 and 3.0 km with several blips of SLWC above 4 km in altitude that are below the noise threshold (right panel, blue line). NIRSS SLWC (black line) output closely mirrors the heights and magnitudes of sensor SLWC for this case. Maximum SLWC heights and magnitudes as well as overall ILW match very well.

The NIRSS volumetric product (Fig. 59) shows “heavy” severity in the vertical profile as well as “heavy” severities in almost all of the approach volumes within 25 km of the terminal. “Moderate to heavy” severities exist out to 50 km range in the west and southwest approaches. The NIRSS volumetric output for this case seems unreasonable given the magnitude of sensor and vertically pointing NIRSS output. A closer reexamination of this case is needed.

The third sensor was released at 15:01 UTC. The sensor’s motion is initially to the north (180° to 190° wind heading) as it moves up through the boundary layer, and gradually veers as it experiences horizontal wind from the west-southwest (Fig. 60). At the first and lowest SLWC maximum, it is on a 238° heading. At the second maximum, it is on a 250° heading. The sounding is above freezing from the surface up to 2.5 km (Fig. 61, left panel). From the surface, it is unsaturated up to 0.7 km, saturated from 0.7 to 2.0 km, and has a second saturated layer from 3.7 up to about 4.3 km. The frequency trace (center) is roughly steady at 44.3 Hz up through the middle altitudes of the lowest saturated non-freezing layer where it decreases by 0.2 Hz over 0.1 km in height before recovering. A second decrease in frequency is

recorded from 4.0 to 4.3 km at the top of the second cloud layer. In the non-saturated heights between the two cloud layers and above the second cloud layer, the slow and steady upward frequency drift is again observed.

Sensor SLWC (right panel, blue line) shows multiple blips with height caused by the higher noise levels in the frequency values. There are also two SLWC signals with maximum values of 0.2 gm^{-3} centered on 1.6 km and 0.3 gm^{-3} centered on 4.25 km, respectively. This lower SLWC layer, which was centered at 1.6 km, exists at +4.0 °C. Perhaps the existence of SLWC in non-freezing conditions has to do with an updraft associated with spring convection or an artifact of the proximity to the freezing level, such as contact with melting snow. The radar brightband is seen to be located at about 2.0 km, as seen in the Ka-band time series at 15:01 UTC (not shown). NIRSS SLWC (black line) has three distinct layers: from 0.5 to 1.6 km, from 2.3 to 3.2 km and from 3.4 to 4.4 km. The tops of sensor liquid layers correspond well to the tops of NIRSS layers, while the bases of NIRSS layers are roughly 0.5 km lower than sensor liquid bases. Layer maximas are approximately half the magnitude for NIRSS compared to the values detected by the sensors in this case. The NIRSS volumetric product (Fig. 62) shows “moderate to heavy” severity in the vertical profile as well as “moderate” or “heavy” severities in almost all of the approach volumes within 50 km of the terminal.

4.1.9 March 26, 2015

On March 26, 2015, Cleveland was experiencing unsettled weather associated with a weak surface low pressure that was located over West Virginia (Fig. 63). Surface temperatures were +2 °C with dewpoints around +1 °C. The winds were out of the north at 2.5 ms^{-1}. Cleveland’s ASOS reported “haze” switching to “rain” at the time of the launches, switching back to “haze” after the launch. PIREPs during the case study period had eight “light rime icing” and one “moderate rime icing” within 100 km of NASA Glenn.

Three SLWC-sensors were released during this case. The first sensor was released at 15:07 UTC. The mean wind direction that influenced the first sensor up to the highest altitude that had SLWC was 250°, or from the west-southwest (Fig. 64). The temperature had dewpoint temperature values over the first 0.6 km (Fig. 65, left panel) are unreasonably high. This was later determined to be caused by a typo in the radiosonde system configuration file for this flight. The erroneous temperature data was removed from the plot. Readings stabilize at around 0.6 km, and the profile is seen to be saturated from this level up to 5.8 km. Temperatures are near zero or very nearly positive from 0.6 up to 1.2 km. Frequency (center) shows a slight depression from 0.5 up to 1.2 km. A more significant frequency decrease begins at 3 km and extends up to 4.2 km. The derived SLWC (right panel, blue line) has several spikes to 0.1 gm^{-3} above 0.5 km of limited vertical extent, and a more significant wedge-shaped SLWC feature from 2.8 up to 4.3 km. This feature reaches a maximum of 0.3 gm^{-3} at 4.0 km. The NIRSS SLWC profile begins at the same height that the lower level sensor SLWC spikes exist at (roughly beginning at 0.5 km) and extend up to 6 km. This height is about 1.7 km higher than the top of the wedge-shaped liquid feature as seen in the sensor profile, but is exactly the height of the saturated layer as determined by the temperature and dewpoint temperature probes on the radiosonde. Based on the NIRSS component instruments’ limitations, the NIRSS profile seen for this case where SLWC does not extend to the cloud top is the best outcome that can be expected.

The NIRSS volumetric product (Fig. 66) shows “heavy” severity in the vertical profile as well as “moderate” to “heavy” severities in almost all of the approach volumes within 50 km of the terminal. The NIRSS volumetric output for this case seems unreasonable from 5 to 25 km range given the magnitude of sensor and vertically pointing NIRSS output. A closer reexamination of this case is needed.

The second sensor was released at 15:51 UTC. The mean wind direction that influenced the second sensor up to the highest altitude that had SLWC was 255°, or from the west-southwest (Fig. 67). The sensor released at 15:51 UTC measured a thermodynamic profile (Fig. 68, left panel) that was very close to freezing up to 1.2 km. Saturated conditions existed from 0.3 to 4.0 km MSL. The frequency (center) has few significant decreases in magnitude during this release. The derived SLWC profile (right panel,

blue line) has a maximum of 0.13 gm^{-3} at 3.7 km MSL and has a few other lesser spikes to near 0.1 gm^{-3}. NIRSS SLWC (black line) bounds the various low-magnitude spikes in SLWC derived from the sensor quite well. NIRSS has a somewhat higher ILW than the sensor does for this case.

NIRSS volumetric product (Fig. 69) has "moderate-heavy" severity icing in the column directly above the ground-based instrumentation (center box) and "moderate-heavy" severity generally out to 25 km distance, with lesser severity values at further ranges and higher altitudes. These severity magnitudes seem high based on the height and magnitude of detected liquid by the sensor, but reasonable based upon the NIRSS SLWC profile. Further assessment is needed on this result.

The third sensor was released at 16:59 UTC and the mean wind direction that influenced the sensor up to the highest altitude that had SLWC was 255°, or from the west-southwest (Fig. 70). The thermodynamic profile (Fig. 71, left panel) was subfreezing from 0.5 km above the surface through the remainder of the profile. A cloud layer existed from 0.1 to 3.0 km, and nearly saturated from 3.0 up to 4.8 km. Above 4.8 km, slightly drier air existed, but the profile was still fairly humid. Frequency (center) was steady at 44.1 Hz up until just below the freezing level at 0.4 km, where a gradual decrease up to 1.2 km occurred. Values increased back toward the initial release frequency up until 2.4 km, where it decreases significantly to the top of the nearly saturated level at 4.8 km. Above this height, a steady frequency increase begins as water mass is gradually sublimated for the ice-accreted wire. The sensor liquid profile (right panel, blue line) begins at 0.4 km with a relative maxima of 0.2 gm^{-3} centered on 1 km altitude. Additional liquid in a wedge-shaped profile begins at 2 km and continues up to 4.7 km, with a maximum SLWC of 0.25 gm^{-3} at 4.3 km. NIRSS SLWC (black line) has a base and top at the same altitudes that the sensor does and has a maximum SLWC of 0.3 gm^{-3} at 4.7 km. Overall, NIRSS shows excellent agreement with the sensor SLWC in this case.

NIRSS volumetric product (Fig. 72) has "heavy" severity icing in the column directly above the ground-based instrumentation (center box) and "heavy" severity generally out to 25 km distance, with lesser severity values at further ranges and higher altitudes. These severity magnitudes seem possible, based on the height and magnitude of detected liquid by the sensor.

4.1.10 April 7, 2015

On April 7, 2015, a stationary front existed from the Cleveland area to a low pressure system which was centered over Kansas (Fig. 73). A stationary front is the surface boundary between two different air masses, neither of which is strong enough to replace the other. Temperatures were around 10 °C with dewpoints closely following the temperature's variations at 8 °C. Surface winds were out of the north at the beginning of the case study time, switching to north-northwesterly flow by the end of the period of interest for the case. Wind speeds varied from 4 to 6 ms^{-1}. ASOS cloud bases were reported near 150 m throughout the event. Cleveland's ASOS reported "light rain" and "moderate rain" just before the sensor launches, switching to "haze" at the time of the launches. There was only one "moderate rime icing" PIREP during the event, the report was at 1435 UTC, which was at the time of the second launch.

Two SLWC-sensors were released during this case. The first sensor was released at 12:56 UTC and rose nearly vertically through the SLWC cloud, with a slight drift to the west (Fig. 74). Temperatures (Fig. 75, left panel) are above freezing from the surface up to 3.0 km. The profile is saturated from the surface up to 1.1 km. Frequency (center) is steady up to 0.8 km, where it begins to decrease by a few tenths of a Hertz to the cloudtop at 1.1 km and then increases back to the starting frequency. Above this height, frequency resumes an upward drift. The frequency change with time and height correlates to a spike in SLWC to about 0.17 gm^{-3} centered on 0.9 km. The sensor SLWC profile (left panel, blue line) has a spike to 0.2 gm^{-3} centered on 0.9 km. There are many other SLWC blips in the profile, but none that exceed the noise threshold of 0.05 gm^{-3}. NIRSS SLWC (black line) exactly bounds the lowest sensor SLWC layer in height, and the maximum SLWC of 0.25 gm^{-3} is similar as well. NIRSS also calls out two other layers of SLWC at 4.2 and 6 km that do not have liquid in the sensor profile. These two elevated layers are seen to have nearly saturated conditions in the thermodynamic profile.

The NIRSS volumetric product (Fig. 76) shows “heavy” severity in the vertical profile as well as “moderate” or “heavy” severities in the furthest three approach volumes of the west, east and southwest flightpaths. Based on the in-situ and vertically-pointing NIRSS profiles, the NIRSS terminal area output seems quite reasonable.

The second sensor was released at 14:35 UTC. The mean wind that influenced the sensor up to the highest altitude that had SLWC at 3.8 km was 270°, or from the west (Fig. 77). Temperatures (Fig. 78, part A) are above freezing from the surface up to 2.9 km. The profile is saturated from very close to the surface up to 4.3 km. The initial sensor frequency (center) is about 43.8 Hz with some noisy outliers in the first 0.2 km. Frequency decreases sharply beginning at 0.5 km up to 1.0 km, where values recover back to the initial value by 1.6 km. Values also decrease from 3.7 to 3.9 km. Between these two liquid layers and above the cloud top height of 4.3 km, the slow upward frequency drift is again evident. These frequency changes with time and height produce maximum SLWCs of 0.28 gm^{-3} (left panel, blue line) centered on 0.7 km and another of 0.22 gm^{-3} centered on 3.8 km, respectively. NIRSS SLWC (black line) also sees two significant discrete SLWC layers. NIRSS closely captures the liquid base altitude of the lowest SLWC layer, but overestimates the liquid top height. NIRSS has a second SLWC layer that is lower than the sensor SLWC layer. The maximum NIRSS SLWC of each layer are quite similar to the sensor maximum values.

The NIRSS volumetric product (Fig. 79) shows “heavy” severity in the vertical profile as well as “moderate” or “heavy” severities in all of the approach volumes out to 50 km in range. Based on the in-situ and vertically-pointing NIRSS profiles, the NIRSS terminal area output seems reasonable, but a recheck of this case is also in order.

4.1.11 April 23, 2015

On April 23, 2015 several weak mid-level troughs were effecting the Cleveland area (Fig. 80). Cleveland surface temperatures were around 3 °C, with dewpoints at –3 °C. Surface winds were out of the northwest at 6.7 ms^{-1} at the time of the single sensor launch. Cleveland’s ASOS reported “light snow” in the hours before the launch. The cloud base was reported at 1.6 kms. During the case study, there were three cases of “trace icing,” nine cases of “light icing” and three cases of “moderate icing”.

The sensor release took place at 17:26 UTC. GPS from the sensor indicates that the sensor rose nearly vertically during its duration within cloud, with a slight eastward motion of a few kilometers (Fig. 81). The sensor indicates above freezing temperatures (Fig. 82, left panel) up to 0.4 km and unsaturated conditions up to 1.5 km. At this height, the profile is only near 100 percent relative humidity for a small range of heights. From 1.6 km up to 2.4 km, conditions approach 90 percent humidity. A 3 °C temperature inversion exists at 2.4 km. The sensor wire frequency (center) drifts upward from the release value of 44.4 Hz up until 1.5 km, where frequency drops very significantly until the inversion height at 2.4 km. Above 2.4 km, frequency begins a gradual recovery toward the initial values. The frequency change with time translates to SLWC (right panel, blue line) from 1.5 to 2.4 km in a classic “wedge-shaped” SLWC profile, with a maximum of 0.85 gm^{-3} at 1.9 km. Once again, the NIRSS SLWC top is exactly collocated with that of the sensor at 2.4 km. NIRSS has a SLWC base at 0.4 km, significantly lower than the sensor SLWC base. The maximum NIRSS SLWC is about 0.4 gm^{-3} at the top of the liquid layer.

The NIRSS volumetric product (Fig. 83) shows “heavy” severity in the vertical profile as well as “heavy” severities in all of the approach volumes out to 50 km in range. Based on the significant SLWCs detected in both the in-situ and vertically-pointing NIRSS profiles, the NIRSS terminal area output seems quite reasonable.

4.2 Overall Statistics

For each of the twenty-three sensor releases detailed in Table 1, vertical profiles of NIRSS SLWC that were closest in time to the sensor when it exited the cloudtop were compared to similar sensor values. The lowest and highest altitudes of NIRSS SLWC were plotted against the lowest and highest altitudes of SLWC as detected by the SLWC-sensors, with results shown in Figure 84. A Pearson's Correlation was run to determine the relation between the maximum and minimum altitudes of SLWC detected by sensor and NIRSS for the twenty-three cases. There was a total of 46 independent base and top heights of SLWC to compare. The correlation factor was found to be 0.78 on a scale of 0 to 1. This value corresponds to a very strong, positive correlation between sensor and NIRSS SLWC heights that was significant at the one tenth of one percent confidence level.

The ILW from the NIRSS and sensor are not directly comparable due to spatial and temporal differences in the measurements. This may be examined and further discussed in a future publication.

5.0 Conclusion

During the winter of 2015, a field campaign was conducted at NASA Glenn Research Center in Cleveland, Ohio with the goal of developing a comparison database to allow the assessment and future refinement of icing remote sensing technologies. As part of this effort the NIRSS vertical pointing and terminal area systems were operated and weather balloons outfitted with SLWC-sensor instrumentation were released into in-flight icing conditions. This dataset is the first to address the assessment of terminal area icing remote sensing technologies.

Forecasts led to twenty-three balloon flights into SLWC conditions aloft. Analysis of each of the individual flights was detailed, including a synoptic case overview followed by comparisons of the base and top heights of SLWC, altitude and amount of maximum SLWC and ILW magnitudes. A statistical analysis also found strong positive correlations between independent SLWC base and top heights when NIRSS SLWCs are compared to SLWC from the sensor database.

The data gathered has proven to be valuable for the assessment of the vertical pointing NIRSS system. Some cases demonstrated significant skill of NIRSS in identifying the location of hazardous icing conditions aloft. Other cases that demonstrated weaker agreement can provide the basis for further NIRSS algorithm refinement. However, the flight path constraints of a free-flying balloon-based instrument for comparisons at specific spatial locations (i.e., specific airport approach paths) have been found to be limiting for the assessment of terminal area icing weather products. Due to the spatial and temporal variability of aircraft icing conditions, a balloon-based sensor system is typically too limited to provide case-by-case comparisons. The limitations of this data set further support the use of instrumented aircraft for future terminal area remote sensing and forecasting method assessments.

Appendix—Acronyms

Algorithms

NIRSS	NASA Icing Remote Sensing System

Organizations

FAA	Federal Aviation Administration
GRC	Glenn Research Center, in Cleveland
NASA	National Aeronautics and Space Administration
NCAR	National Center for Atmospheric Research
NSF	National Science Foundation
NWS	National Weather Service

Miscellaneous

AGL	above ground level
ASOS	Automated Surface Observing Station
CCL	cloud condensation level
ILW	integrated liquid water
LWC	liquid water content
MSL	mean sea level
NOTAM	“Notice to Airmen”
PIREP	pilot report
QC	quality control
SLW	supercooled liquid water
SLWC	supercooled liquid water content

References

1. Reehorst, A., Brinker, D., Politovich, M., Serke, D., Ryerson, C., Pazmany, A. and Solheim, F., "Progress Towards the Remote Sensing of Aircraft Icing Hazards," NASA/TM—2009-215828, November 2009.
2. "Meteorologische Messtechnik GmbH, Doppler Radar 35 GHz," METEK GmbH, Elmshorn, Germany, viewed March 26, 2014 <http://www.metek.de/product-variants/doppler-radar-35-ghz.html>.
3. "MP-Series Profilers," Radiometrics Corporation, Boulder, CO, viewed March 26, 2014 <http://radiometrics.com/products-services/product/mp-series/>.
4. Reehorst, A., and Serke, D., "A Terminal Area Icing Remote Sensing System," NASA/TM—2014-218417, November 2014.
5. Serke, D., Hall, E., Bognar, J., Jordan, A., Abdo, S., Baker, K., Seitel, T., Nelson, M., Ware, R., McDonough, F. and Politovich, M., "Supercooled liquid water content profiling case studies with a new vibrating wire sonde compared to a ground-based microwave radiometer," *Atmos. Res.* 149, 77–87, November, 2014.
6. Rogers, R., and Yau, M., "A Short Course in Cloud Physics," Elsevier Science, Oxford, UK, 1988.
7. Politovich, M.K., B.B. Stankov, and B.E. Martner, "Determination of liquid water altitudes using combined remote sensors," *J. Appl. Meteor*., 34, pp. 2060–2075, 1995.
8. Bernstein, B., McDonough, F., Politovich, M., Brown, B., Ratvasky, T., Miller, D., Wolff, C., and Cunning, G., "Current Icing Potential: algorithm description and comparison to aircraft observations," *J. Appl. Meteor*., 44, pp. 969–986, 2005.
9. Hill, G.E. and Woffinden, D., "A Balloonborne Instrument for the Measurement of Vertical Profiles of Supercooled Liquid Water Concentration," *J. Appl. Meteorol*., 19, pp. 1285–1292, 1980.
10. Hill, G. E., "Analysis of Supercooled Liquid Water Measurements Using Microwave Radiometer and Vibrating Wire Devices," *J. Atmos. Ocean. Technol.*, 11, pp. 1242–1252, 1994.
11. Serke, D., Doyle, R., King, M., Geerts, B., Steiger, S. and Politovich, M., A new SLW-sonde compared to research aircraft flights, AMS 17th Symposium on Meteorological Observation and Instrumentation, June 9–13, Westminster, CO, 2014.
12. King, M., "Supercooled liquid water content instrument analysis and winter 2014 data with comparisons to the NASA Icing Remote Sensing System and pilot reports," NASA/TM, 2015, In Review.
13. Hogg, D.C., F.O. Guiraud, J.B. Snider, M.T. Decker and E.R. Westwater, 1983: A steerable dual-channel microwave radiometer for measurements of water vapor and liquid water in the troposphere. *J. Climate Appl. Meteor.*, 22, 789–806.
14. Solheim, F., Godwin, J., Westwater, E., Han, Y., Keihm, S., Marsh, K., and Ware, R., "Radiometric profiling of temperature, water vapor and cloud liquid water using various inversion methods," *Radio Sci.*, 33, pp. 393–404, 1998.
15. Reehorst, A.L., Brinker, D.J., Ratvasky, T.P., "NASA Icing Remote Sensing System: comparisons from AIRS–II," NASA/TM—2005-213592, 2005.
16. Zednik, S., "NIRSS Display Upgrades- Cloud and Icing Logic," Undergraduate Studies Program Final Report, 2004, Available upon request.
17. Johnston, Christopher J.; Serke, David J.; Adriaansen, Daniel R.; Reehorst, Andrew L.; Politovich, Marcia K.; Wolff, Cory A.; and McDonough, Frank, "Comparison of In-Situ, Model and Ground Based In-Flight Icing Severity," NASA/TM—2011-217141, December, 2011.
18. Guirong Xu, Randolph Ware, Wengang Zhang, Guangliu Feng, Kewen Liao, and Yibing Liu, "Effect of off-zenith observations on reducing the impact of precipitation on ground-based microwave radiometer measurement accuracy," *Atmos. Res.*, Volumes 140–141, pgs. 85–94, April-May 2014.
19. Tuttle, John D., and Foote, G. Brant, "Determination of the Boundary Layer Airflow from a Single Doppler Radar," *J. Atmos. and Ocean. Tech.*, Volume 7, pgs. 218–232, 1990.

TABLE 1.—DATE, TIME, AND MAXIMUM OBSERVED LWC OF THE SENSOR RELEASES DURING THE 2015 FIELD CAMPAIGN

Sonde date		Sonde time		max LWC
[yyyymmdd]		[hh:mm]		[gm-3]
20150122		14:17		0.30
20150129		19:25		0.50
20150129		20:06		0.35
20150204		13:42		0.20
20150204		17:07		0.20
20150211		20:00		0.50
20150211		21:10		0.80
20150313		20:43		0.10
20150313		21:59		0.20
20150313		23:38		0.15
20150317		13:54		0.30
20150317		14:47		1.40
20150320		15:00		0.40
20150320		15:49		0.20
20150325		12:22		0.10
20150325		14:18		0.20
20150325		15:01		0.30
20150326		15:07		0.25
20150326		15:51		0.10
20150326		16:59		0.20
20150407		12:56		0.20
20150407		14:35		0.20
20150423		17:26		0.80

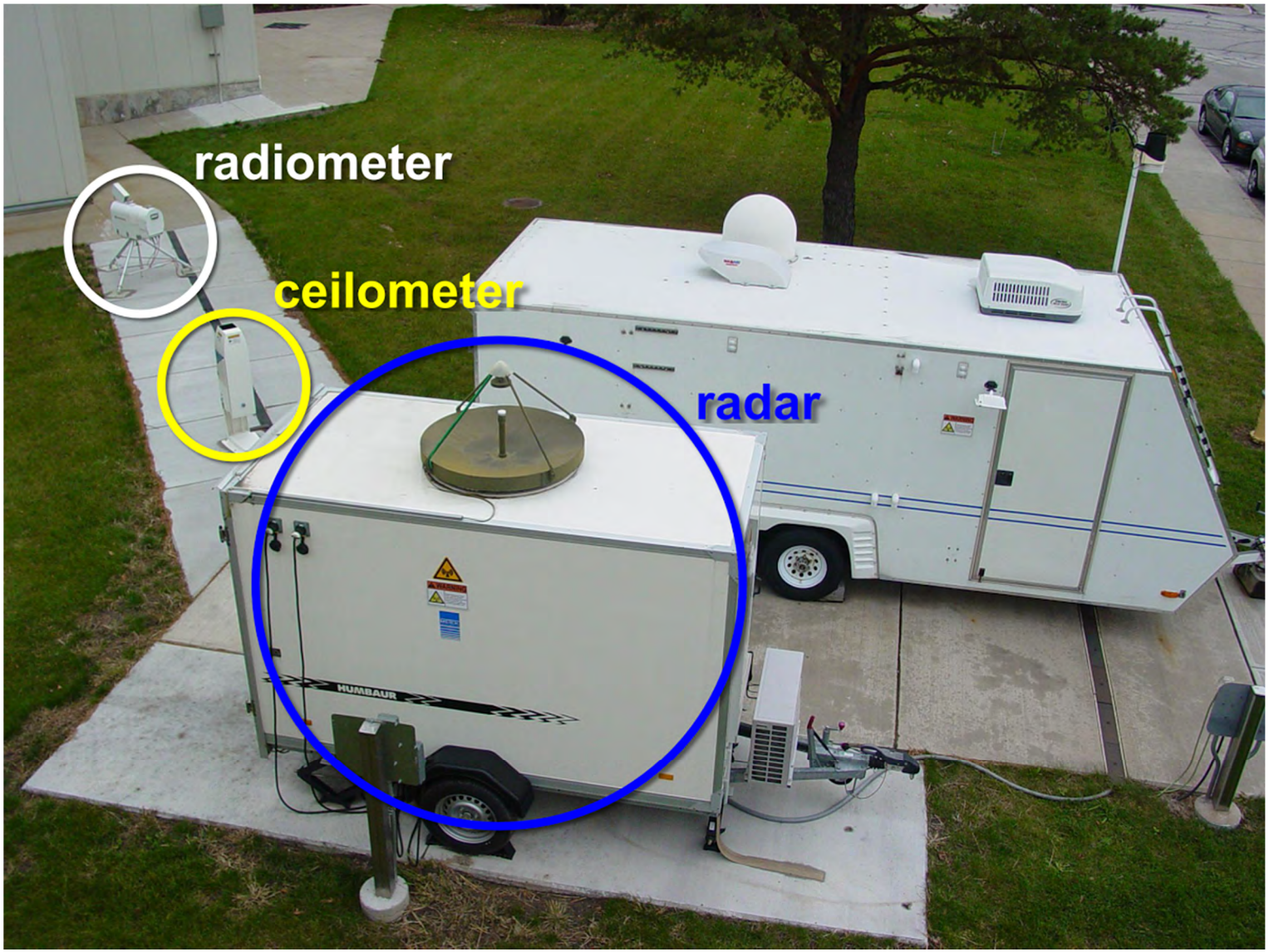

Figure 1.—NIRSS hardware components.

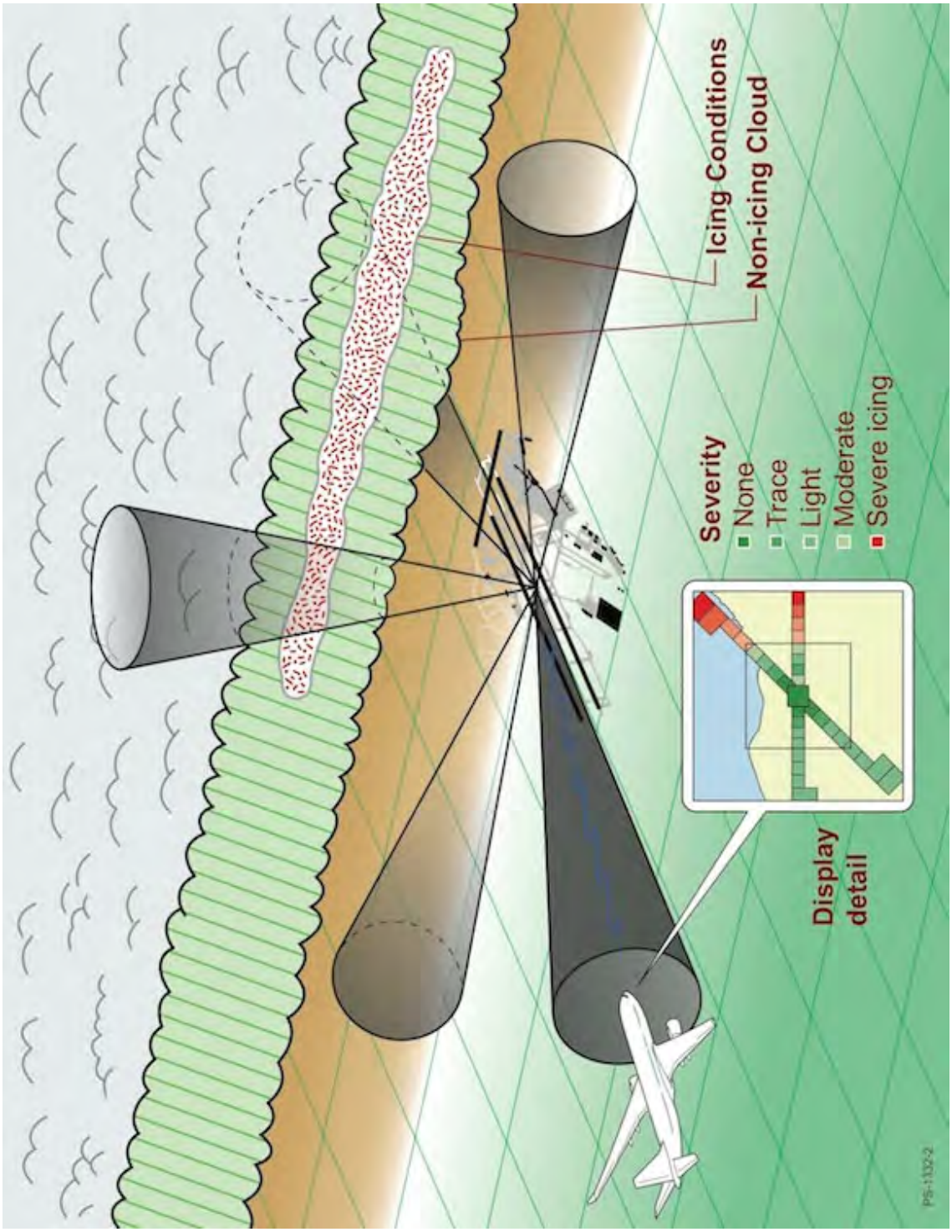

Figure 2.—Conceptual drawing of a ground-based remote sensing system for the detection of in-flight icing hazards.

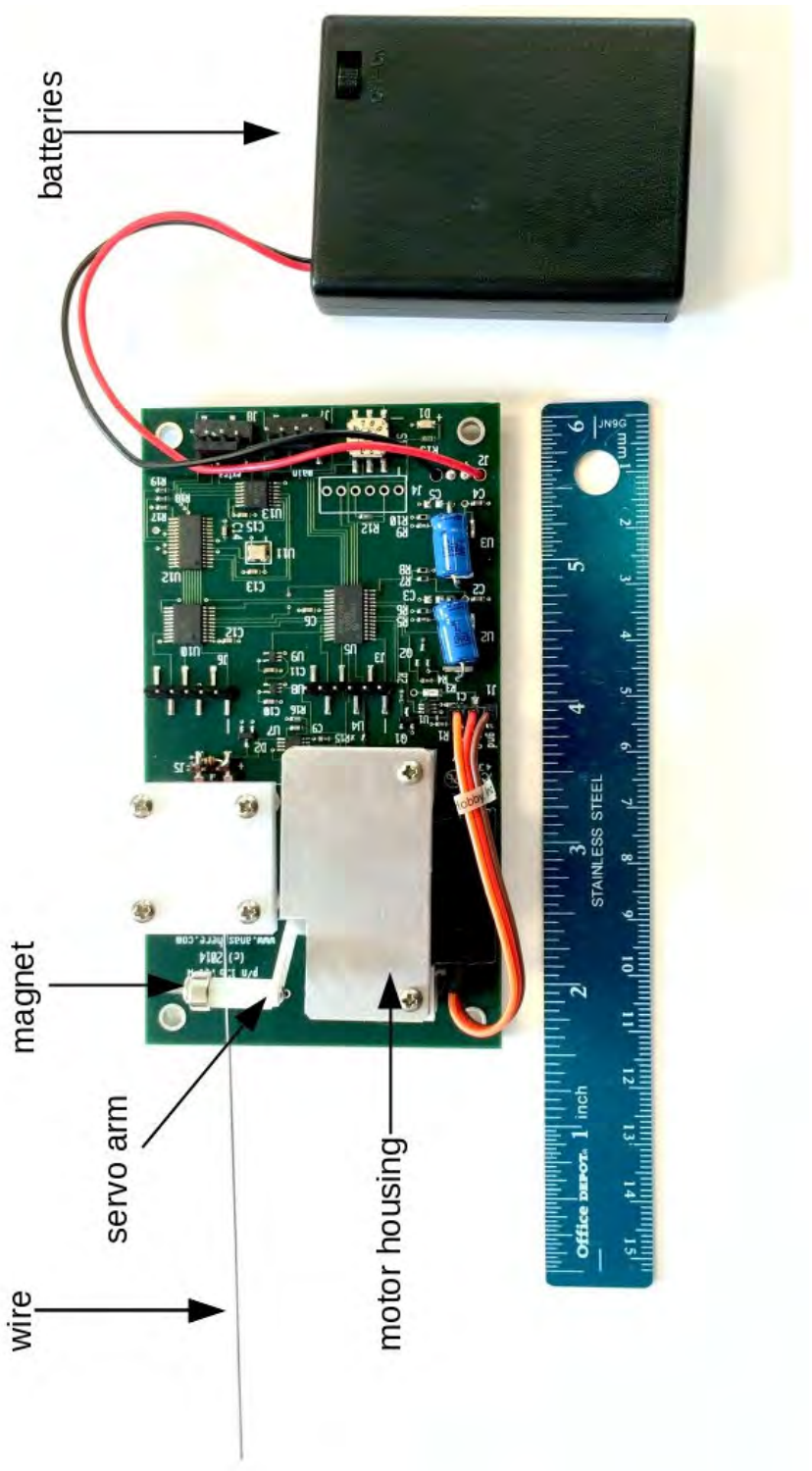

Figure 3.—SLW-sensor.

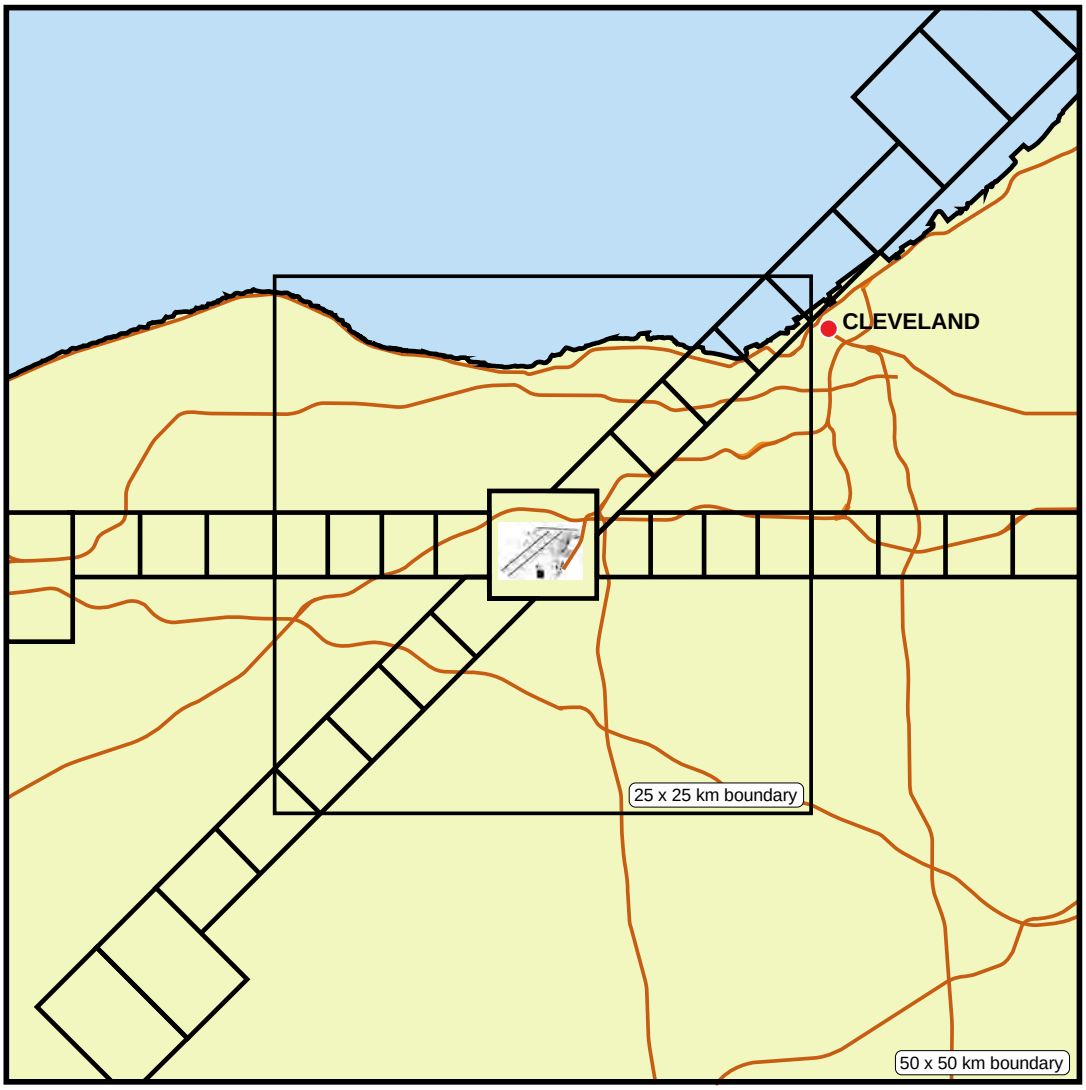

PS-1332-3

Figure 4.—Terminal area approach zones for Cleveland Hopkins Airport, planview.

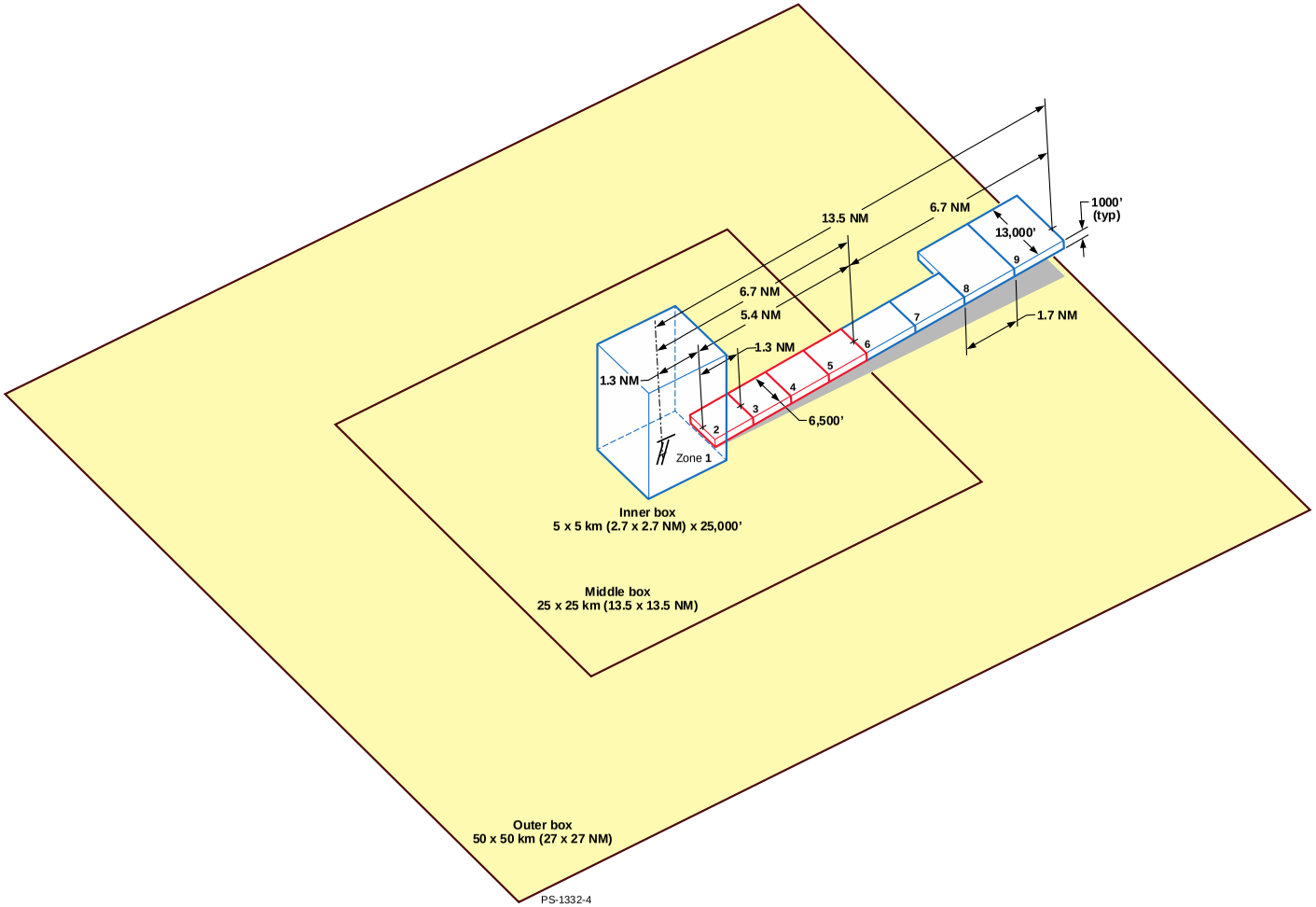

Figure 5.—Terminal area approach zones detail, 3-D view.

Figure 6.—Map of field campaign sensor locations at NASA Glenn Research Center in Cleveland, Ohio. Imagery ©2016 Google, Map data ©2016 Google.

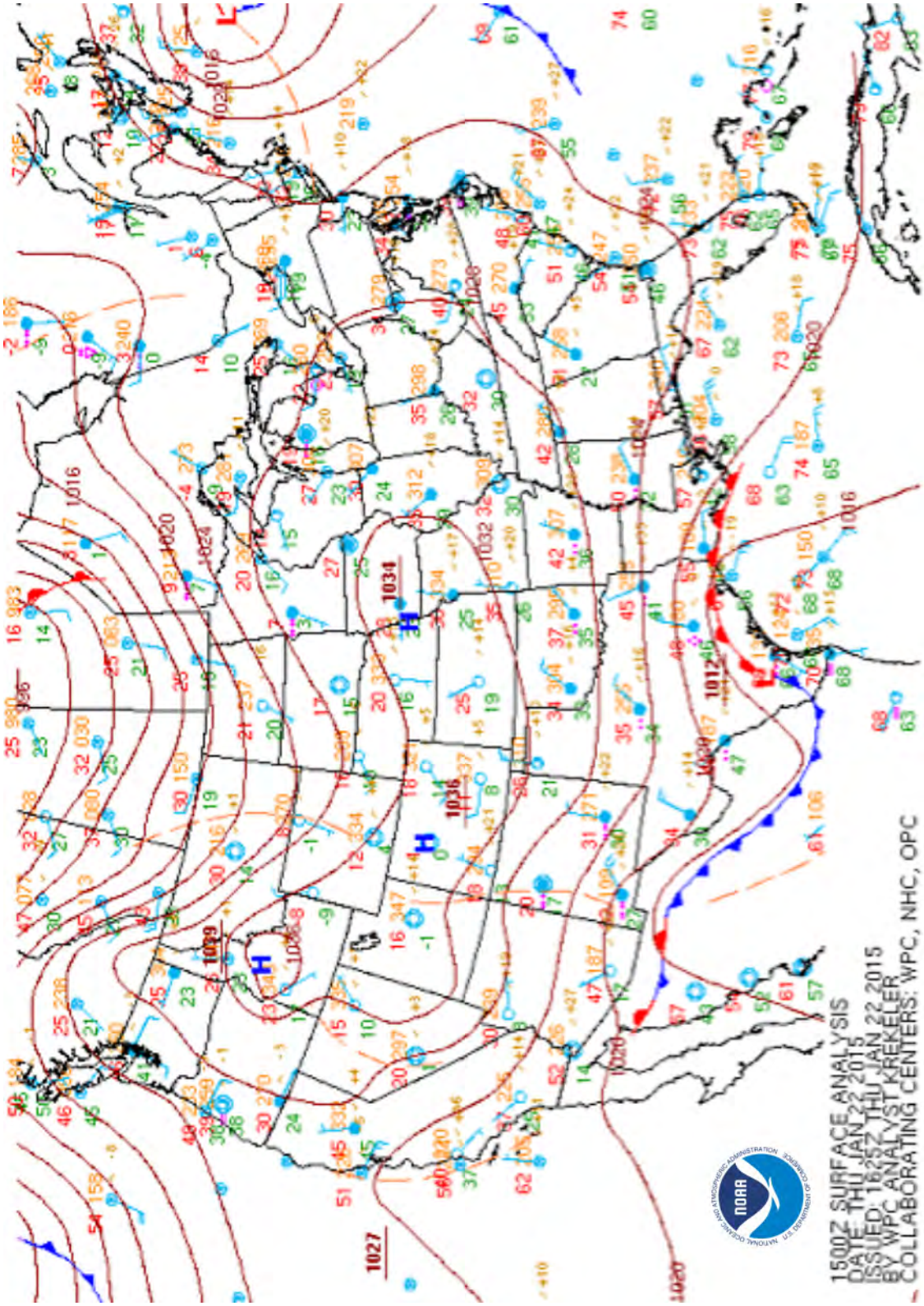

Figure 7.—Surface analysis chart form 15:00 UTC on January 22, 2015.

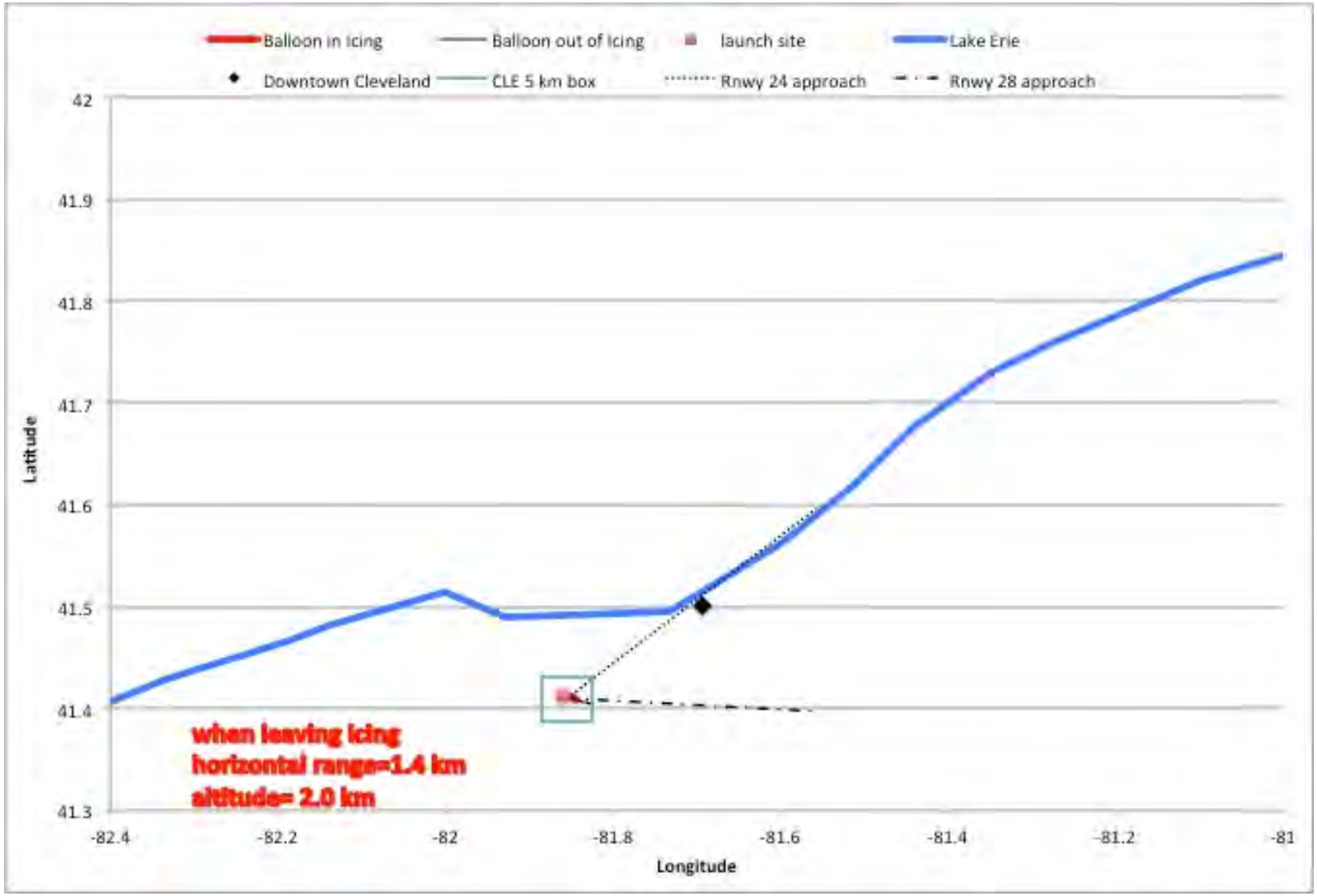

Figure 8.—Map of SLW-sensor trajectory (red) from 14:17 UTC on January 22, 2015.

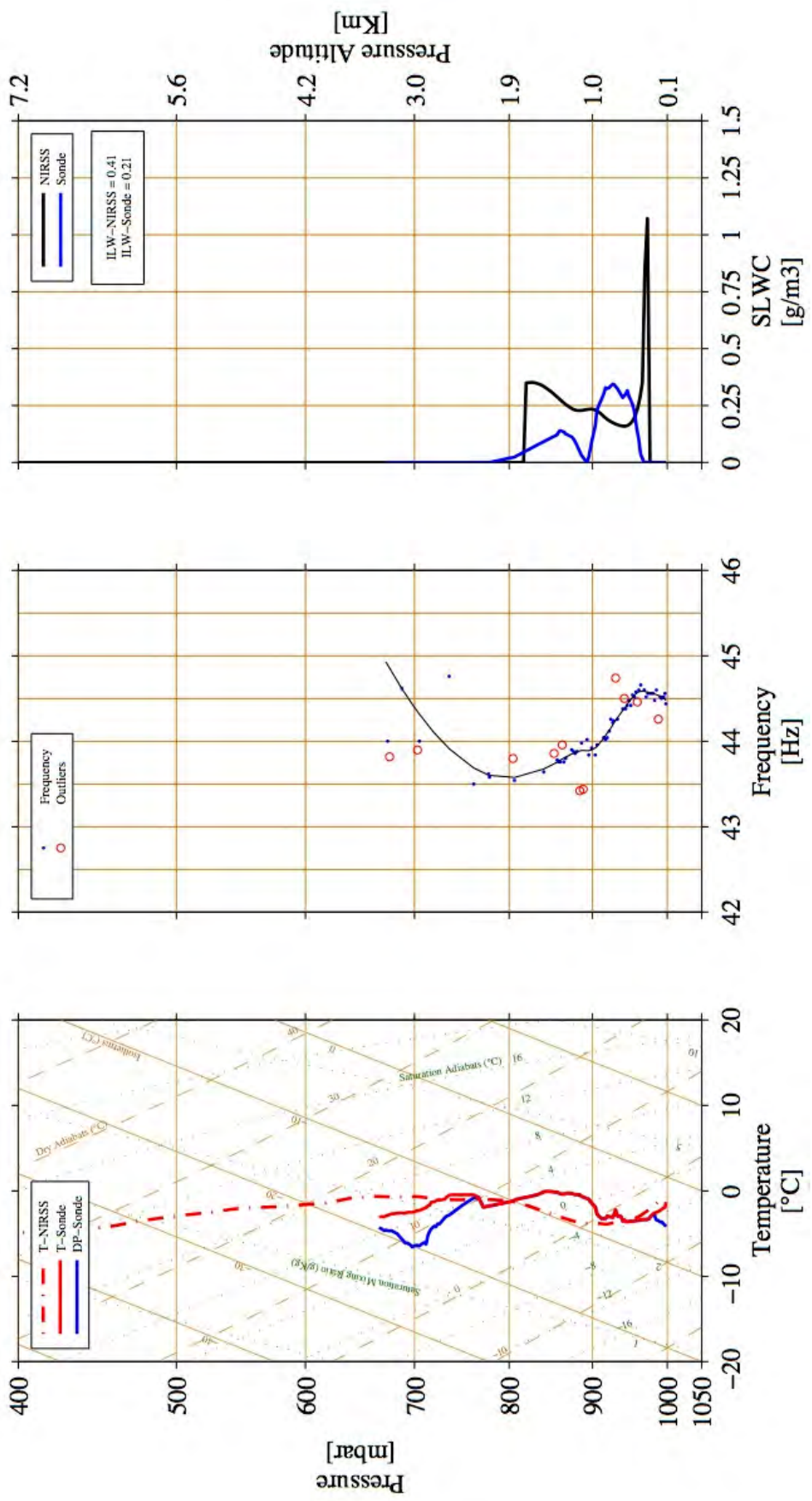

Figure 9.—Skew-T log P profile of SLW-sensor temperature (left, red line) and dewpoint temperature (left, blue line), SLW-sensor wire frequency (center, black line), and SLW-sensor LWC (right, blue line) with NIRSS LWC (right, black line) from 14:17 UTC, January 22, 2015.

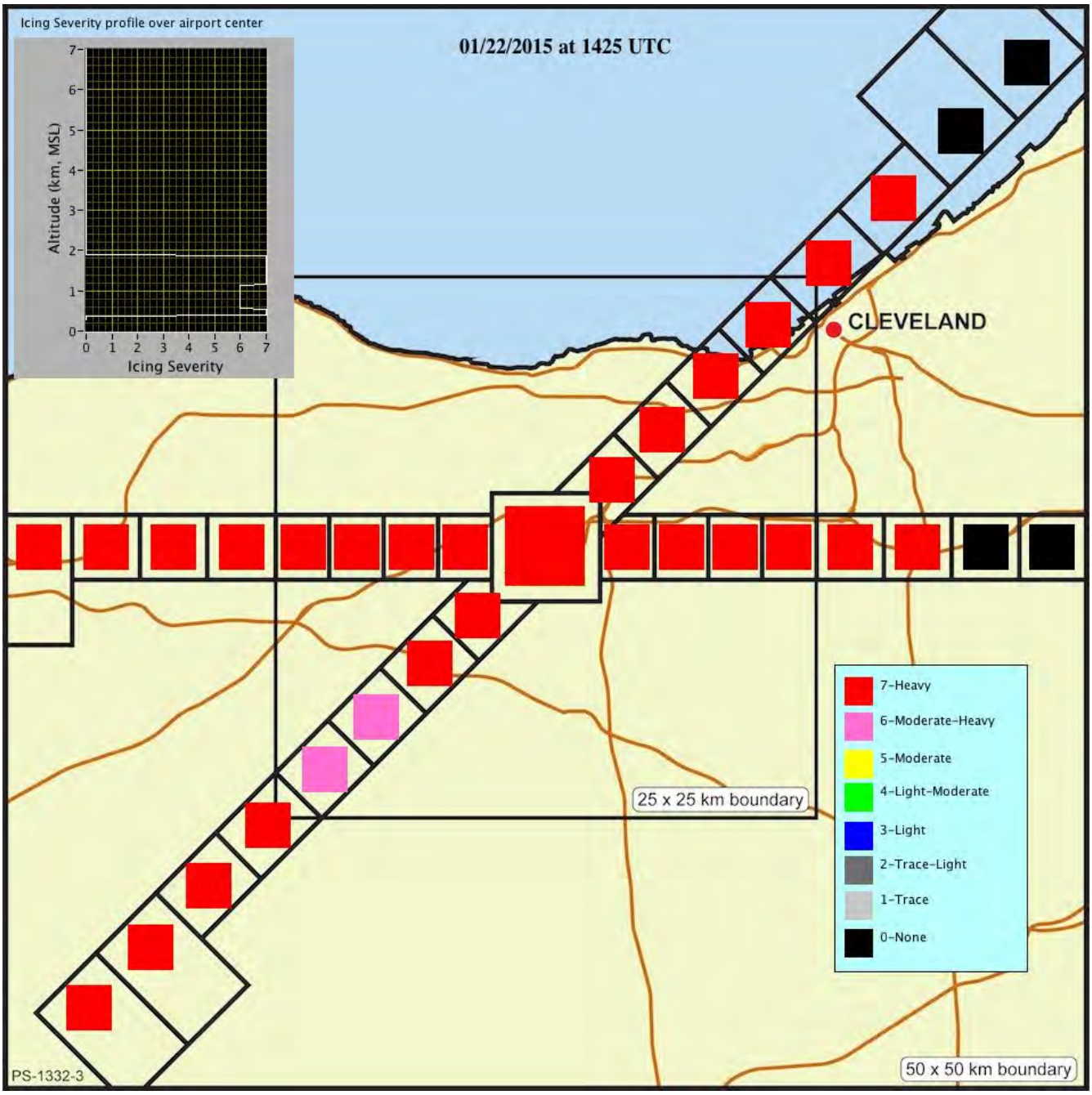

Figure 10.—NIRSS terminal area qualitative in-flight icing hazard classification from 14:25 UTC on January 22, 2015.

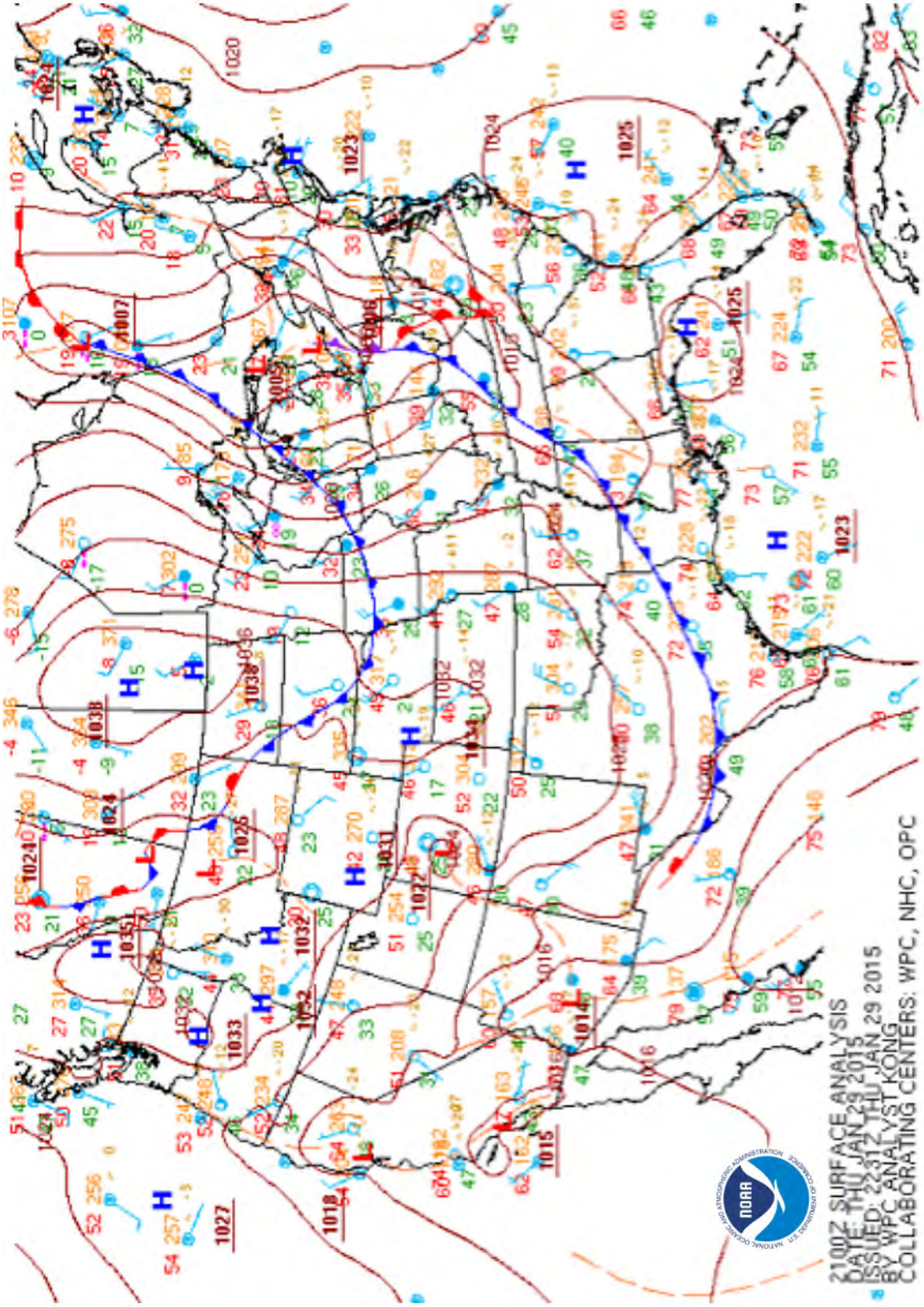

Figure 11.—Surface analysis chart from 20:00 UTC on January 29, 2015.

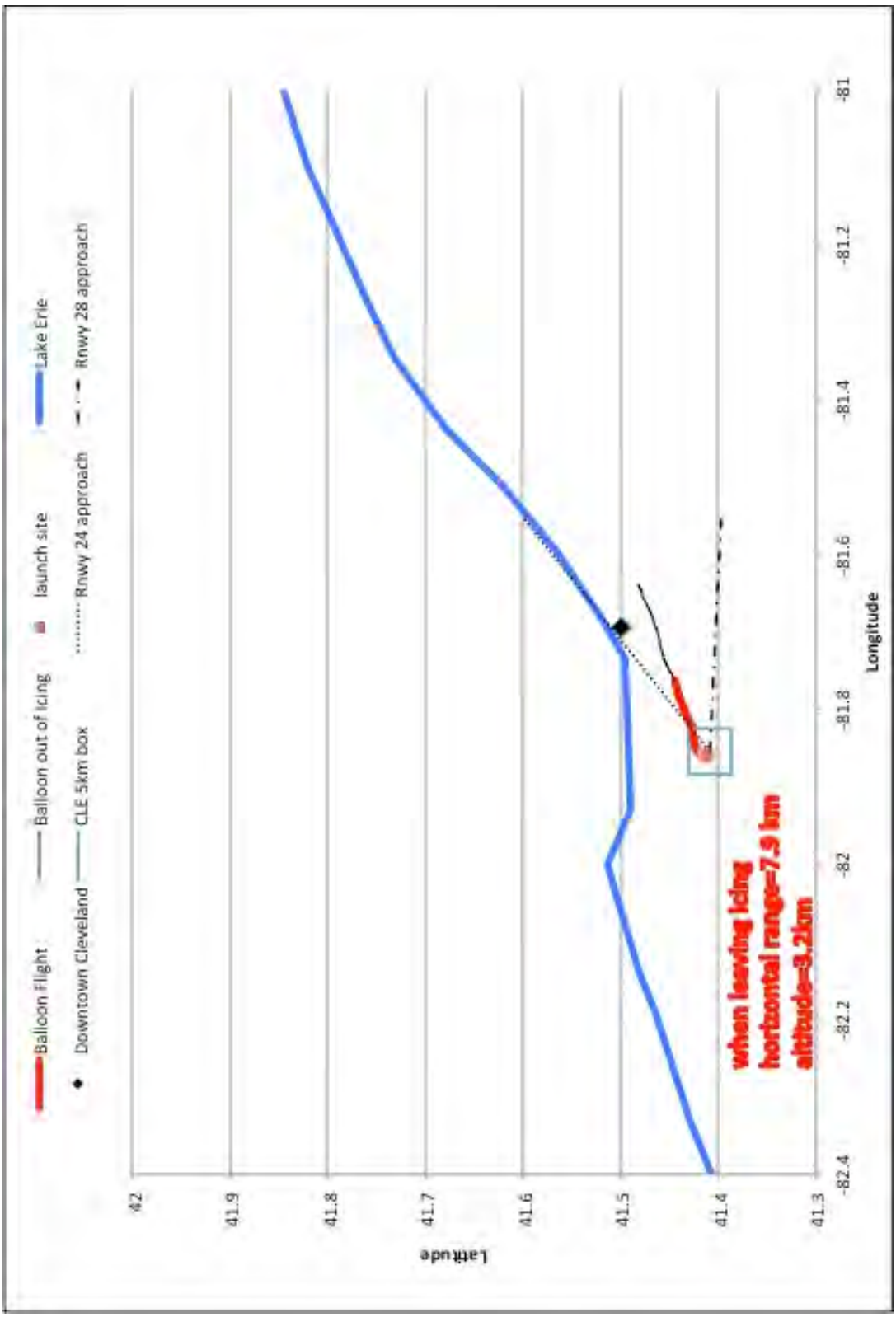

Figure 12.—Map of SLW-sensor trajectory (red) from 19:25 UTC on January 29, 2015.

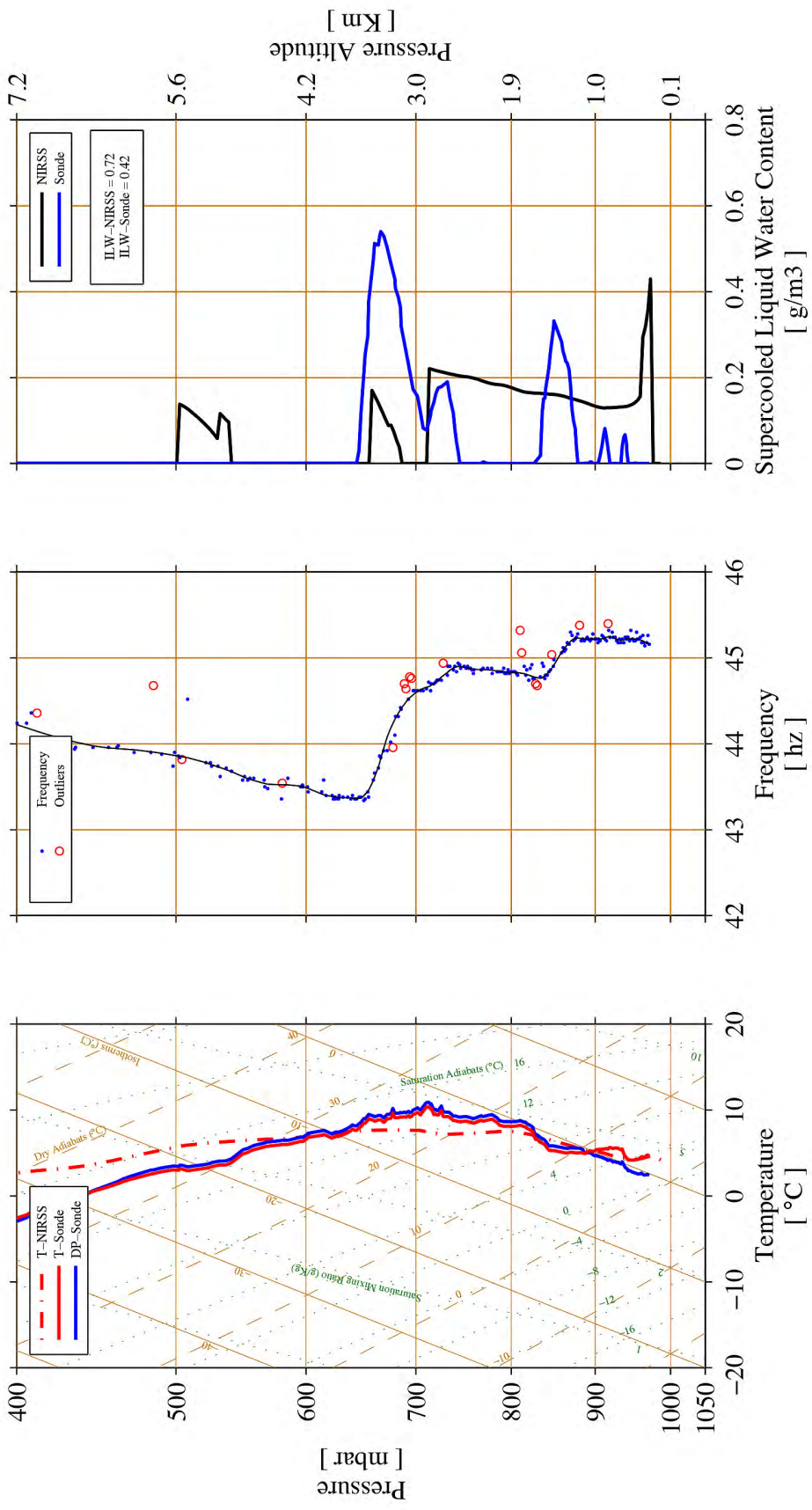

Figure 13.—Skew-T log P profile of SLW-sensor temperature (left, red line) and dewpoint temperature (left, blue line), SLW-sensor wire frequency (center, black line), and SLW-sensor LWC (right, blue line) with NIRSS LWC (right, black line) from 19:25 UTC, January 29, 2015.

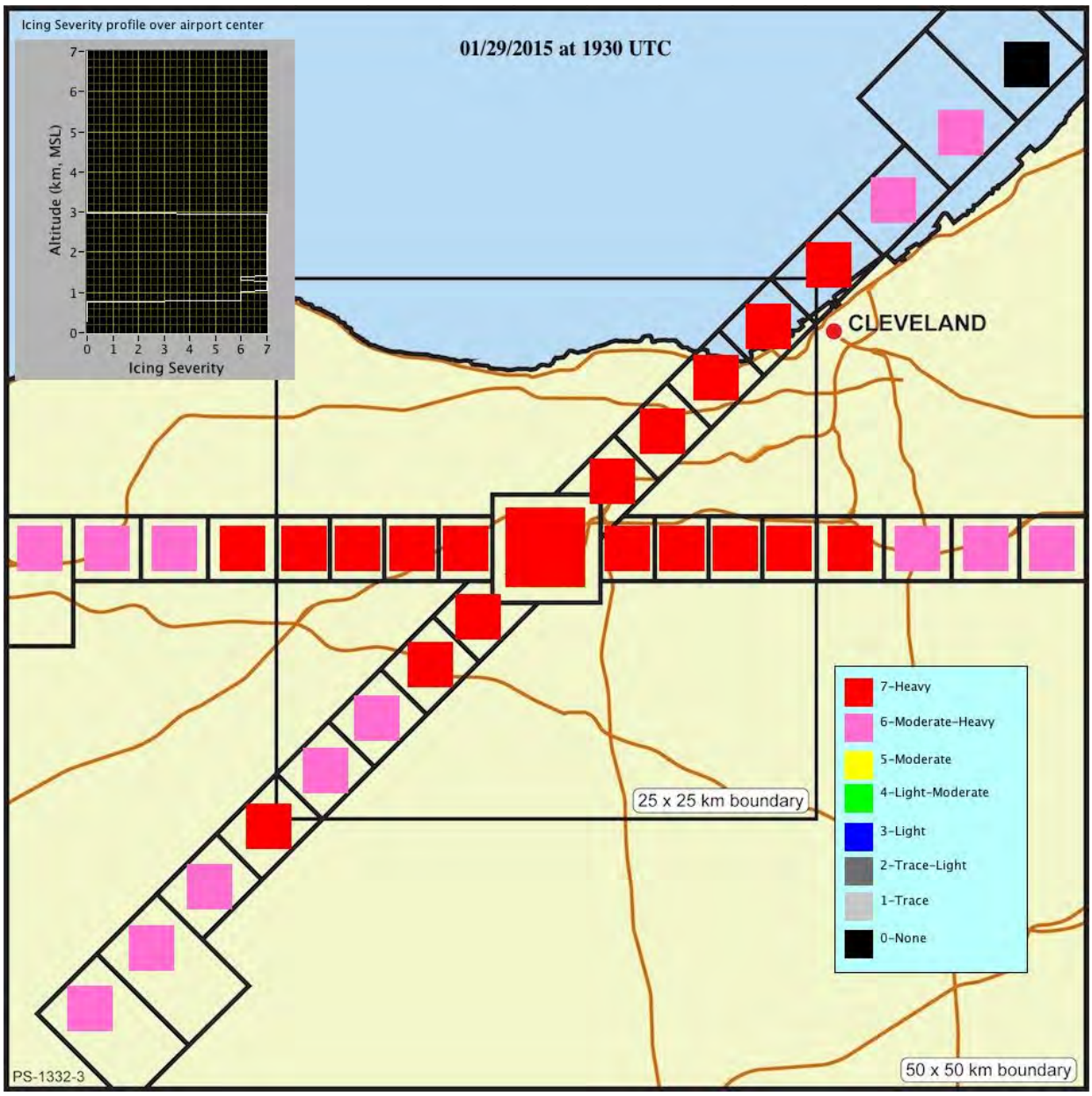

Figure 14.—NIRSS terminal area qualitative in-flight icing hazard classification from 19:34 UTC on January 29, 2015.

Figure 15.—Map of SLW-sensor trajectory (red) from 20:06 UTC on January 29, 2015.

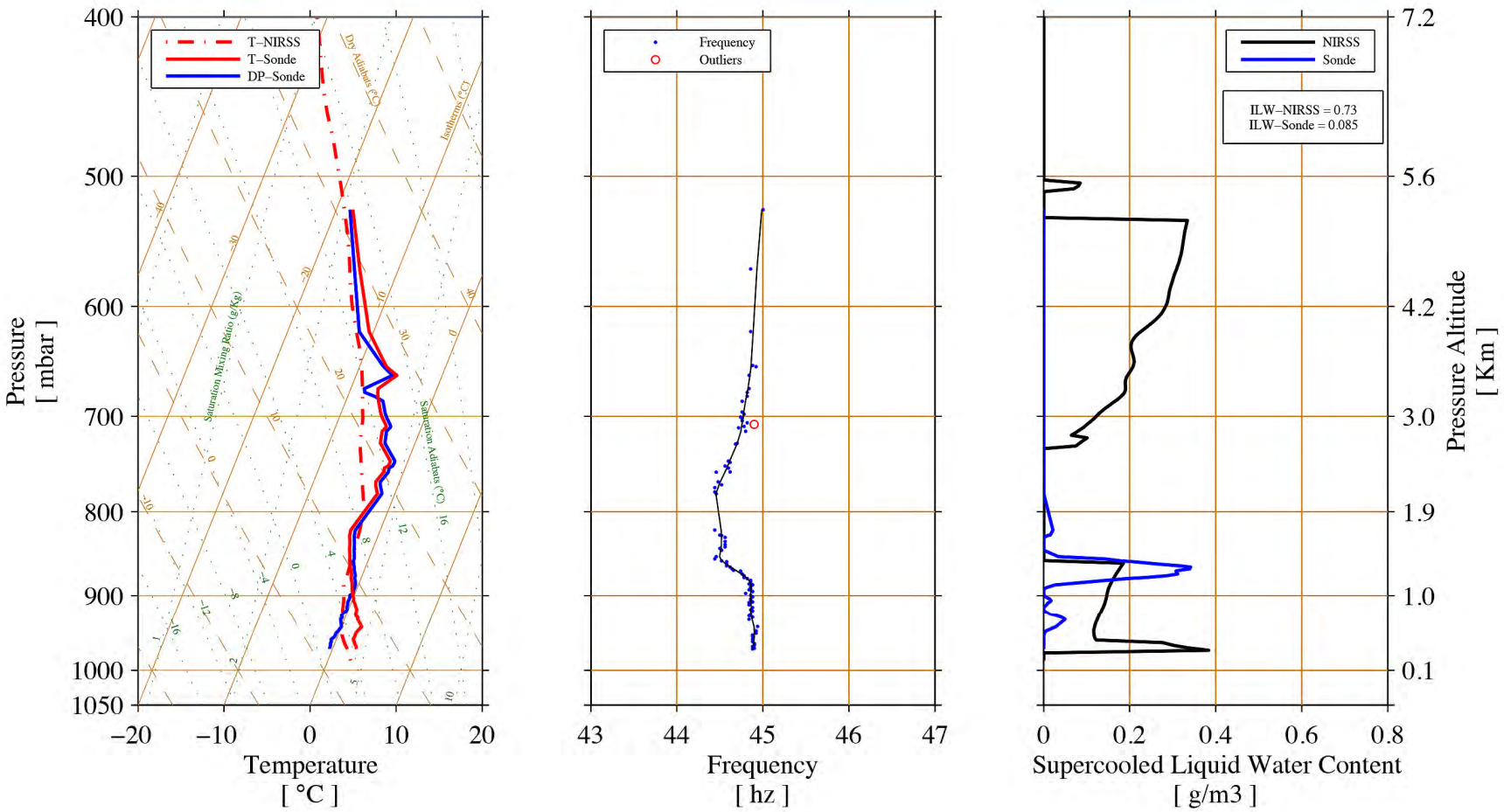

Figure 16.—Skew-T log P profile of SLW-sensor temperature (left, red line) and dewpoint temperature (left, blue line), SLW-sensor wire frequency (center, black line) and SLW-sensor LWC (right, blue line) with NIRSS LWC (right, black line) from 20:06 UTC on January 29, 2015.

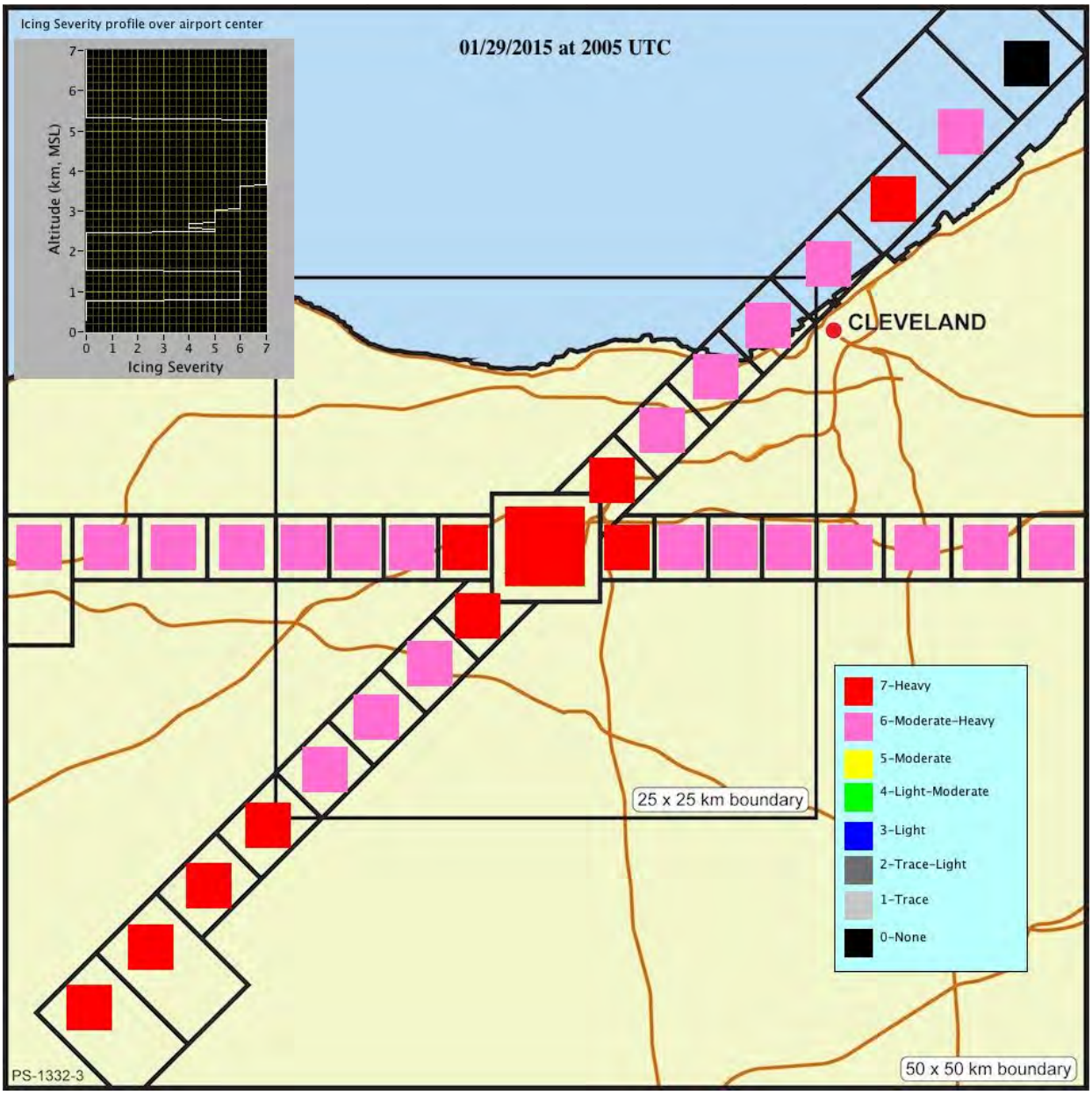

Figure 17.—NIRSS terminal area qualitative in-flight icing hazard classification from 20:05 UTC on January 29, 2015.

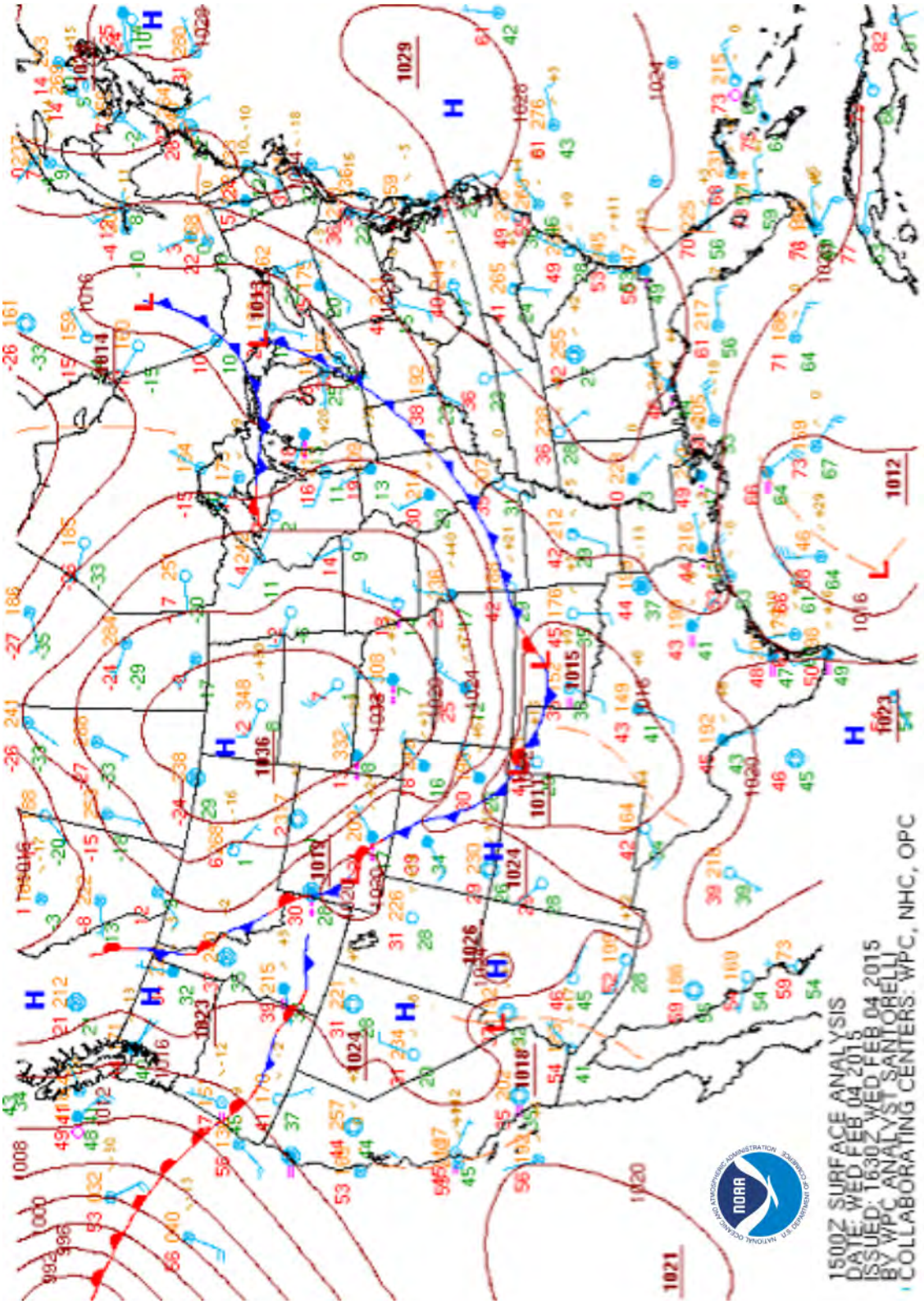

Figure 18.—Surface analysis chart from 15:00 UTC on February 4, 2015.

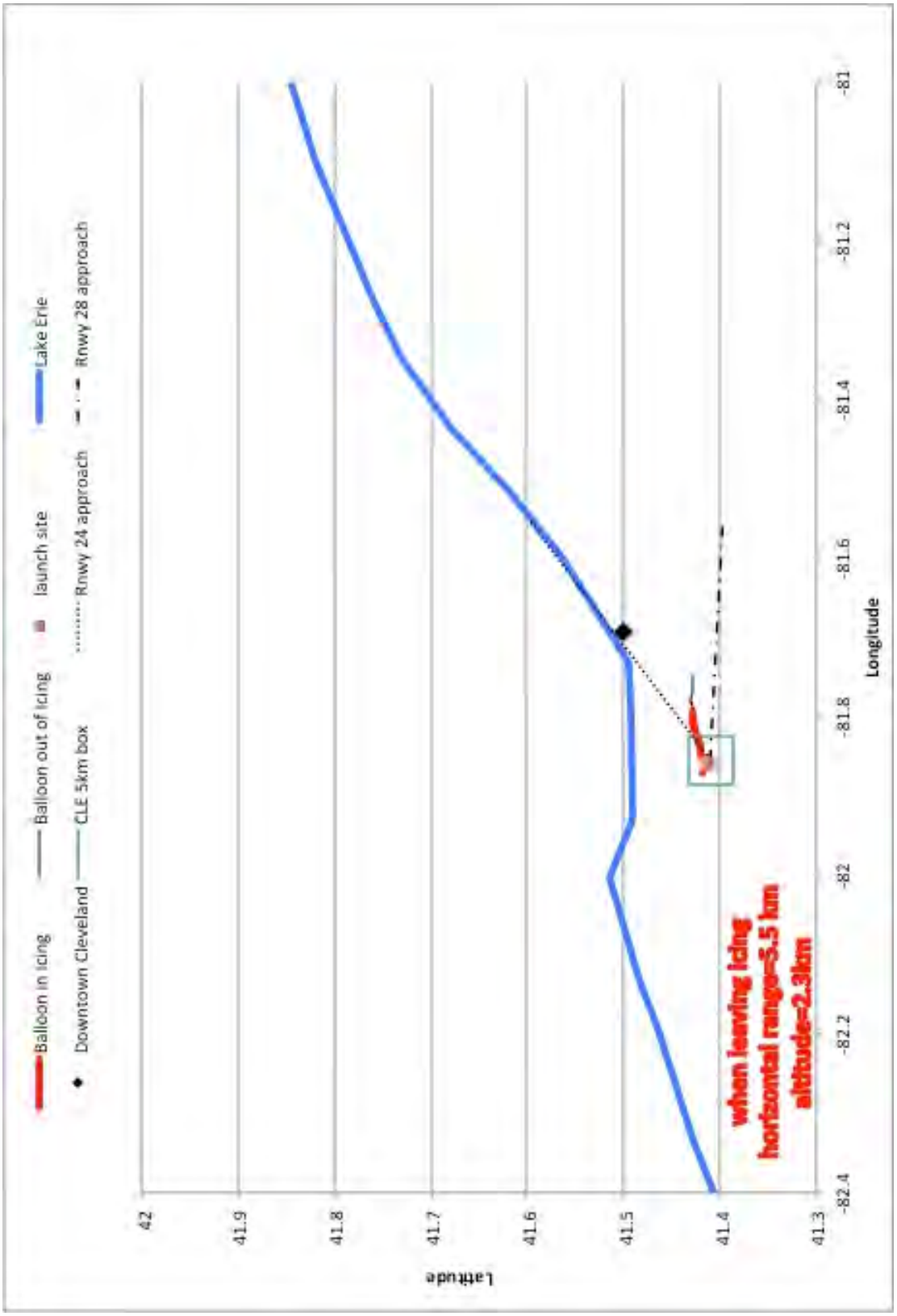

Figure 19.—Map of SLW-sensor trajectory (red) from 13:42 UTC on February 4, 2015.

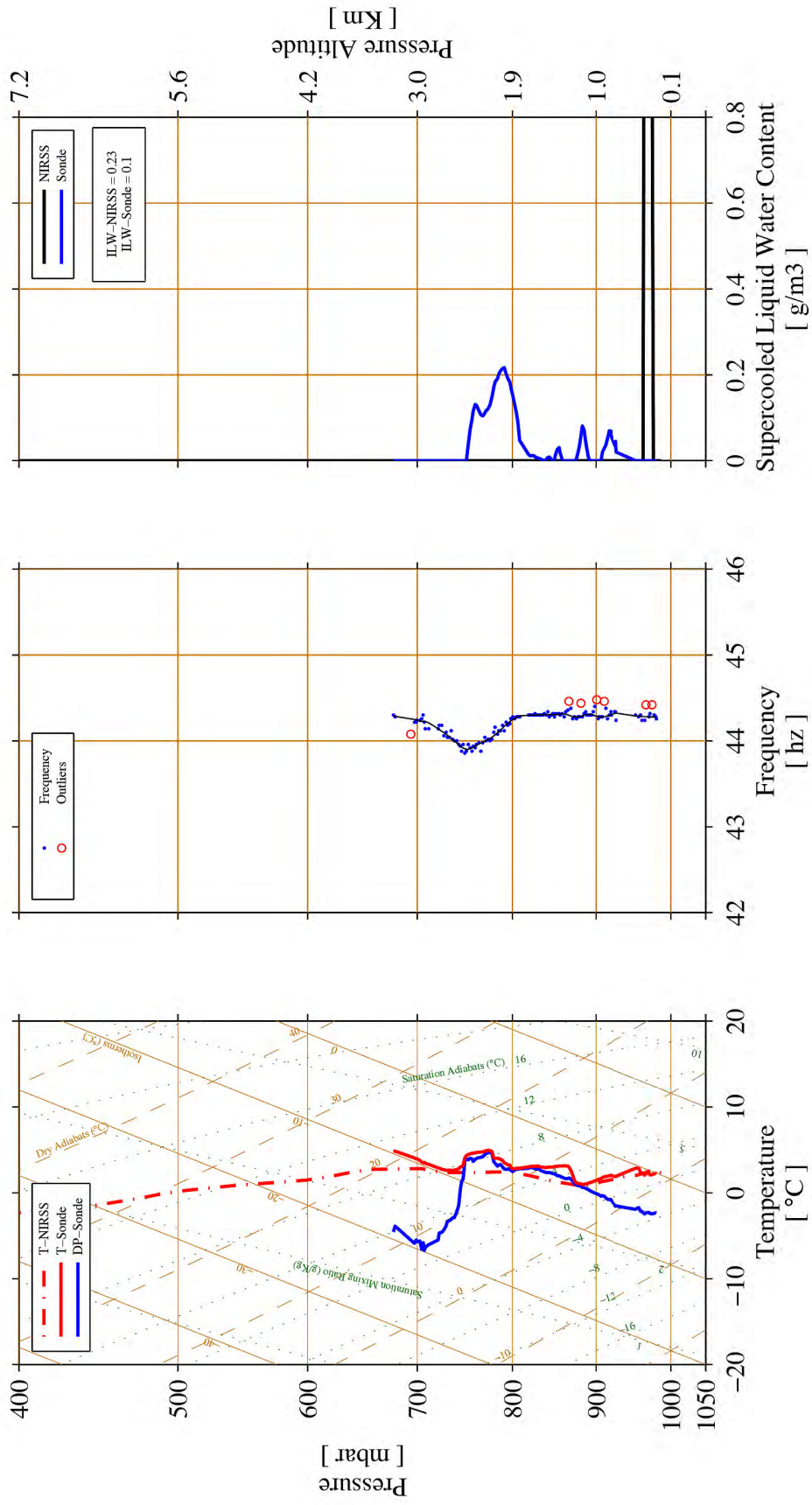

Figure 20.—Skew-T log P profile of SLW-sensor temperature (left, red line) and dewpoint temperature (left, blue line), SLW-sensor wire frequency (center, black line) and SLW-sensor LWC (right, blue line) with NIRSS LWC (right, black line) from 13:42 UTC on February 4, 2015.

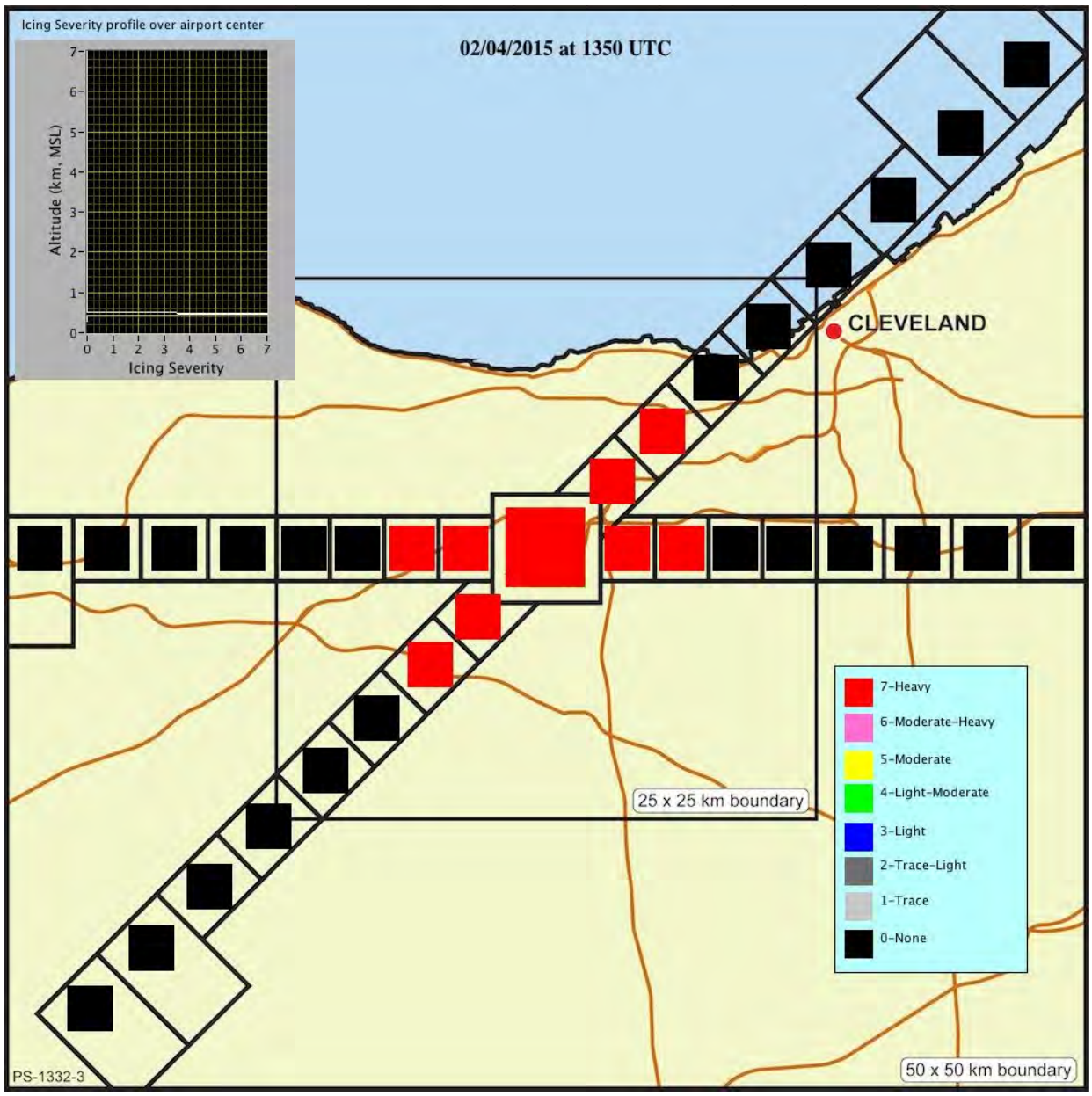

Figure 21.—NIRSS terminal area qualitative in-flight icing hazard classification from 13:50 UTC on February 4, 2015.

Figure 22.—Map of SLW-sensor trajectory (red) from 17:07 UTC on February 4, 2015.

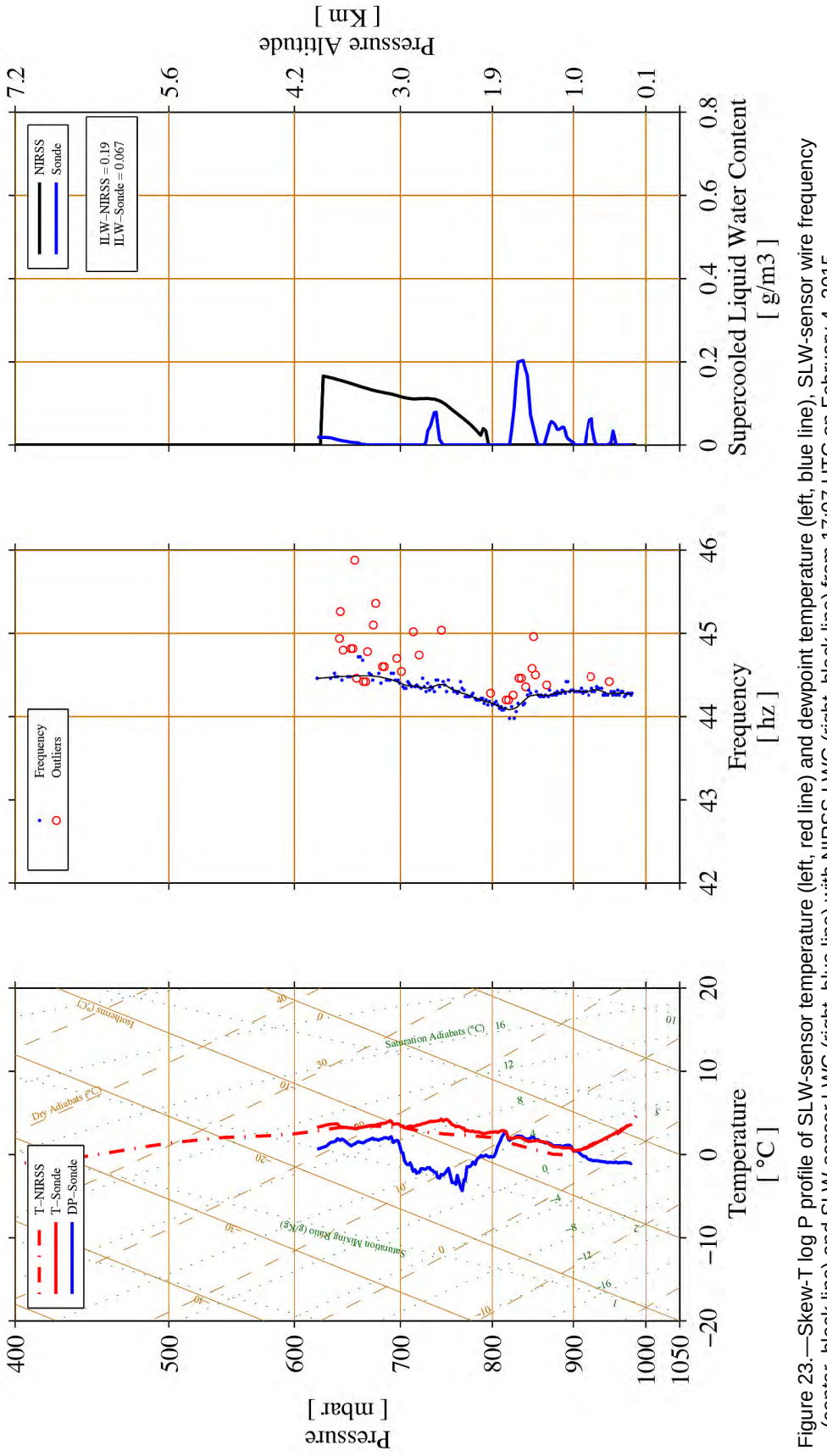

Figure 23.—Skew-T log P profile of SLW-sensor temperature (left, red line) and dewpoint temperature (left, blue line), SLW-sensor wire frequency (center, black line) and SLW-sensor LWC (right, blue line) with NIRSS LWC (right, black line) from 17:07 UTC on February 4, 2015.

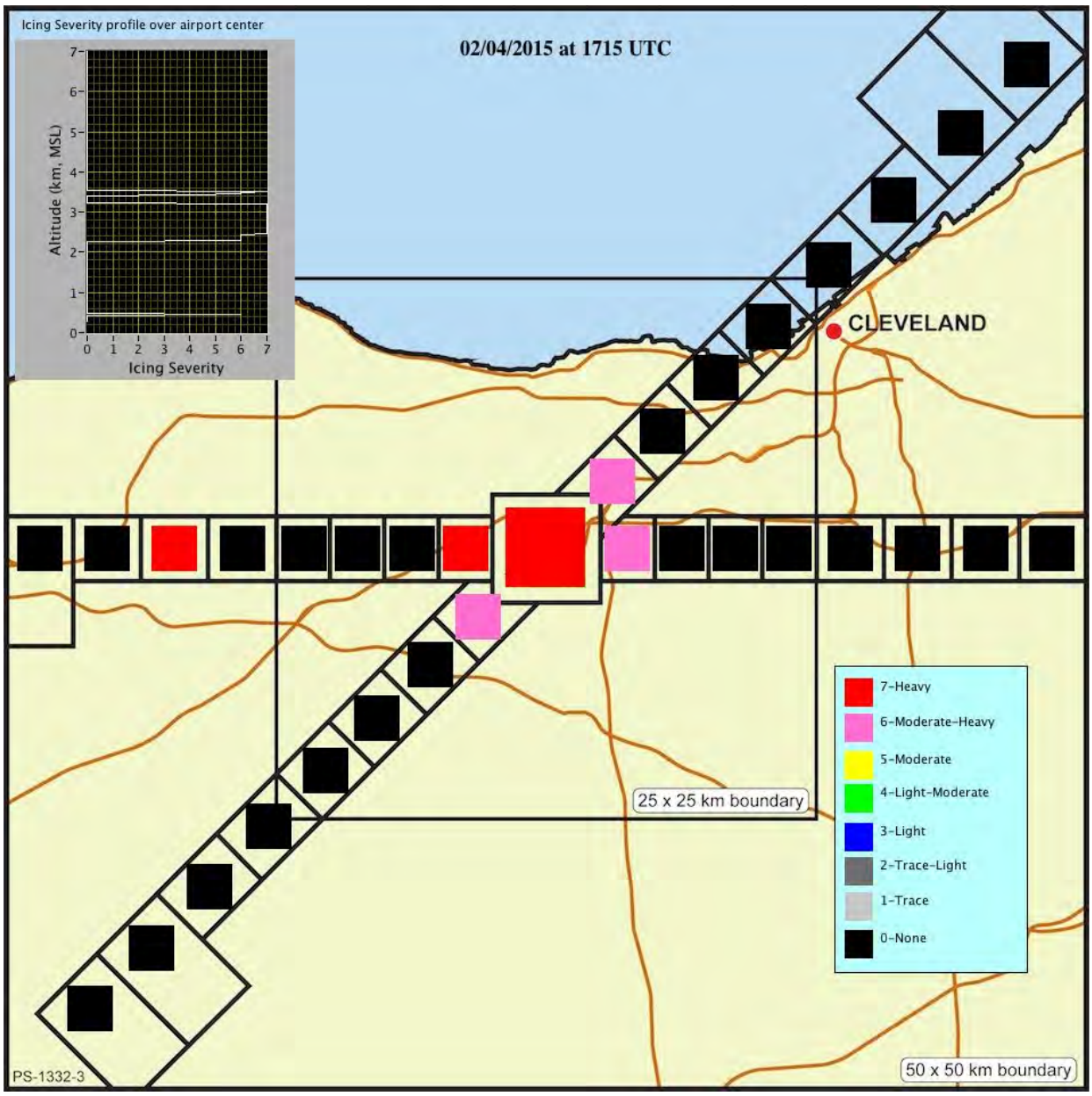

Figure 24.—NIRSS terminal area qualitative in-flight icing hazard classification from 17:15 UTC on February 4, 2015.

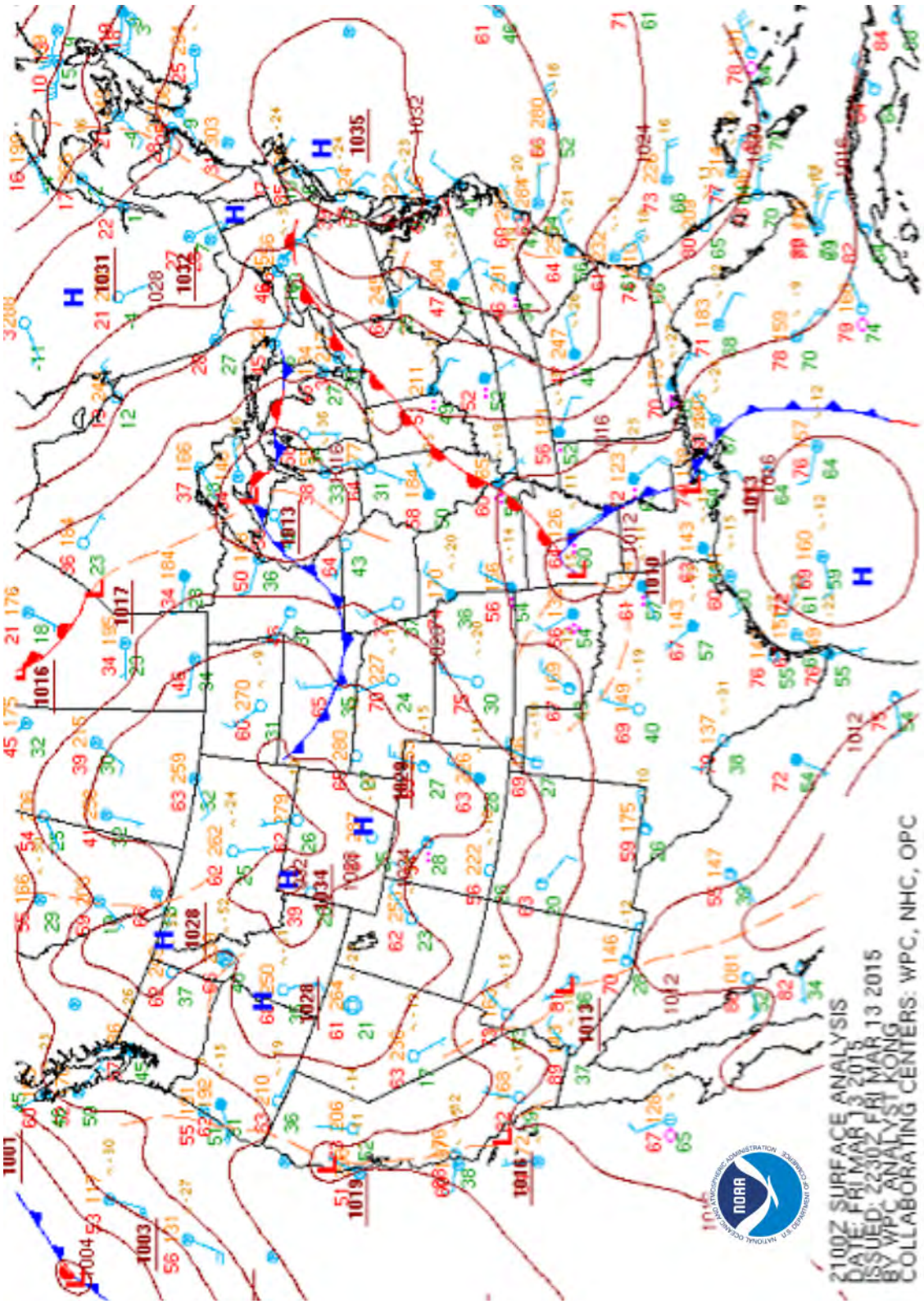

Figure 25.—Surface analysis chart from 21:00 UTC on February 11, 2015.

Figure 26.—Map of SLW-sensor trajectory (red) from 20:00 UTC on February 11, 2015.

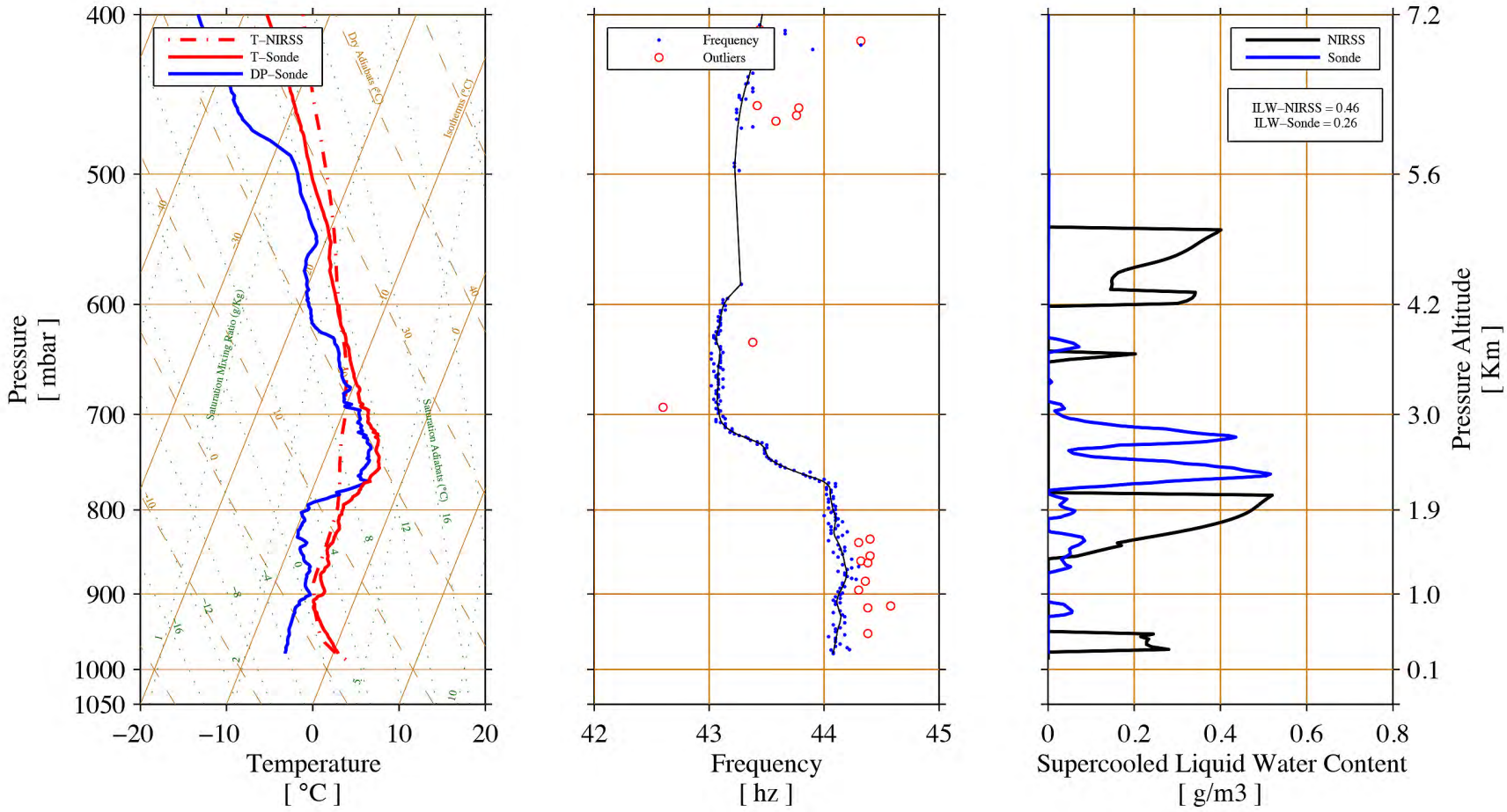

Figure 27.—Skew-T log P profile of SLW-sensor temperature (left, red line) and dewpoint temperature (left, blue line), SLW-sensor wire frequency (center, black line) and SLW-sensor LWC (right, blue line) with NIRSS LWC (right, black line) from 20:00 UTC on February 11, 2015.

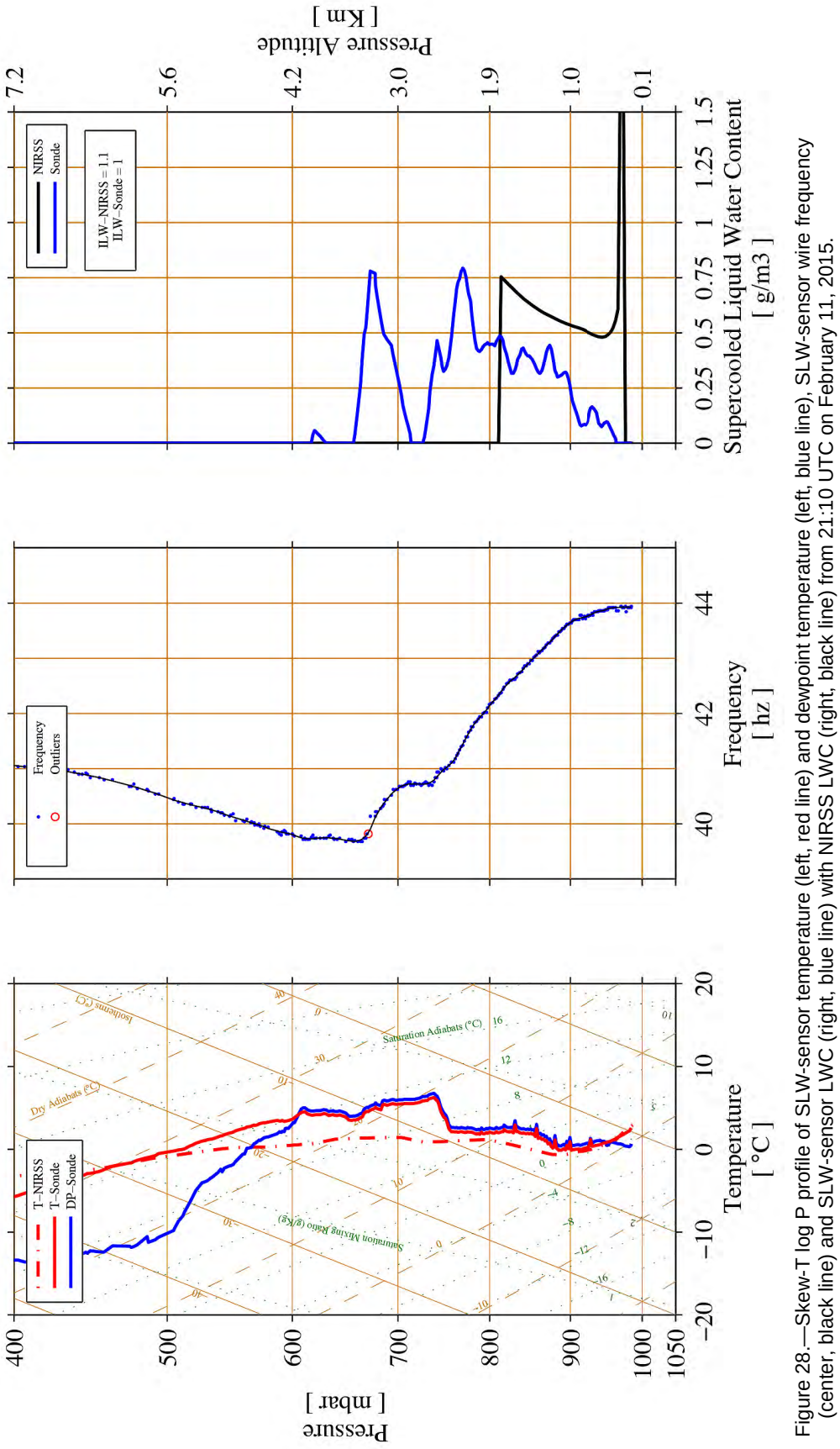

Figure 28.—Skew-T log P profile of SLW-sensor temperature (left, red line) and dewpoint temperature (left, blue line), SLW-sensor wire frequency (center, black line) and SLW-sensor LWC (right, blue line) with NIRSS LWC (right, black line) from 21:10 UTC on February 11, 2015.

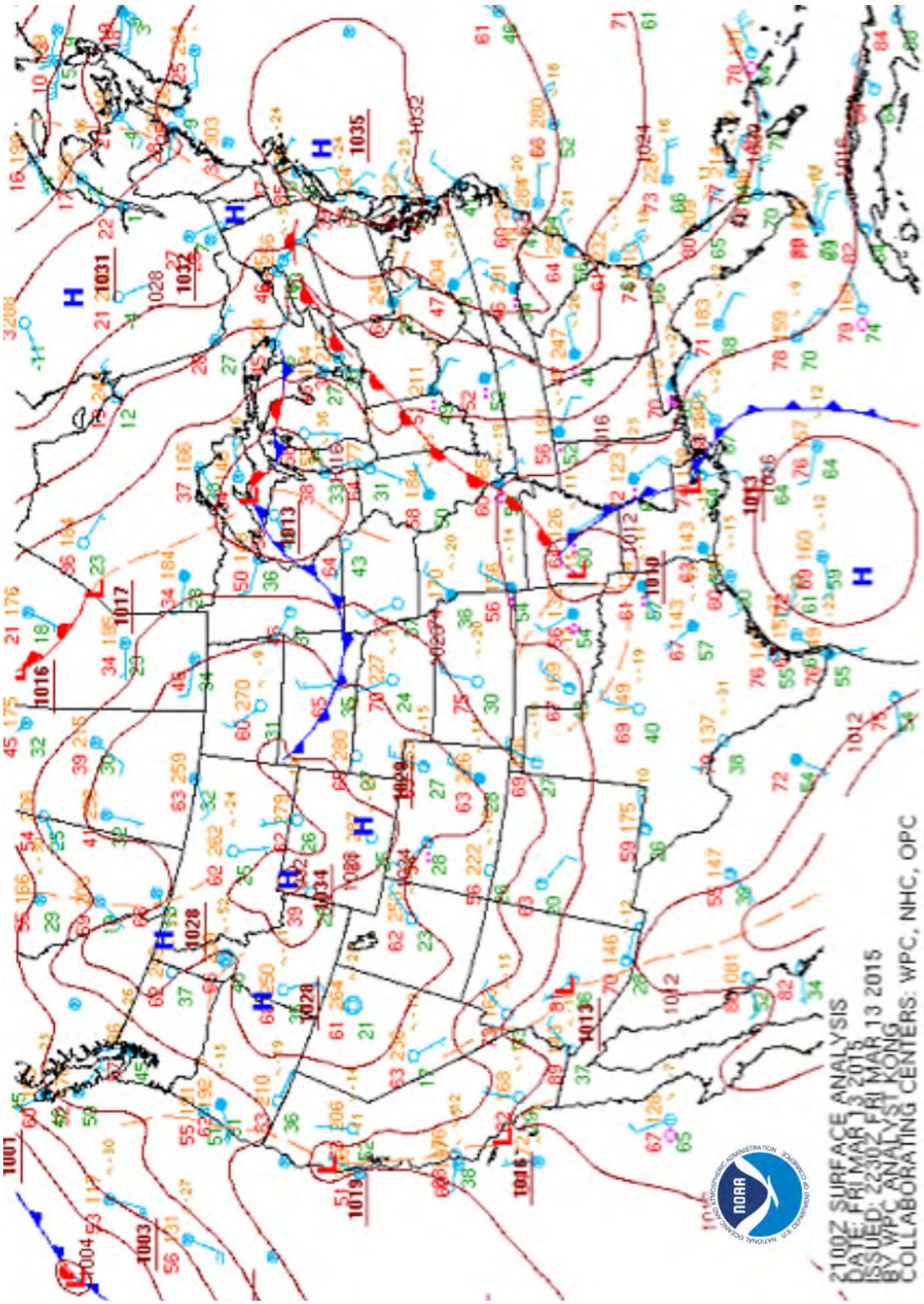

Figure 29.—Surface analysis chart from 21:00 UTC on March 13, 2015.

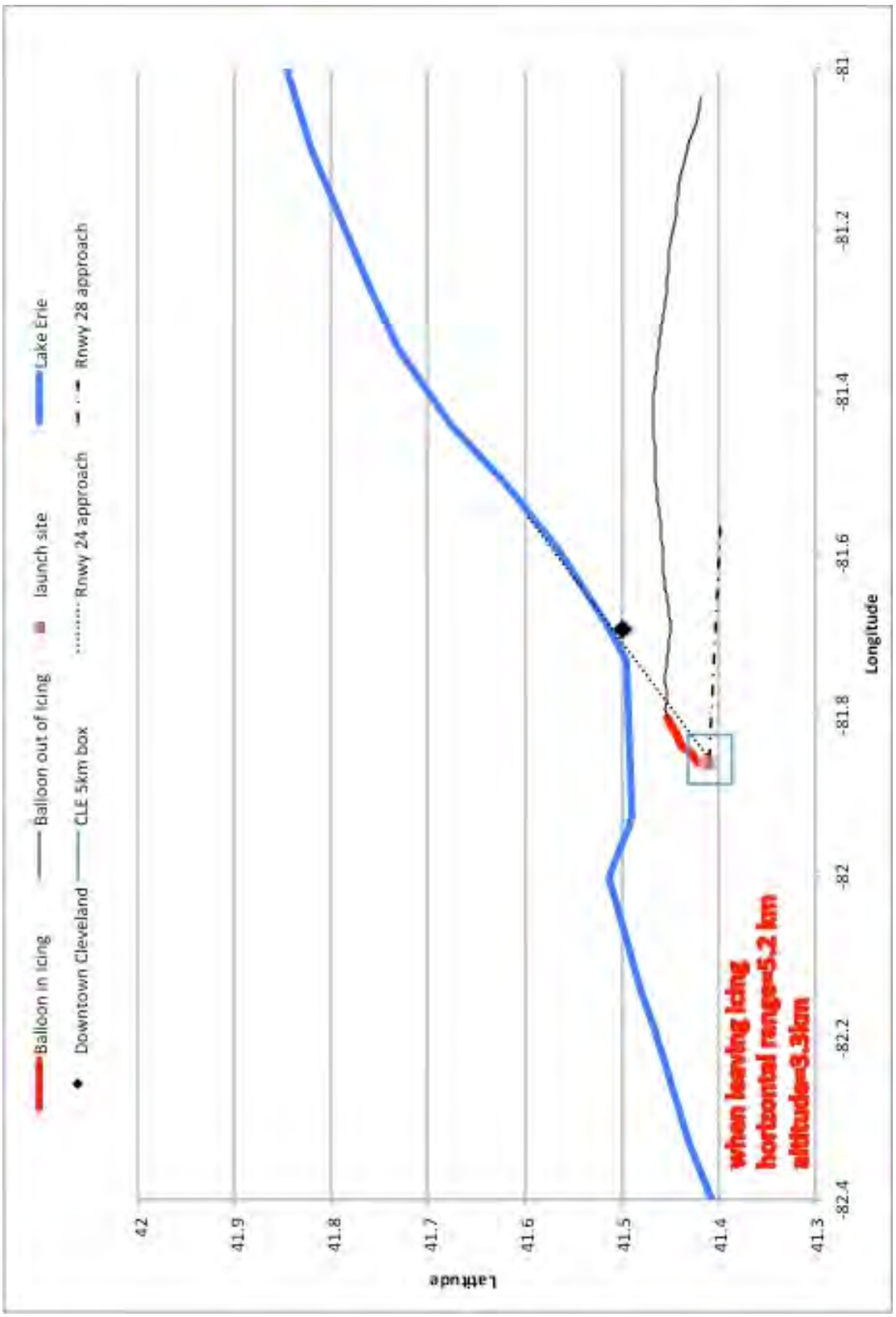

Figure 30.—Map of SLW-sensor trajectory (red) from 20:43 UTC on March 13, 2015.

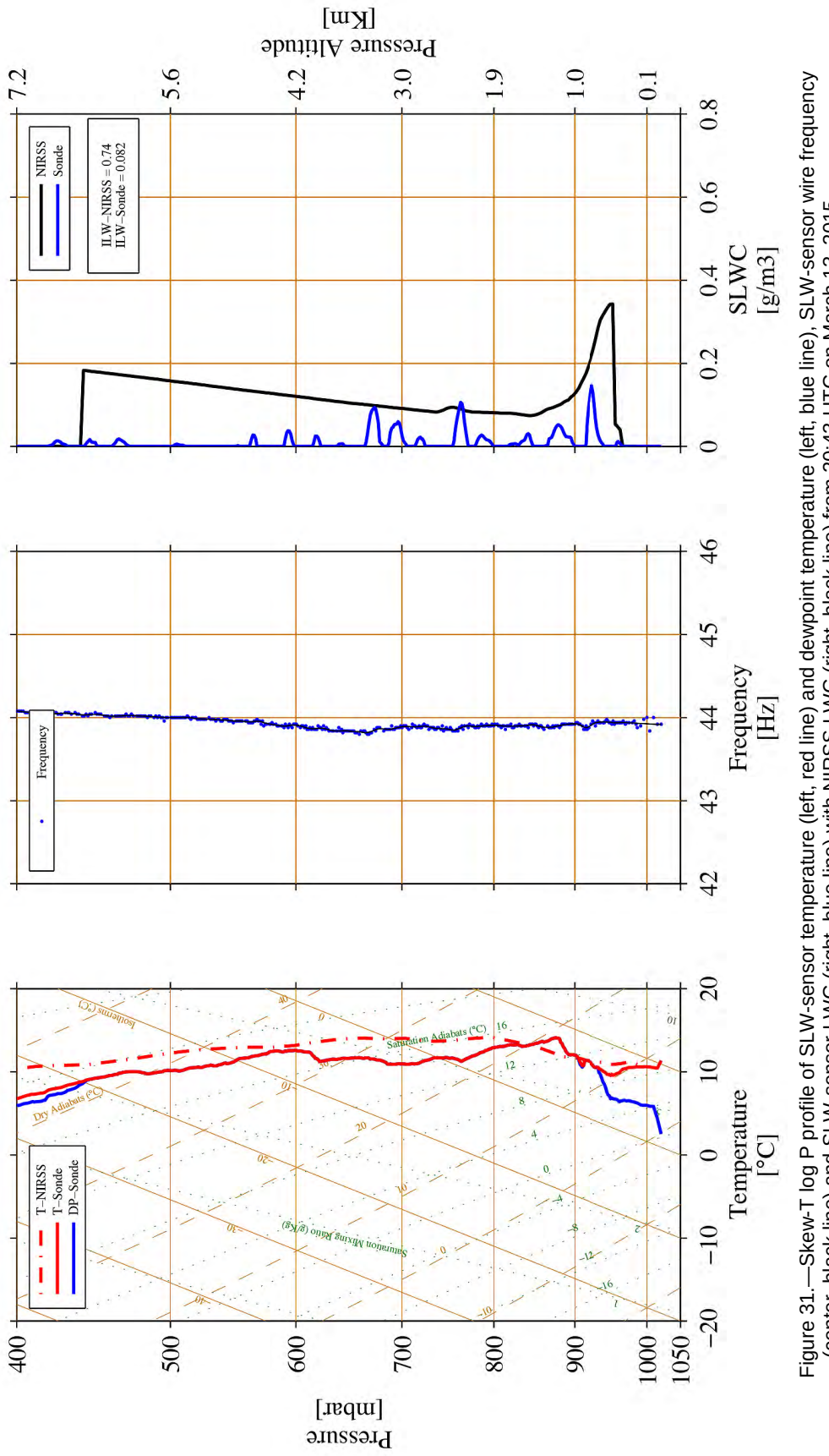

Figure 31.—Skew-T log P profile of SLW-sensor temperature (left, red line) and dewpoint temperature (left, blue line), SLW-sensor wire frequency (center, black line) and SLW-sensor LWC (right, blue line) with NIRSS LWC (right, black line) from 20:43 UTC on March 13, 2015.

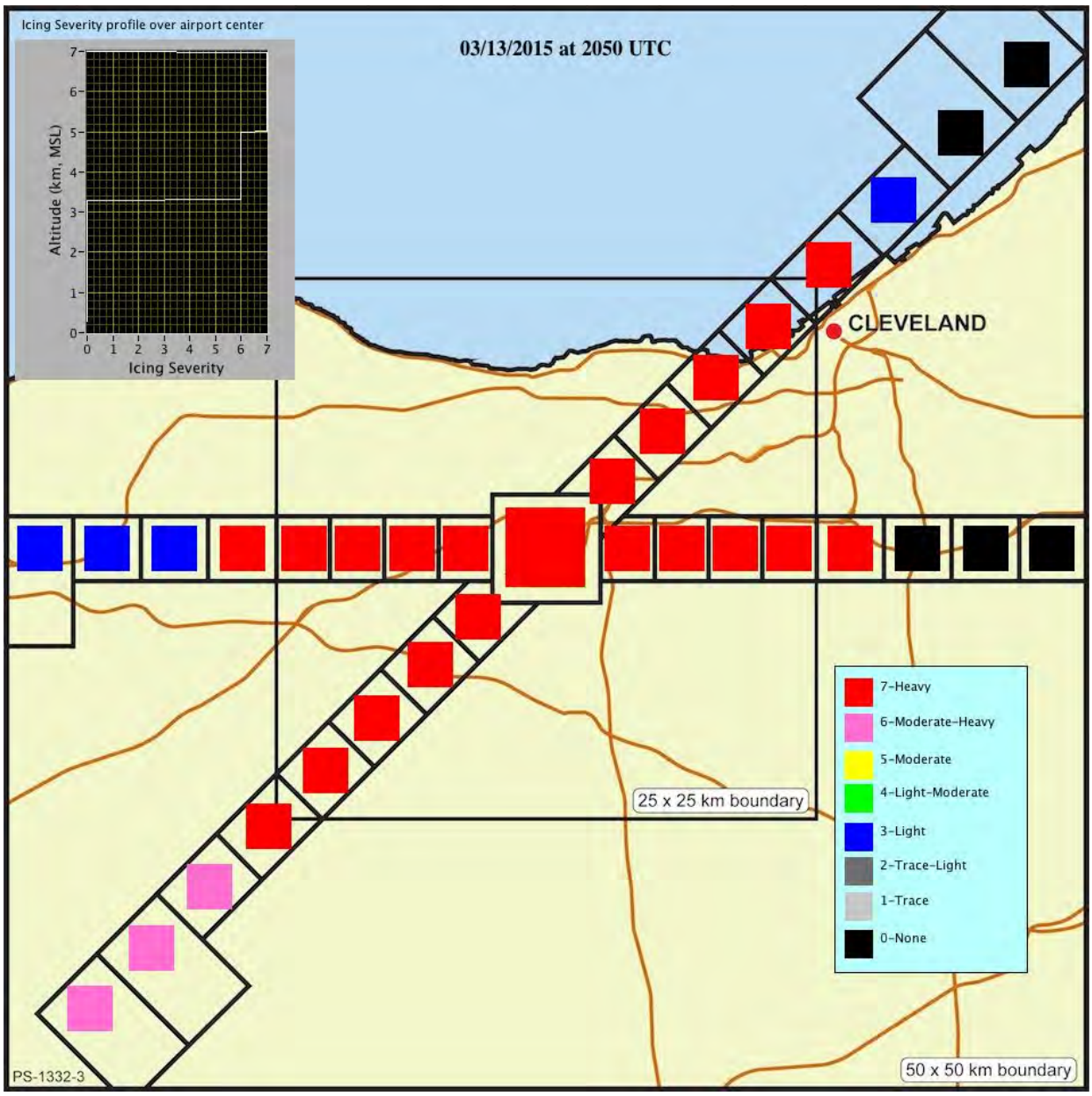

Figure 32.—NIRSS terminal area qualitative in-flight icing hazard classification from 17:15 UTC on March 13, 2015.

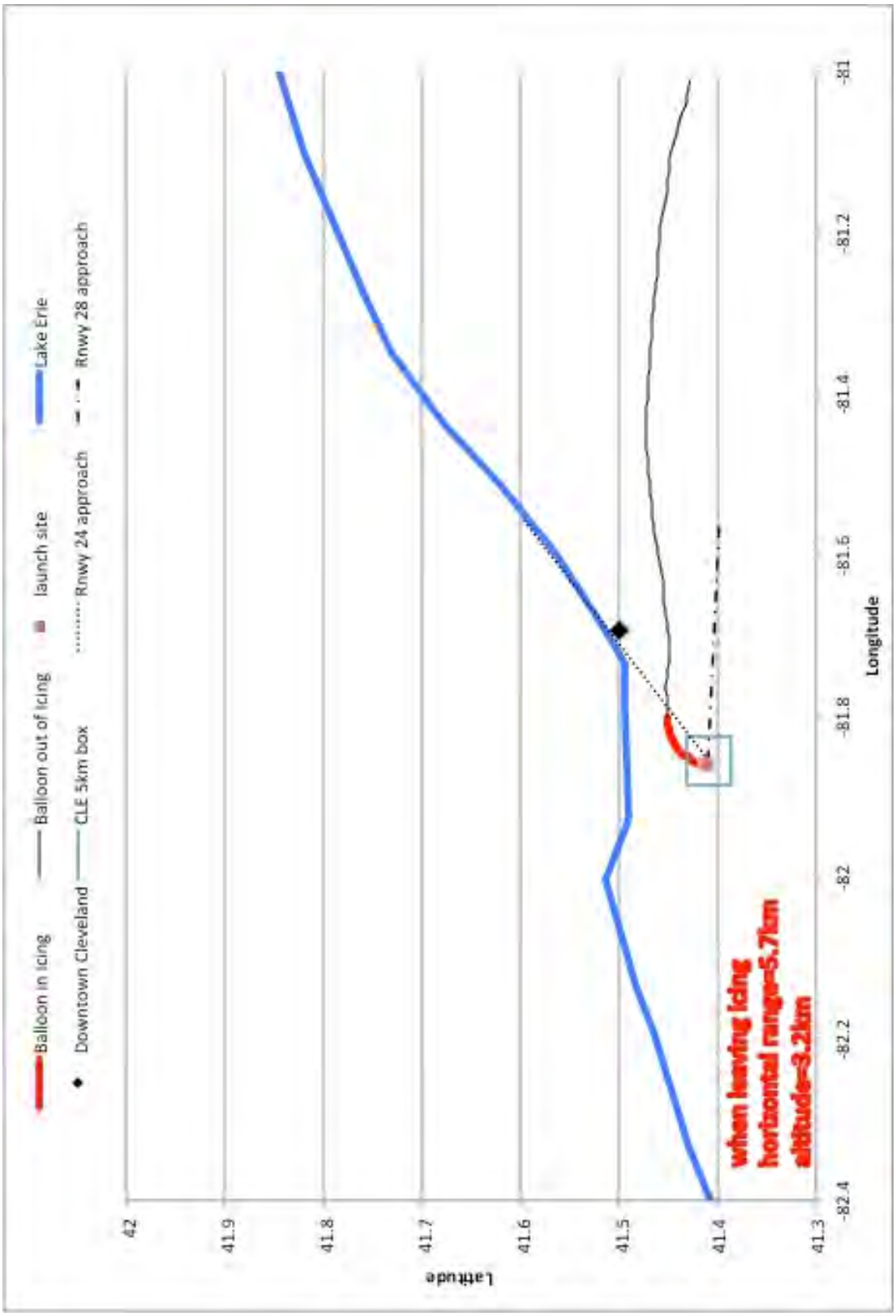

Figure 33.—Map of SLW-sensor trajectory (red) from 21:59 UTC on March 13, 2015.

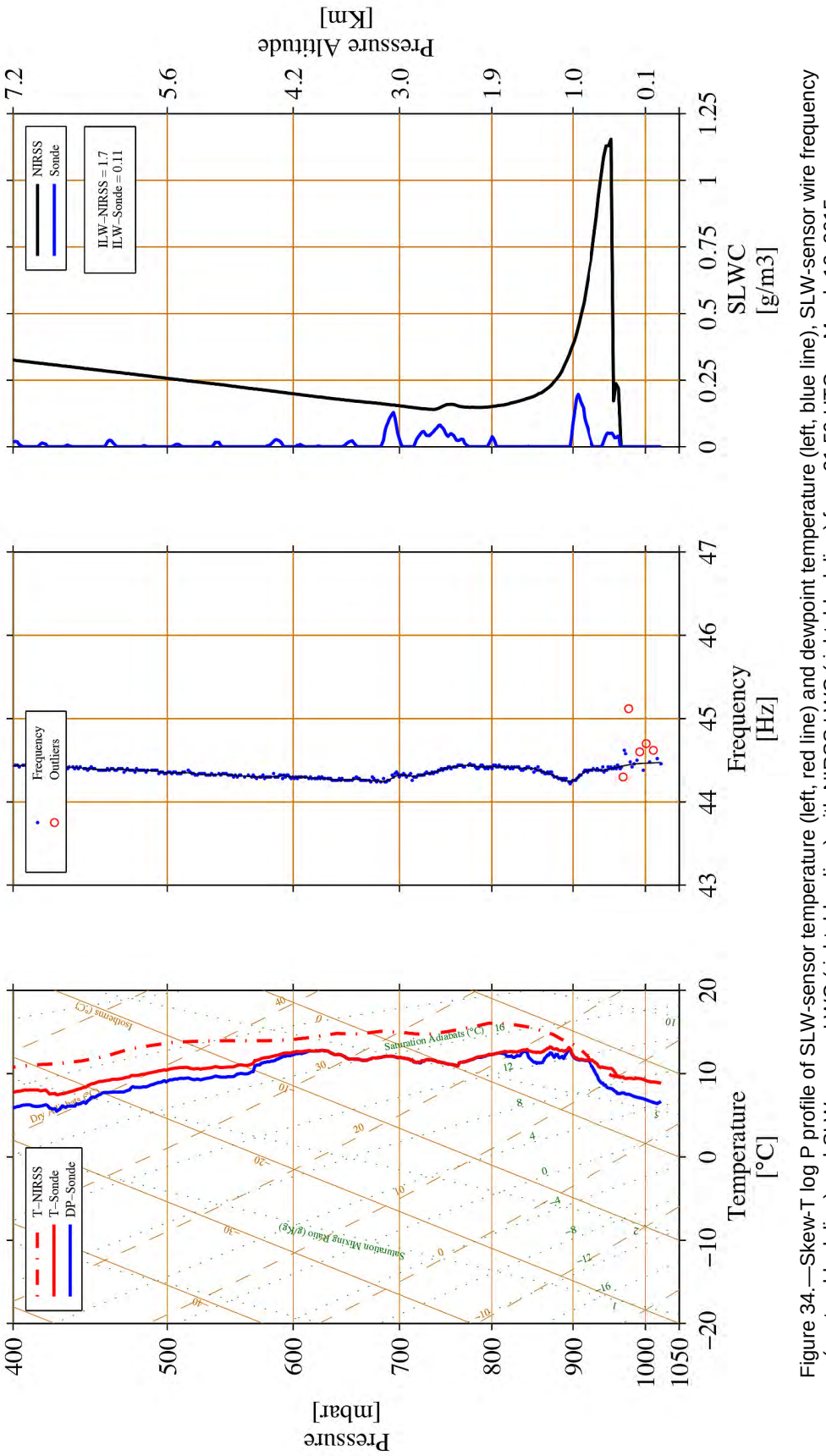

Figure 34.—Skew-T log P profile of SLW-sensor temperature (left, red line) and dewpoint temperature (left, blue line), SLW-sensor wire frequency (center, black line) and SLW-sensor LWC (right, blue line) with NIRSS LWC (right, black line) from 21:59 UTC on March 13, 2015.

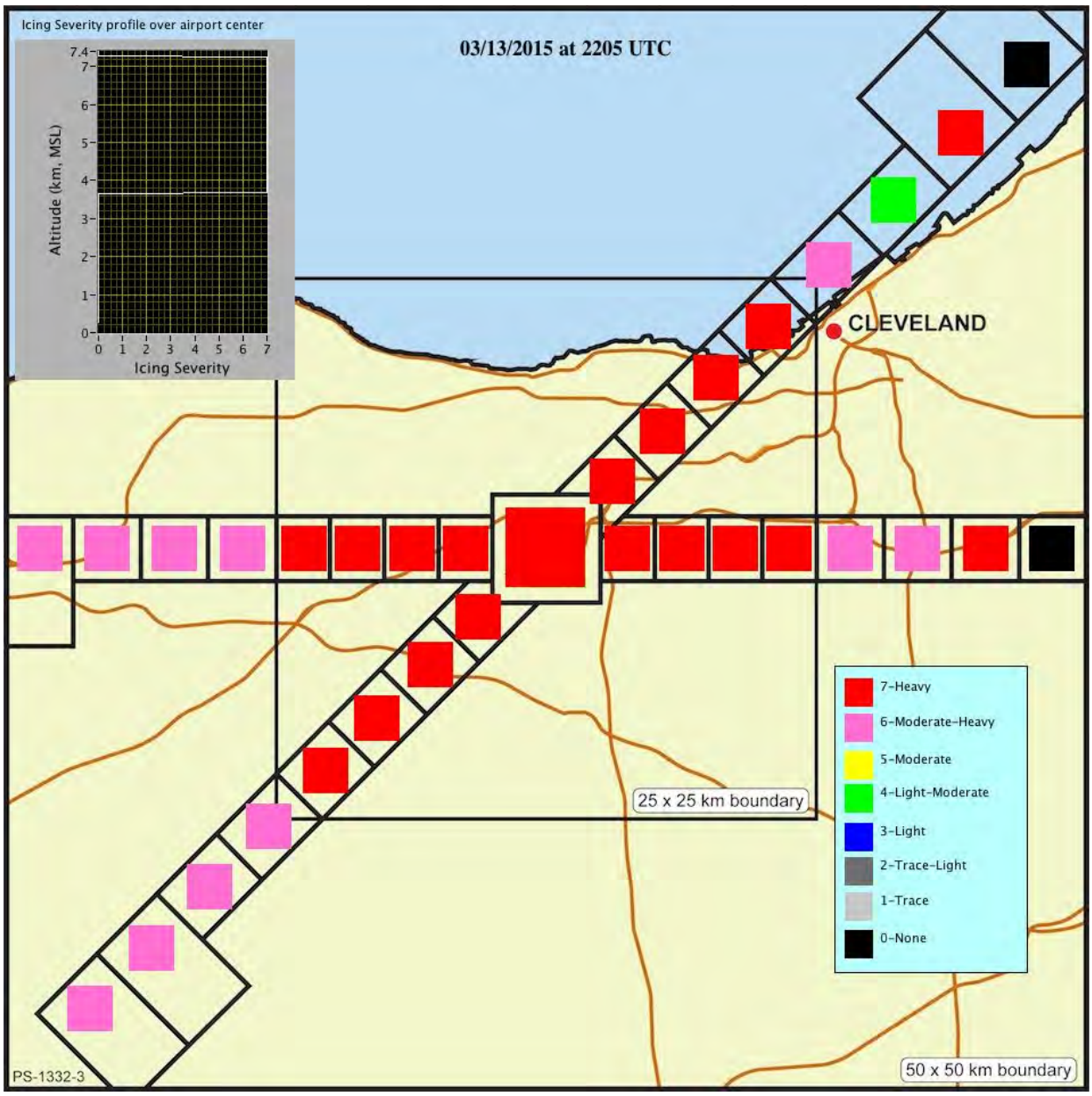

Figure 35.—NIRSS terminal area qualitative in-flight icing hazard classification from 22:05 UTC on March 13, 2015.

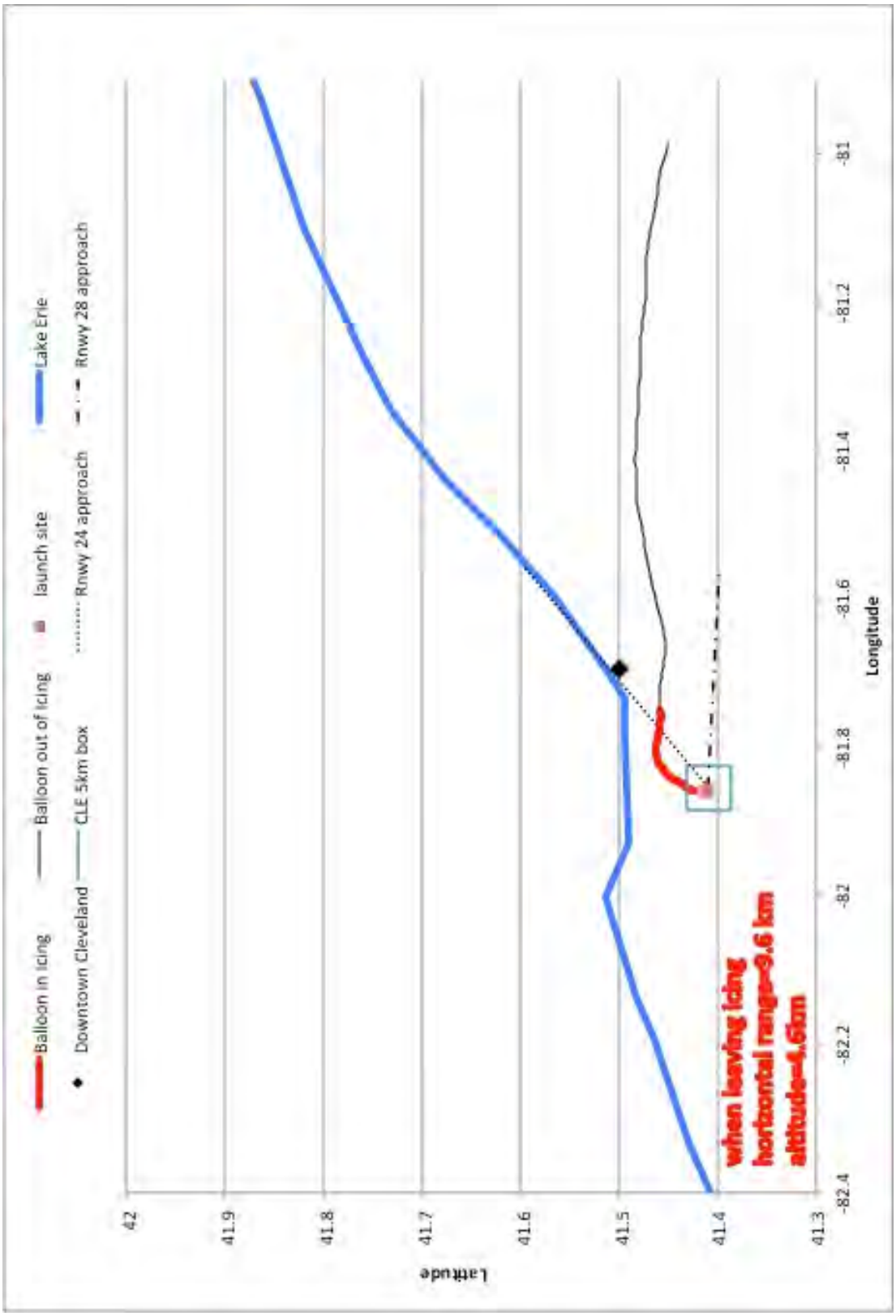

Figure 36.—Map of SLW-sensor trajectory (red) from 23:38 UTC on March 13, 2015.

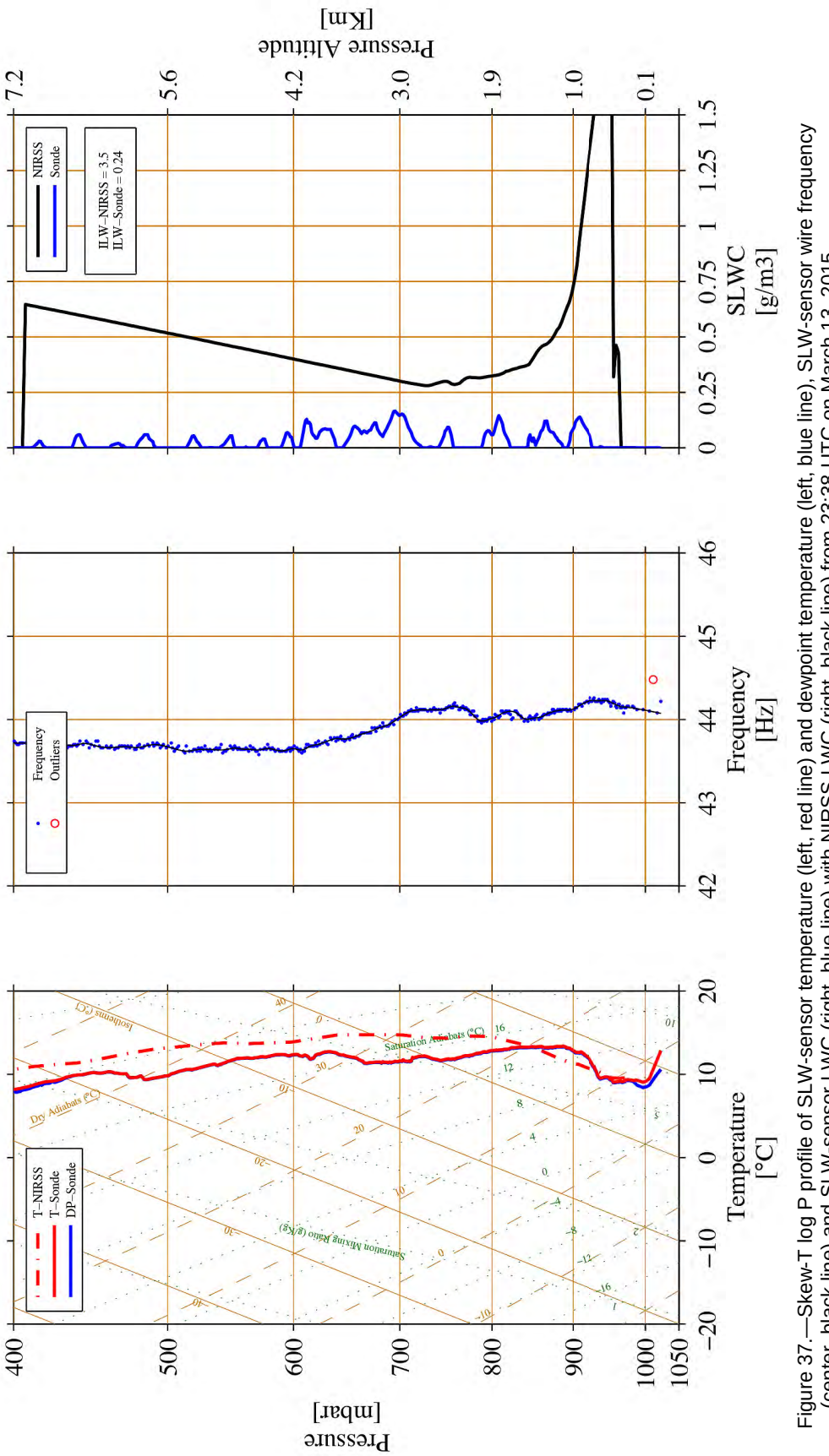

Figure 37.—Skew-T log P profile of SLW-sensor temperature (left, red line) and dewpoint temperature (left, blue line), SLW-sensor wire frequency (center, black line) and SLW-sensor LWC (right, blue line) with NIRSS LWC (right, black line) from 23:38 UTC on March 13, 2015.

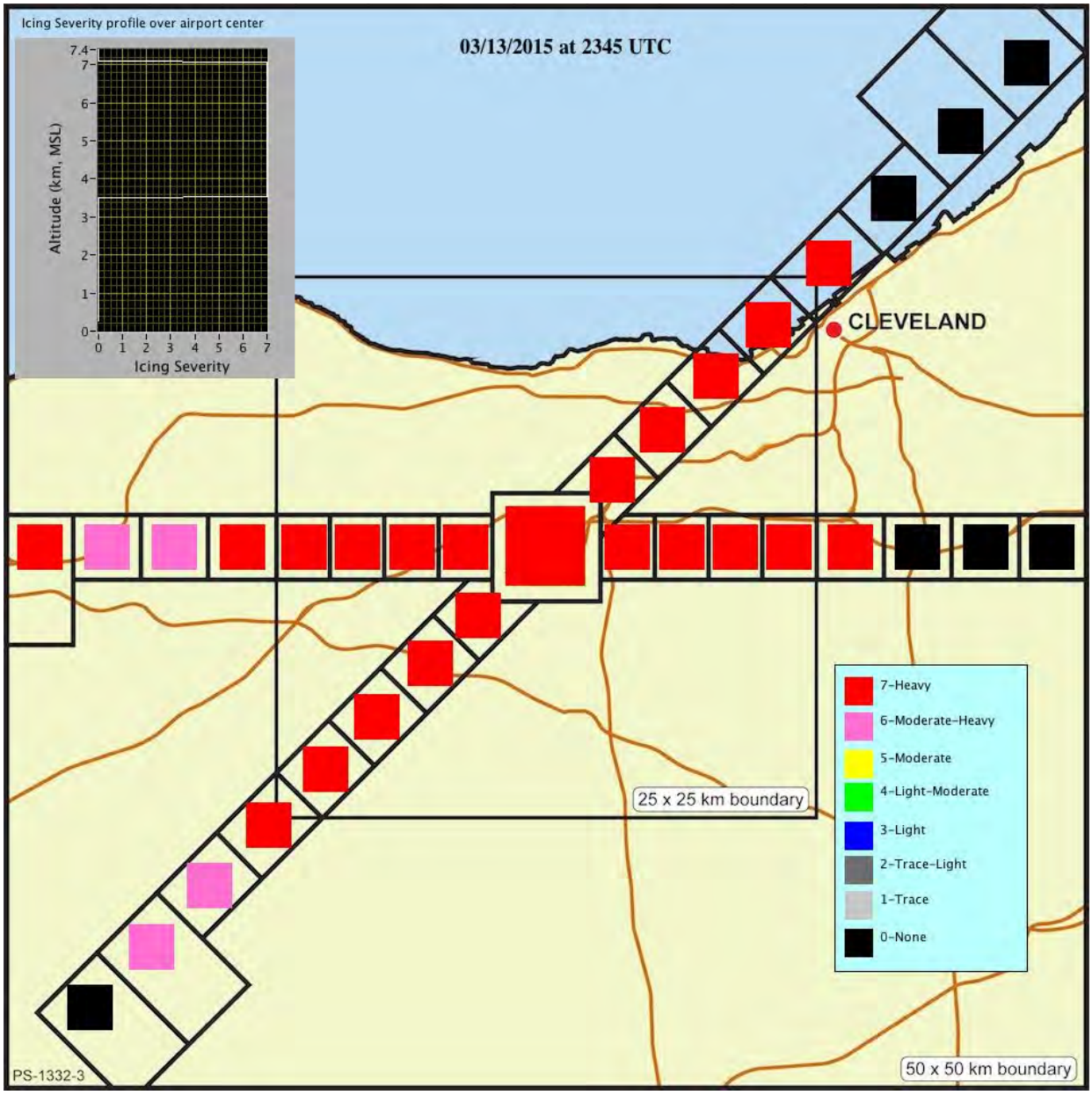

Figure 38.—NIRSS terminal area qualitative in-flight icing hazard classification from 23:45 UTC on March 13, 2015.

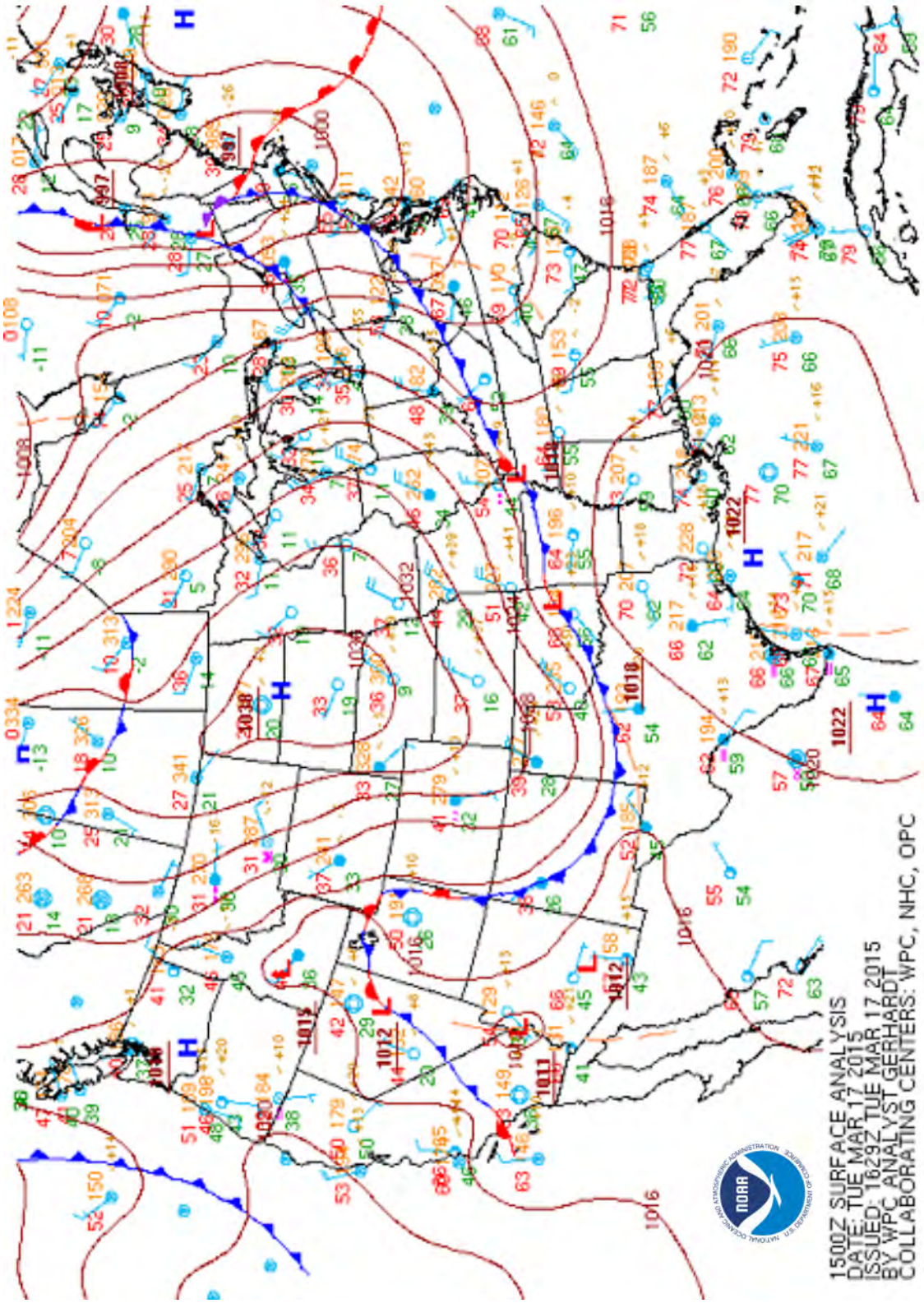

Figure 39.—Surface analysis chart from 15:00 UTC on March 17, 2015.

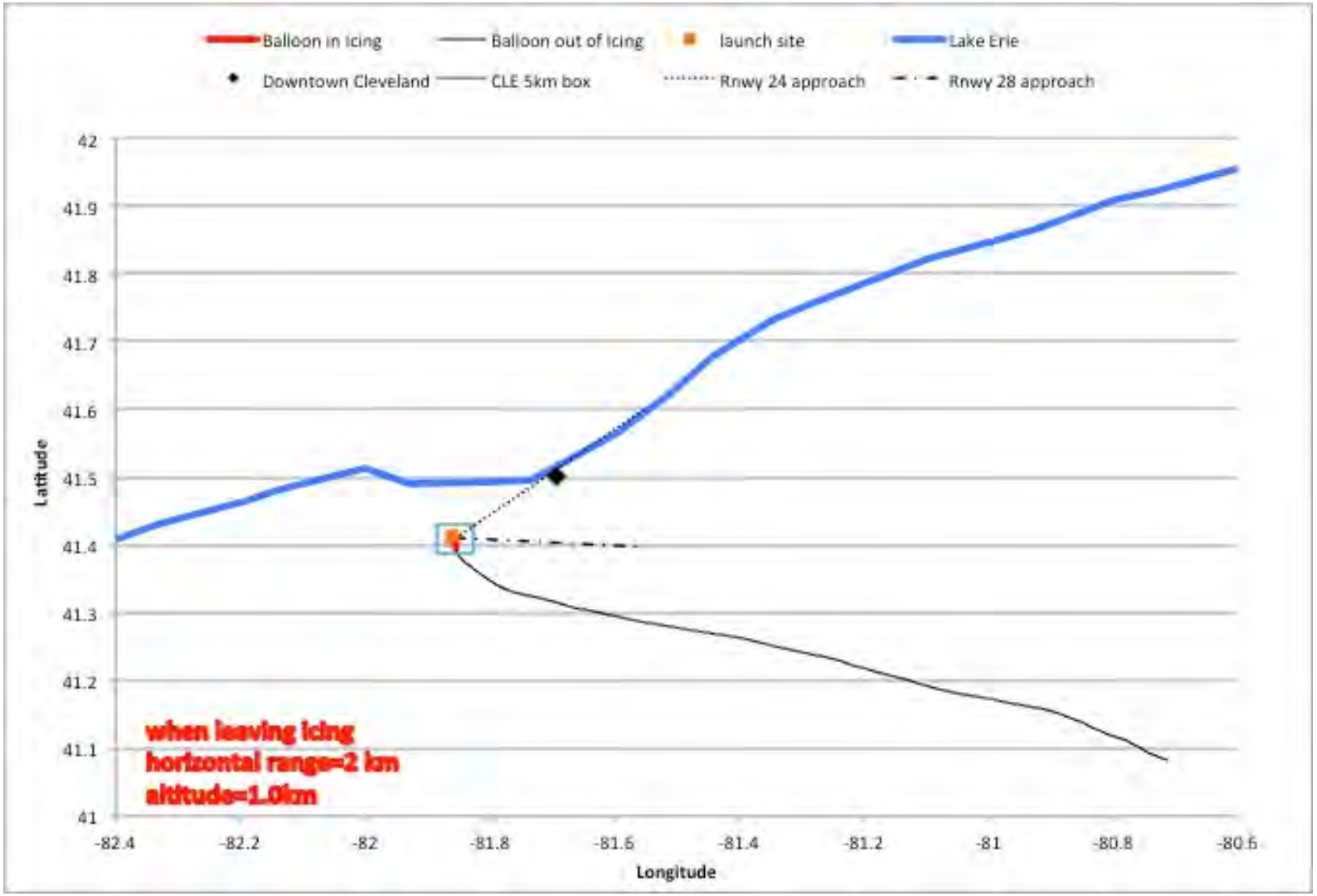

Figure 40.—Map of SLW-sensor trajectory (red) from 13:54 UTC on March 17, 2015.

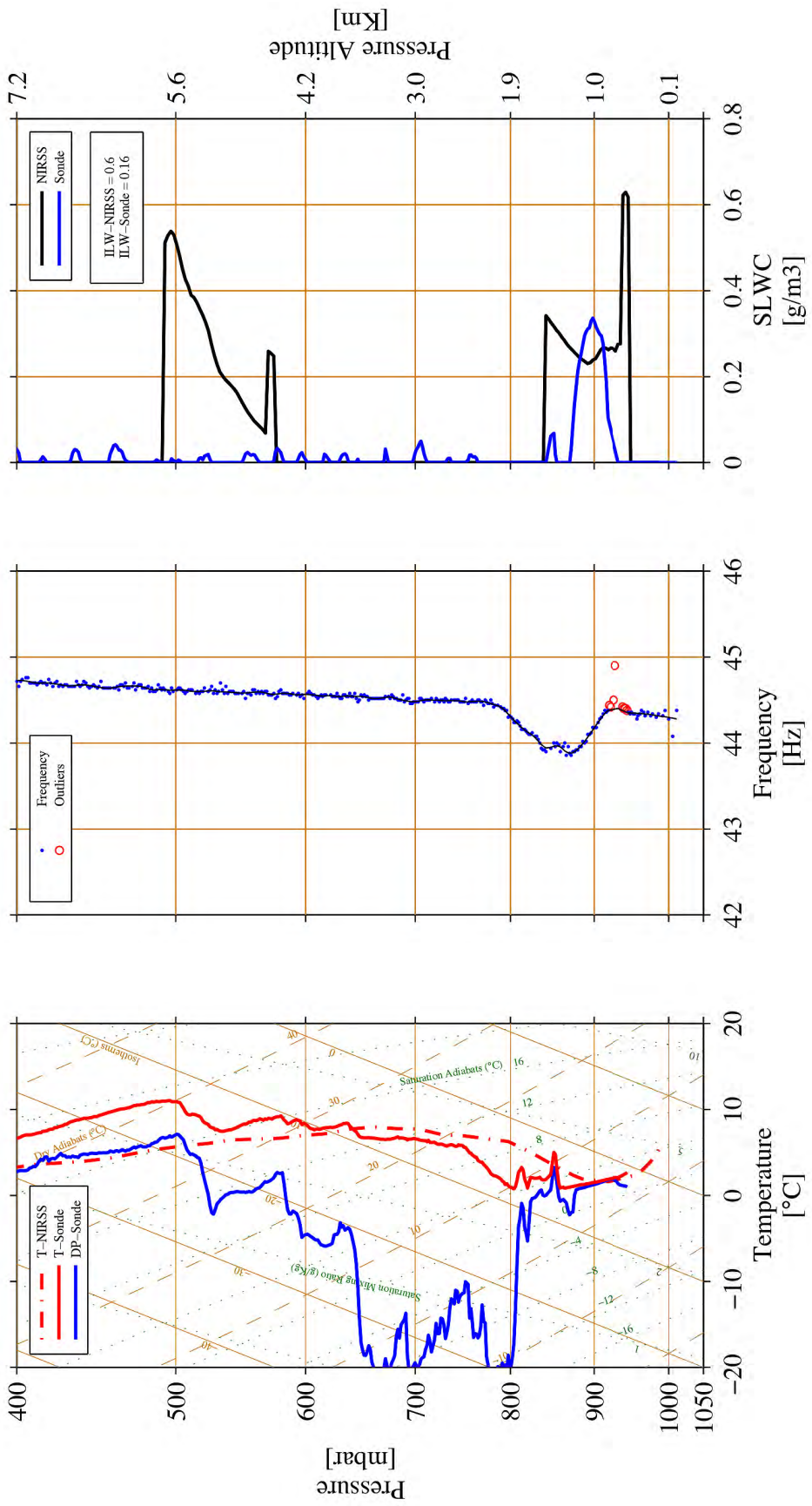

Figure 41.—Skew-T log P profile of SLW-sensor temperature (left, red line) and dewpoint temperature (left, blue line), SLW-sensor wire frequency (center, black line) and SLW-sensor LWC (right, blue line) with NIRSS LWC (right, black line) from 13:54 UTC on March 17, 2015.

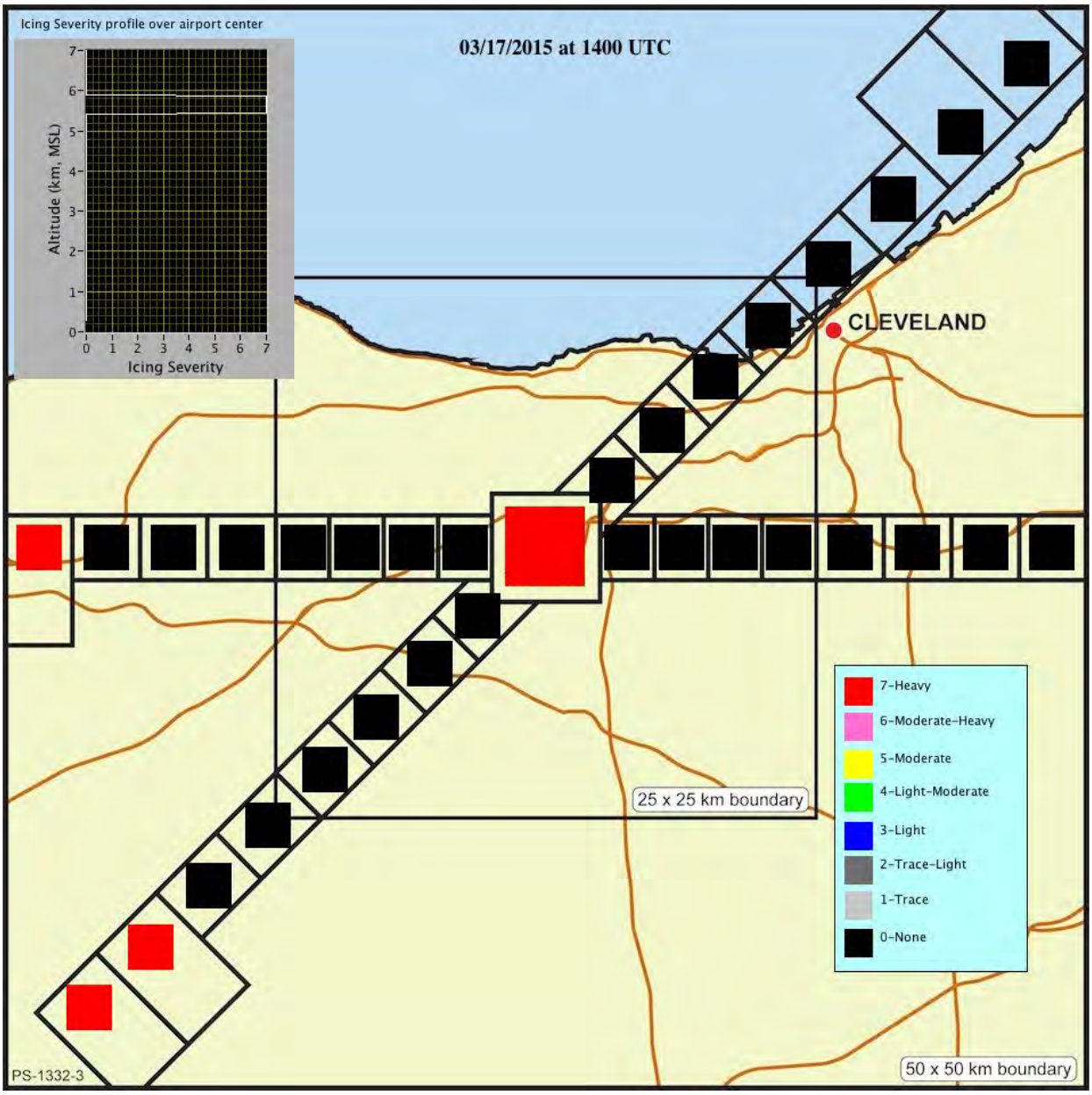

Figure 42.—NIRSS terminal area qualitative in-flight icing hazard classification from 14:00 UTC on March 17, 2015.

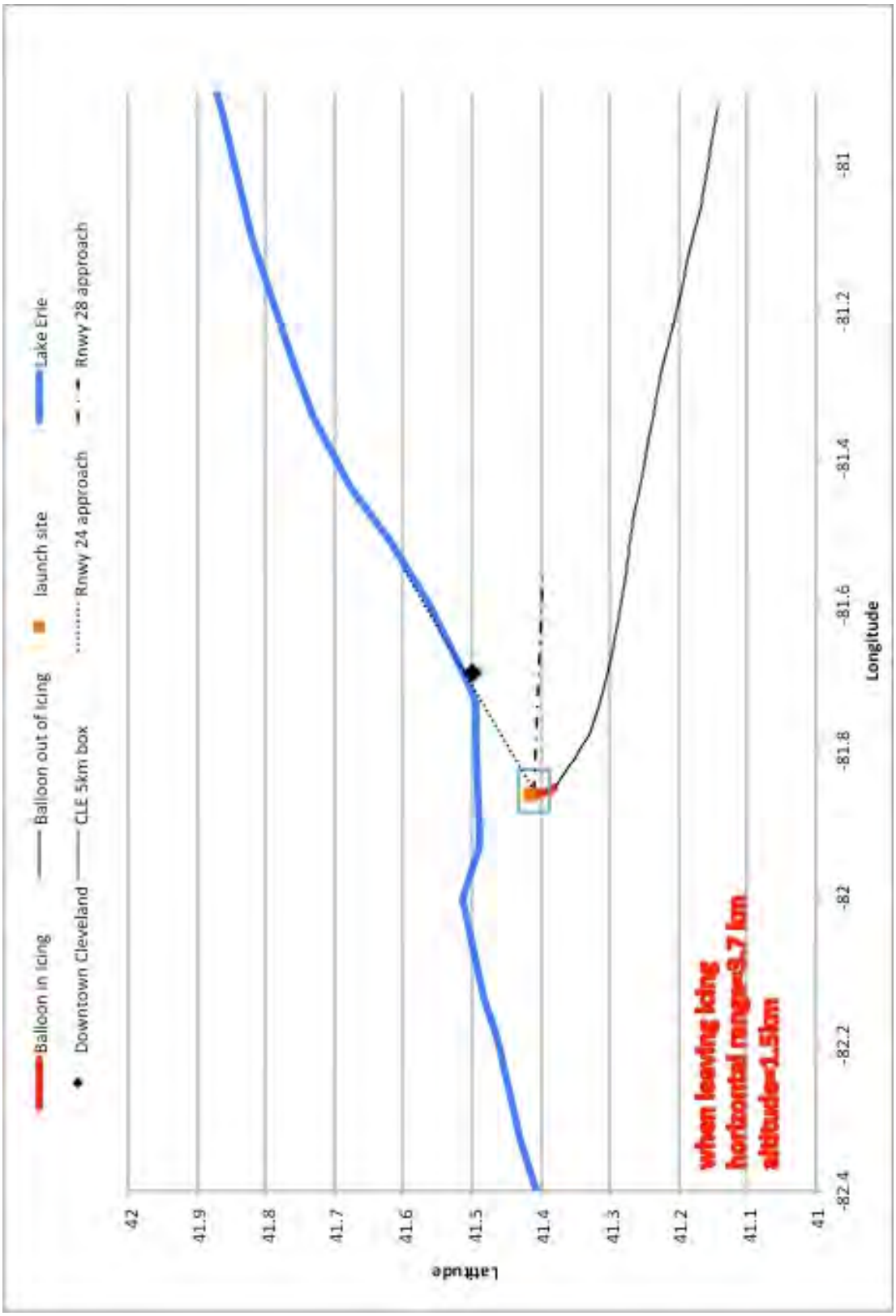

Figure 43.—Map of SLW-sensor trajectory (red) from 14:47 UTC on March 17, 2015.

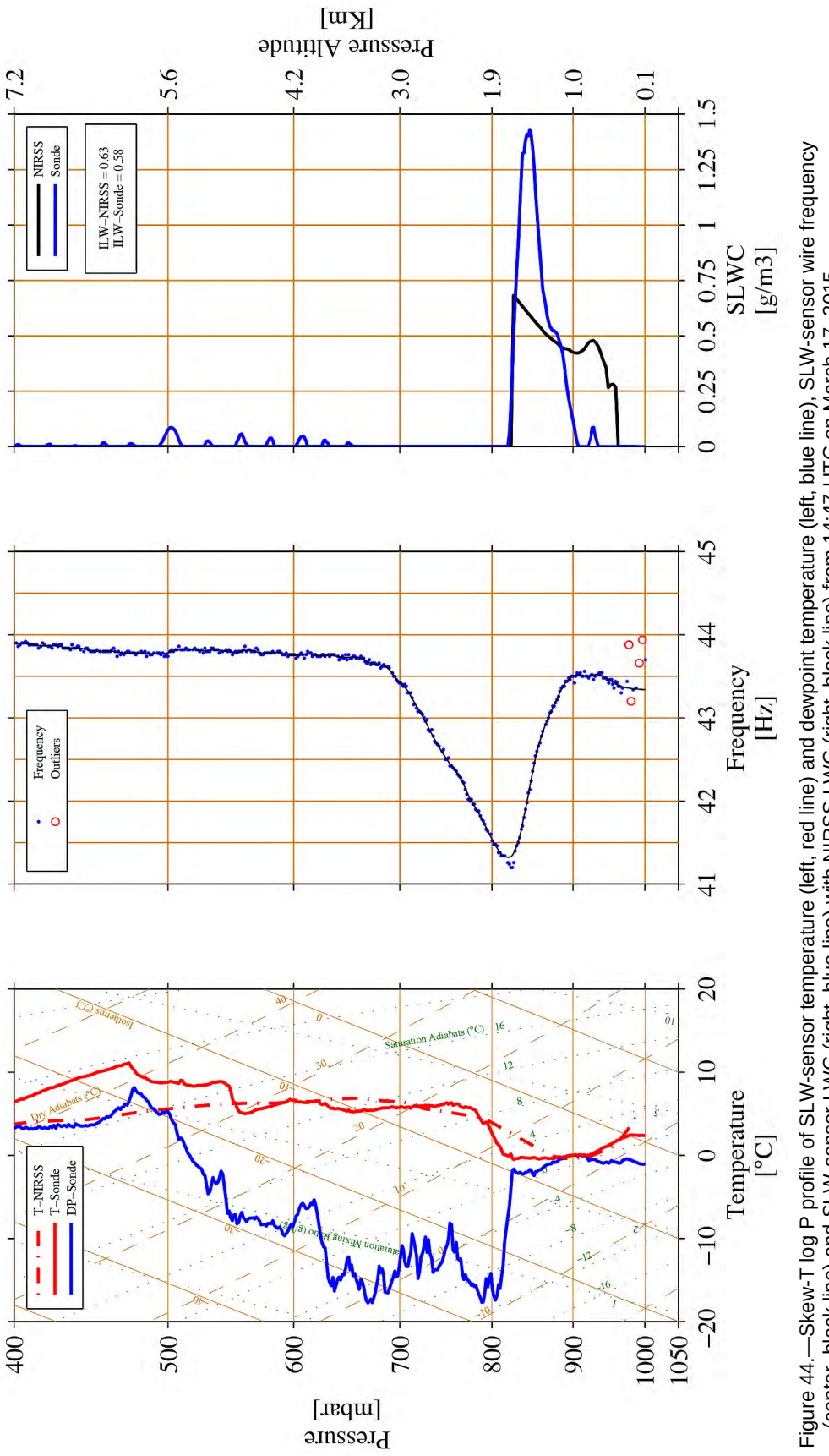

Figure 44.—Skew-T log P profile of SLW-sensor temperature (left, red line) and dewpoint temperature (left, blue line), SLW-sensor wire frequency (center, black line) and SLW-sensor LWC (right, blue line) with NIRSS LWC (right, black line) from 14:47 UTC on March 17, 2015.

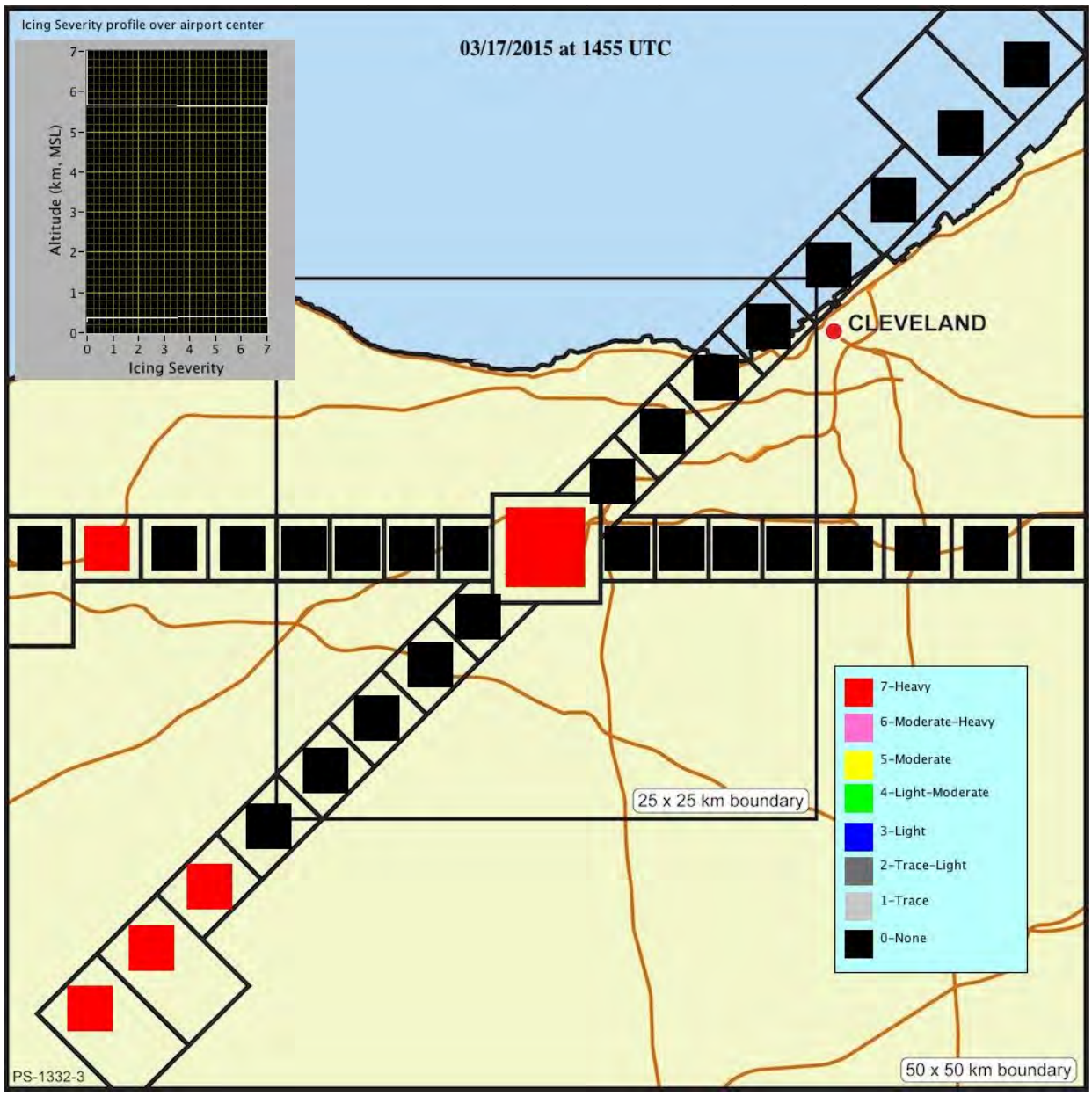

Figure 45.—NIRSS terminal area qualitative in-flight icing hazard classification from 14:55 UTC on March 17, 2015.

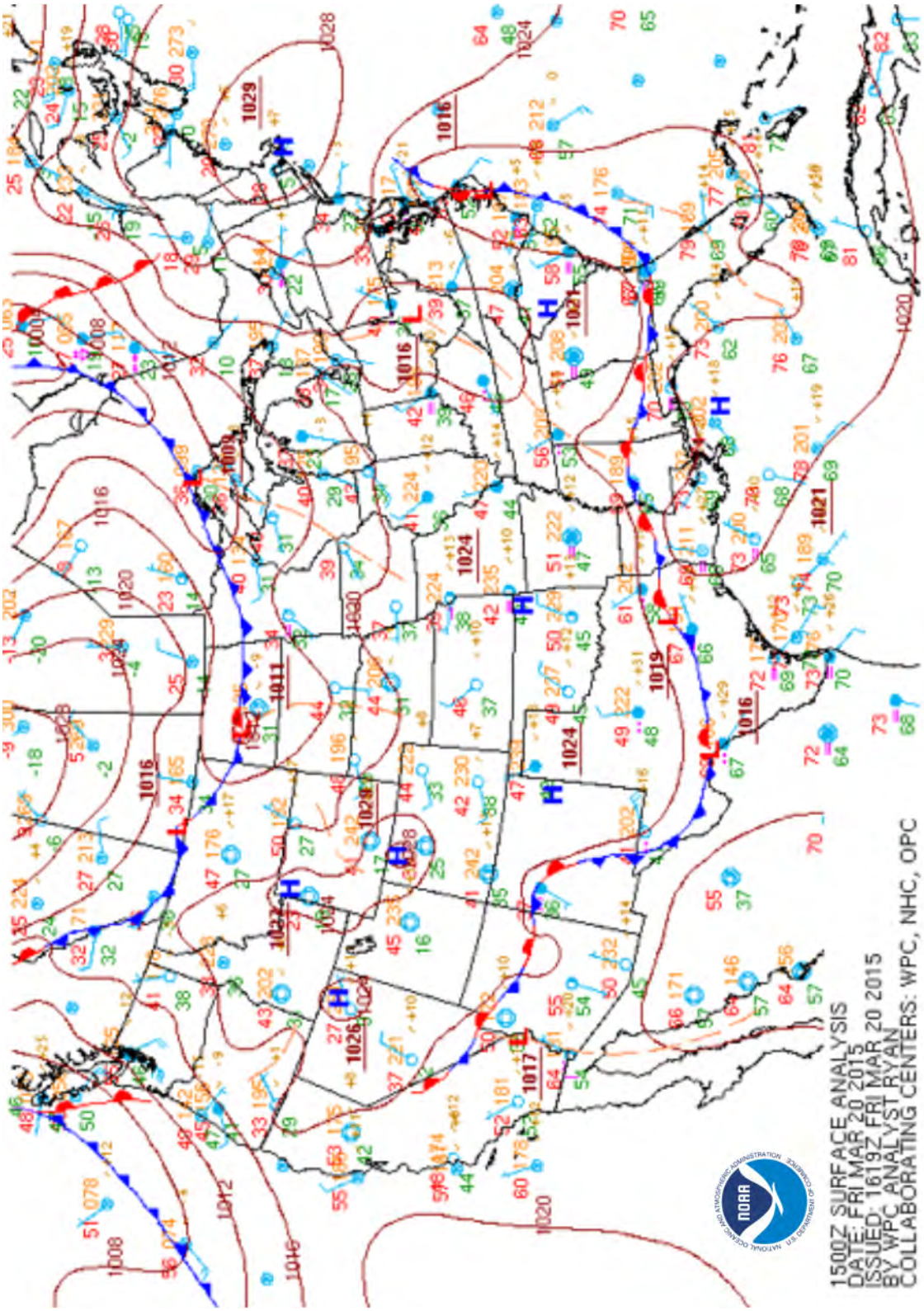

Figure 46.—Surface analysis chart from 15:00 UTC on March 20, 2015.

Figure 47.—Map of SLW-sensor trajectory (red) from 15:00 UTC on March 20, 2015.

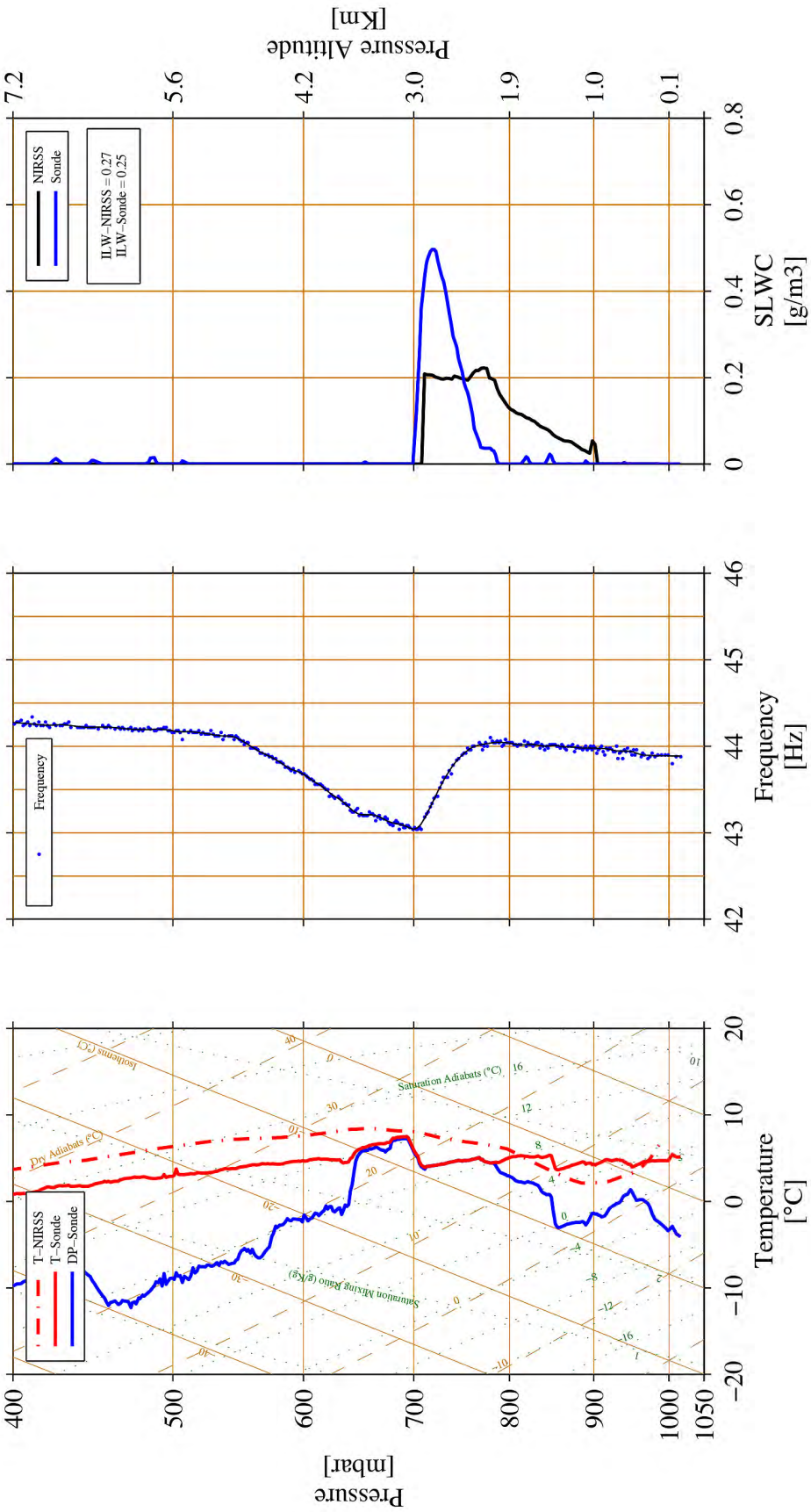

Figure 48.—Skew-T log P profile of SLW-sensor temperature (left, red line) and dewpoint temperature (left, blue line), SLW-sensor wire frequency (center, black line) and SLW-sensor LWC (right, blue line) with NIRSS LWC (right, black line) from 15:00 UTC on March 20, 2015.

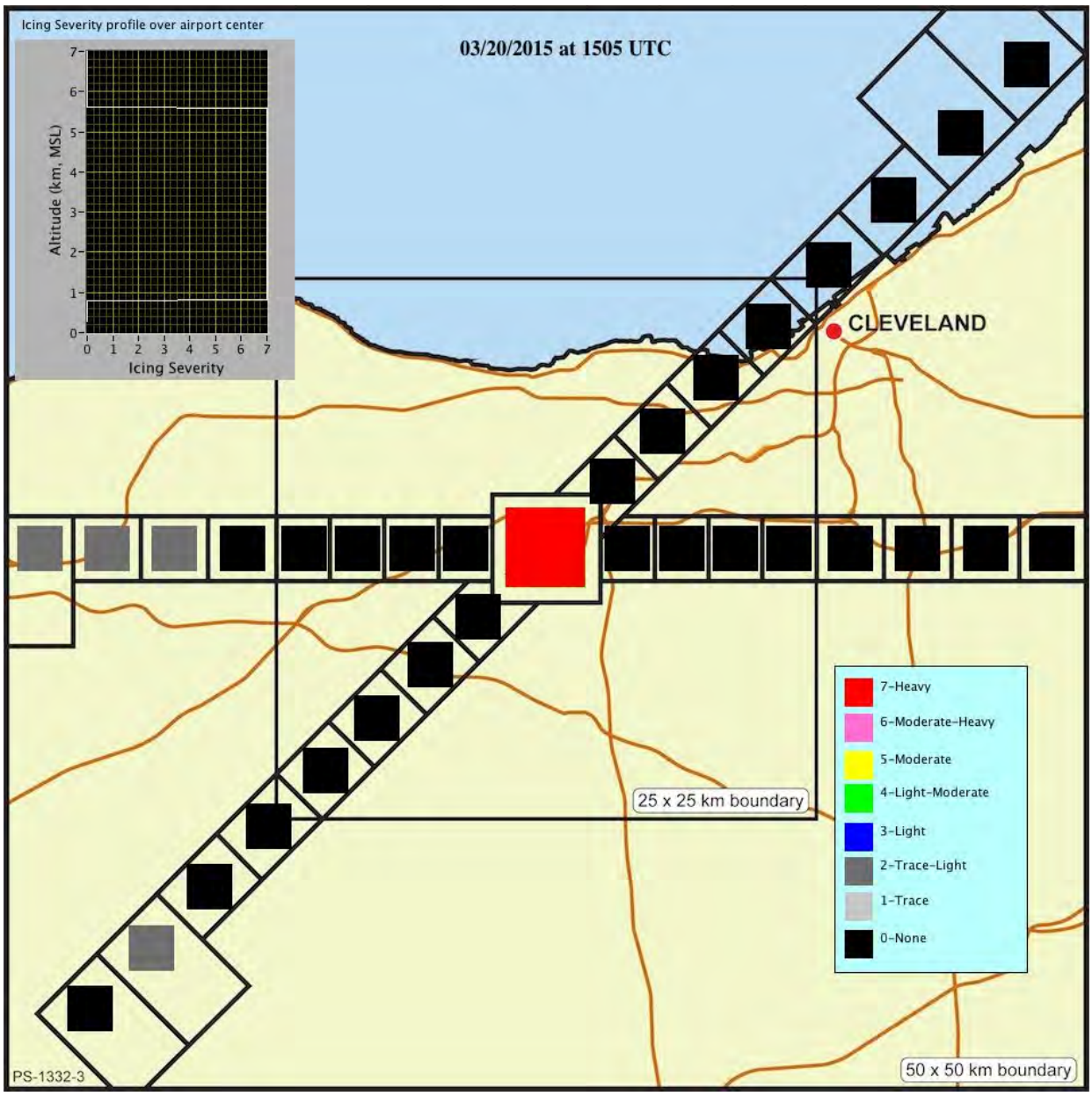

Figure 49.—NIRSS terminal area qualitative in-flight icing hazard classification from 15:05 UTC on March 20, 2015.

Figure 50.—Map of SLW-sensor trajectory (red) from 15:49 UTC on March 20, 2015.

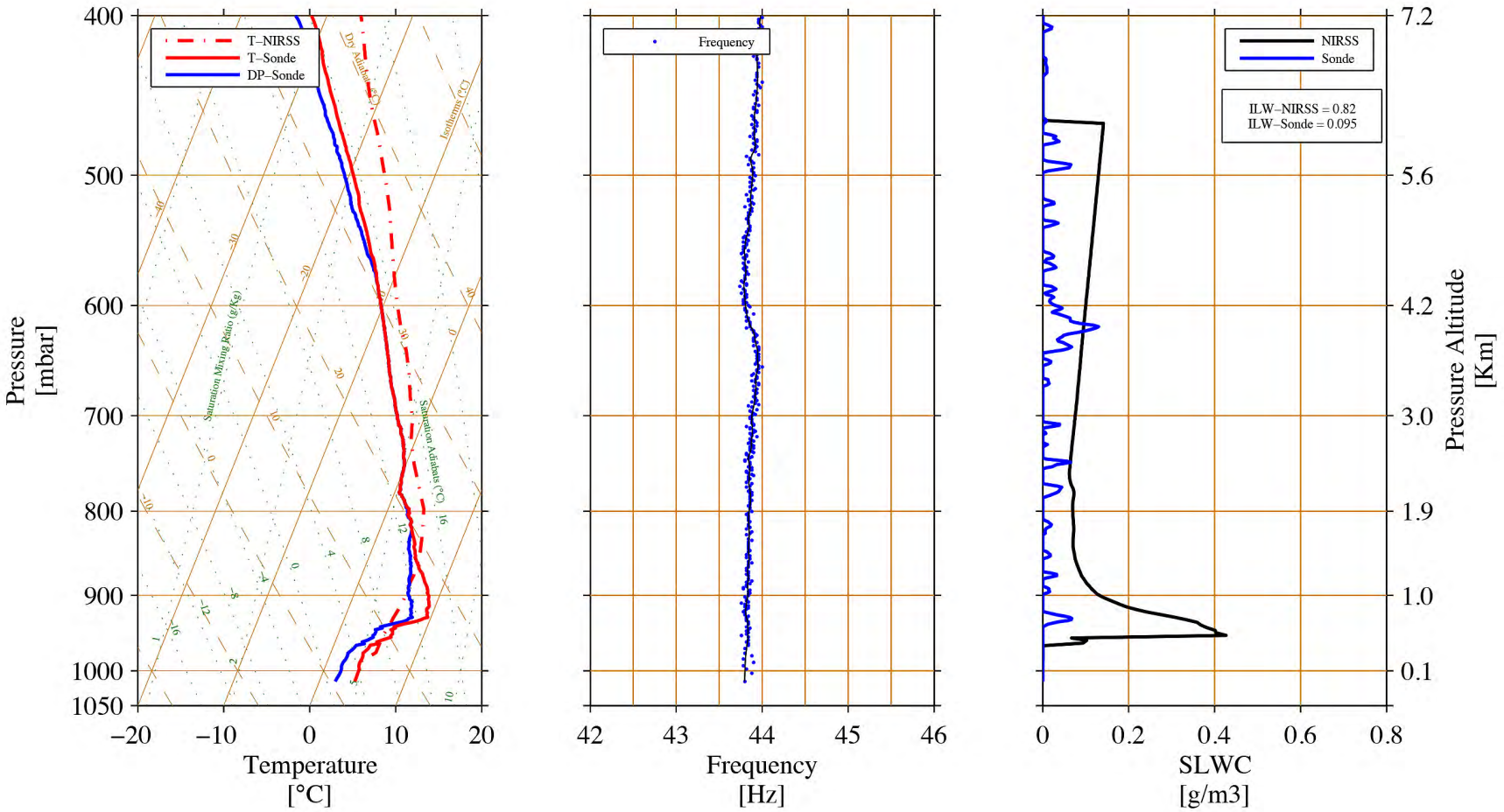

Figure 51.—Skew-T log P profile of SLW-sensor temperature (left, red line) and dewpoint temperature (left, blue line), SLW-sensor wire frequency (center, black line) and SLW-sensor LWC (right, blue line) with NIRSS LWC (right, black line) from 15:49 UTC on March 20, 2015.

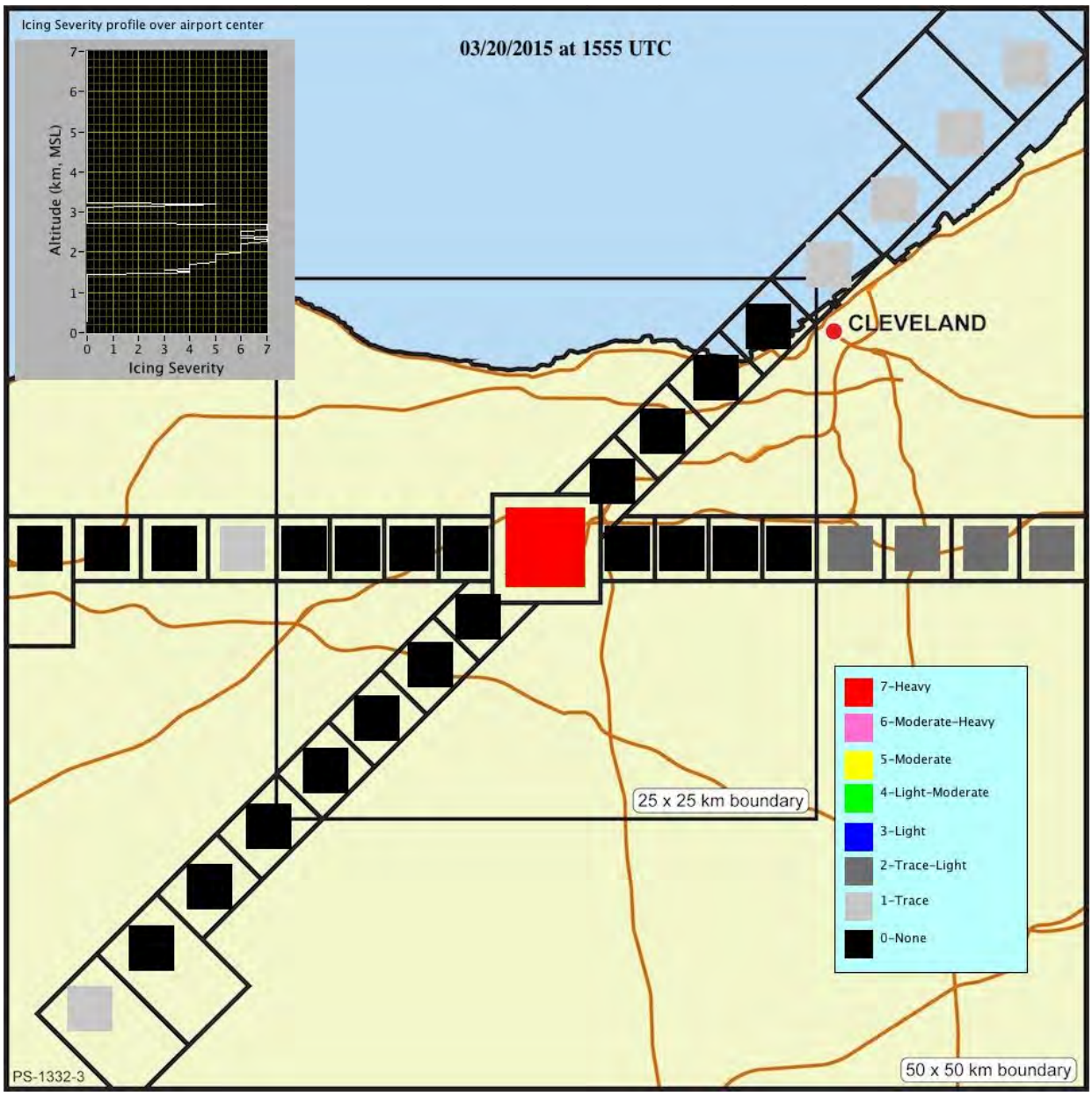

Figure 52.—NIRSS terminal area qualitative in-flight icing hazard classification from 15:55 UTC on March 20, 2015.

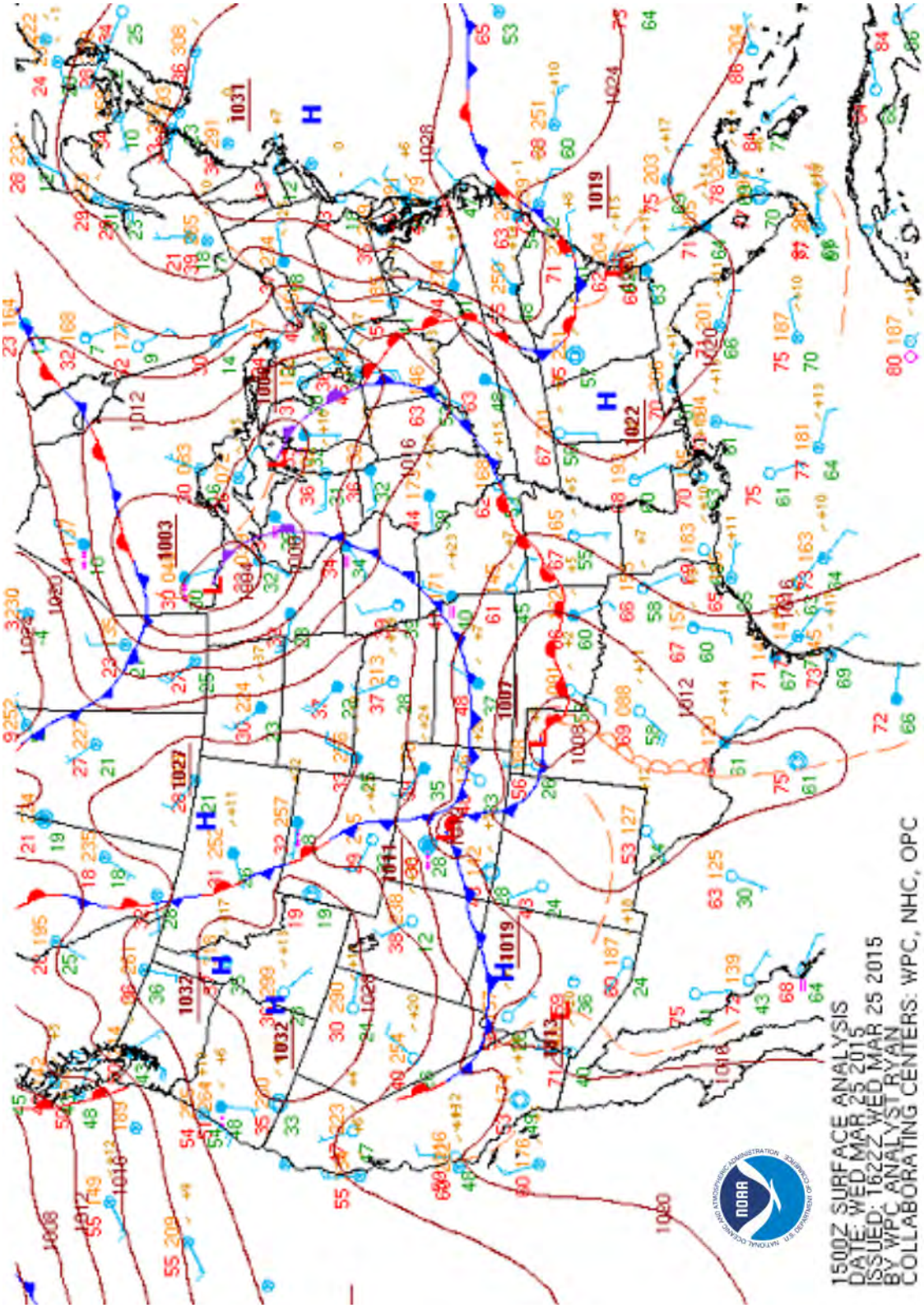

Figure 53.—Surface analysis chart from 15:00 UTC on March 25, 2015.

Figure 54.—Map of SLW-sensor trajectory (red) from 12:22 UTC on March 25, 2015.

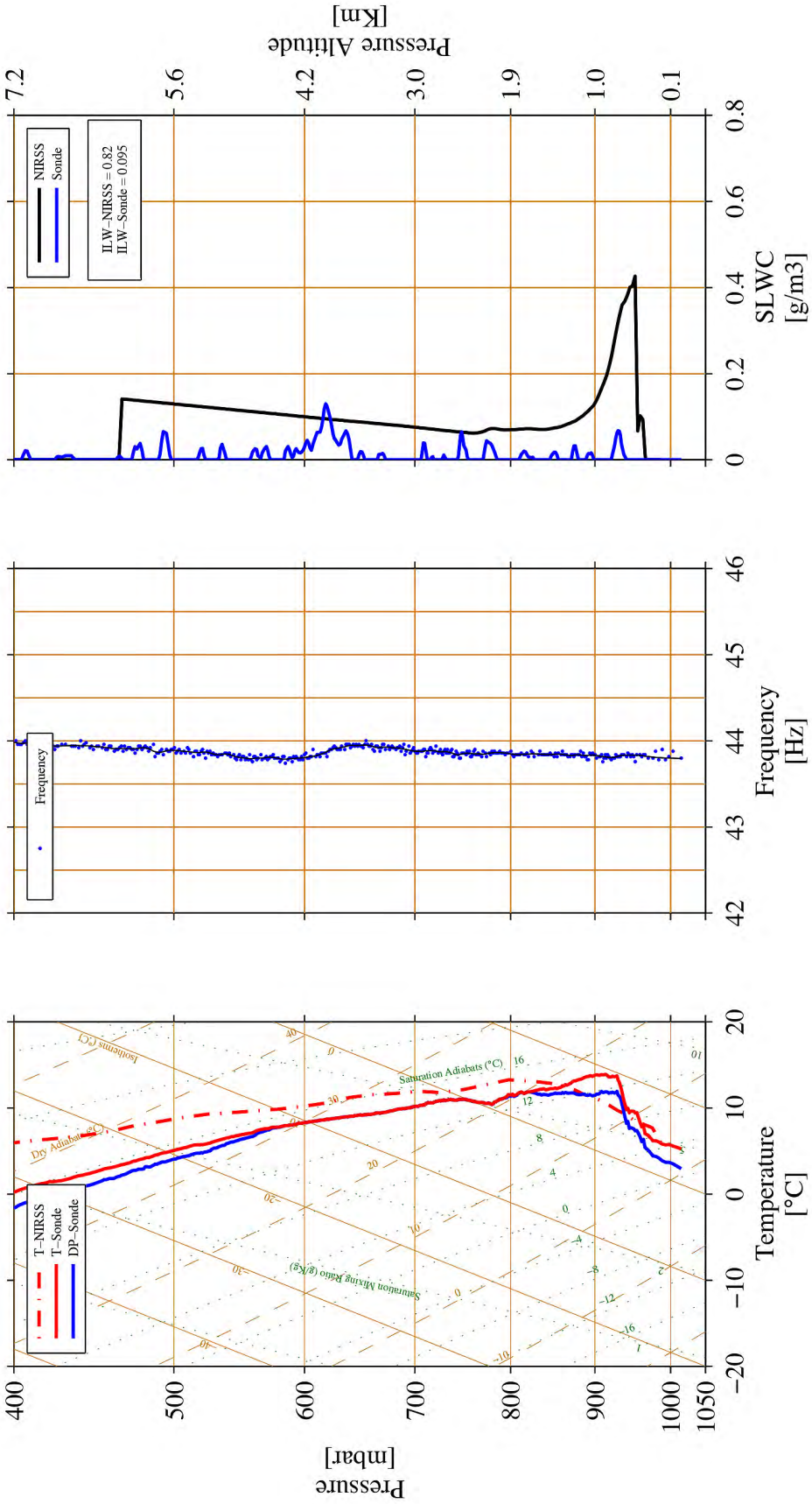

Figure 55.—Skew-T log P profile of SLW-sensor temperature (left, red line) and dewpoint temperature (left, blue line), SLW-sensor wire frequency (center, black line) and SLW-sensor LWC (right, blue line) with NIRSS LWC (right, black line) from 12:22 UTC on March 25, 2015.

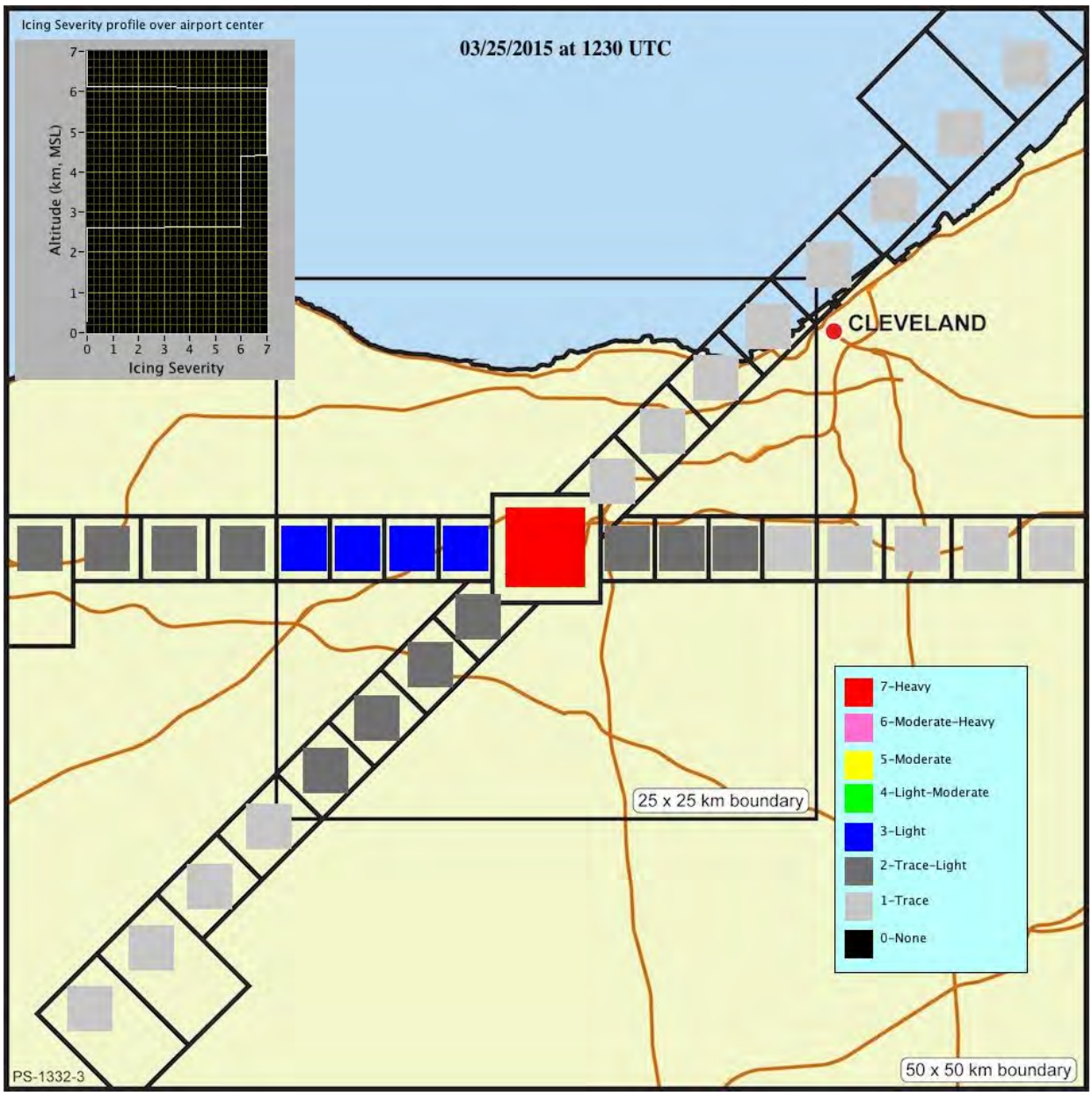

Figure 56.—NIRSS terminal area qualitative in-flight icing hazard classification from 12:30 UTC on March 25, 2015.

Figure 57.—Map of SLW-sensor trajectory (red) from 14:18 UTC on March 25, 2015.

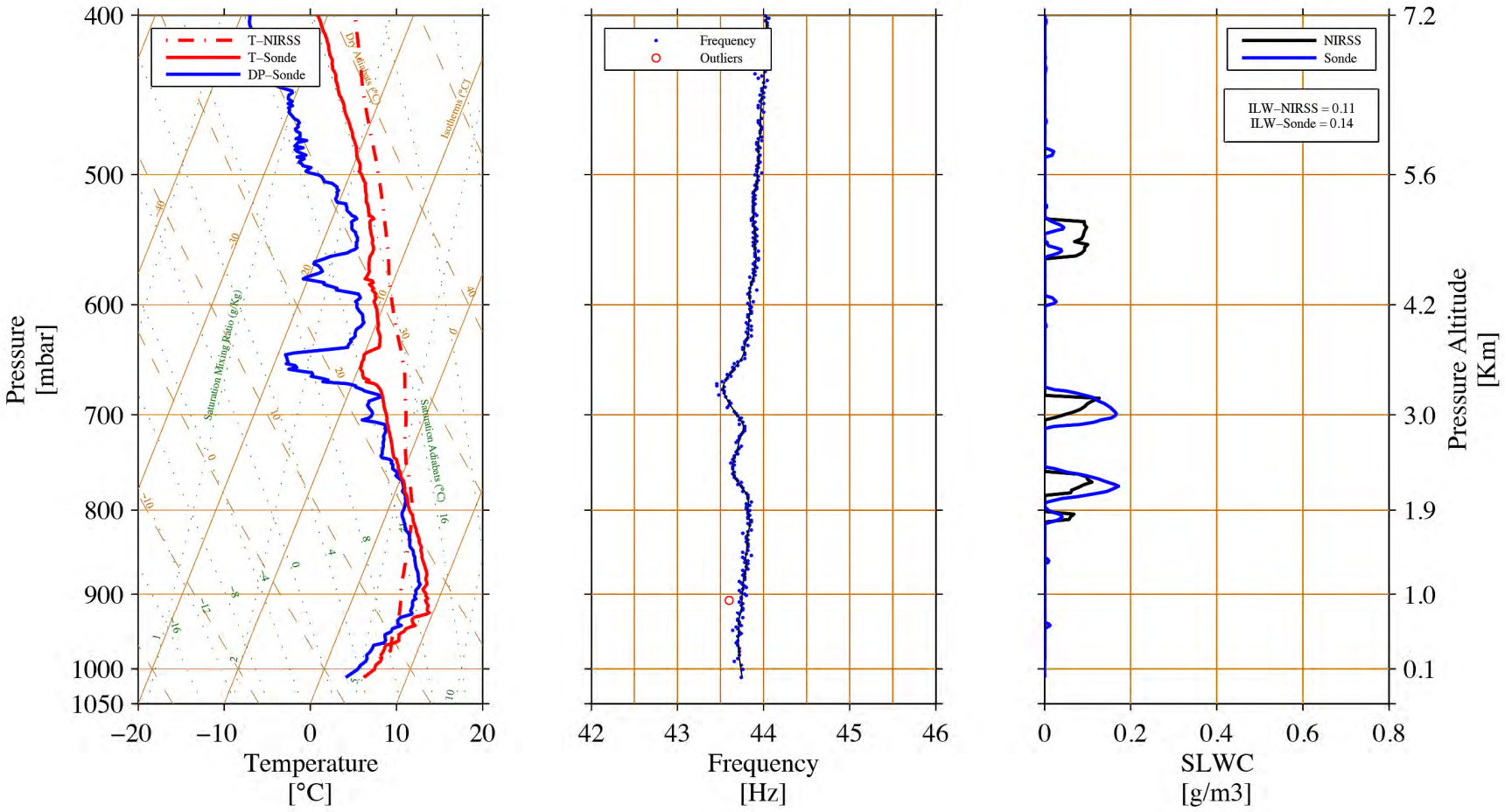

Figure 58.—Skew-T log P profile of SLW-sensor temperature (left, red line) and dewpoint temperature (left, blue line), SLW-sensor wire frequency (center, black line) and SLW-sensor LWC (right, blue line) with NIRSS LWC (right, black line) from 14:18 UTC on March 25, 2015.

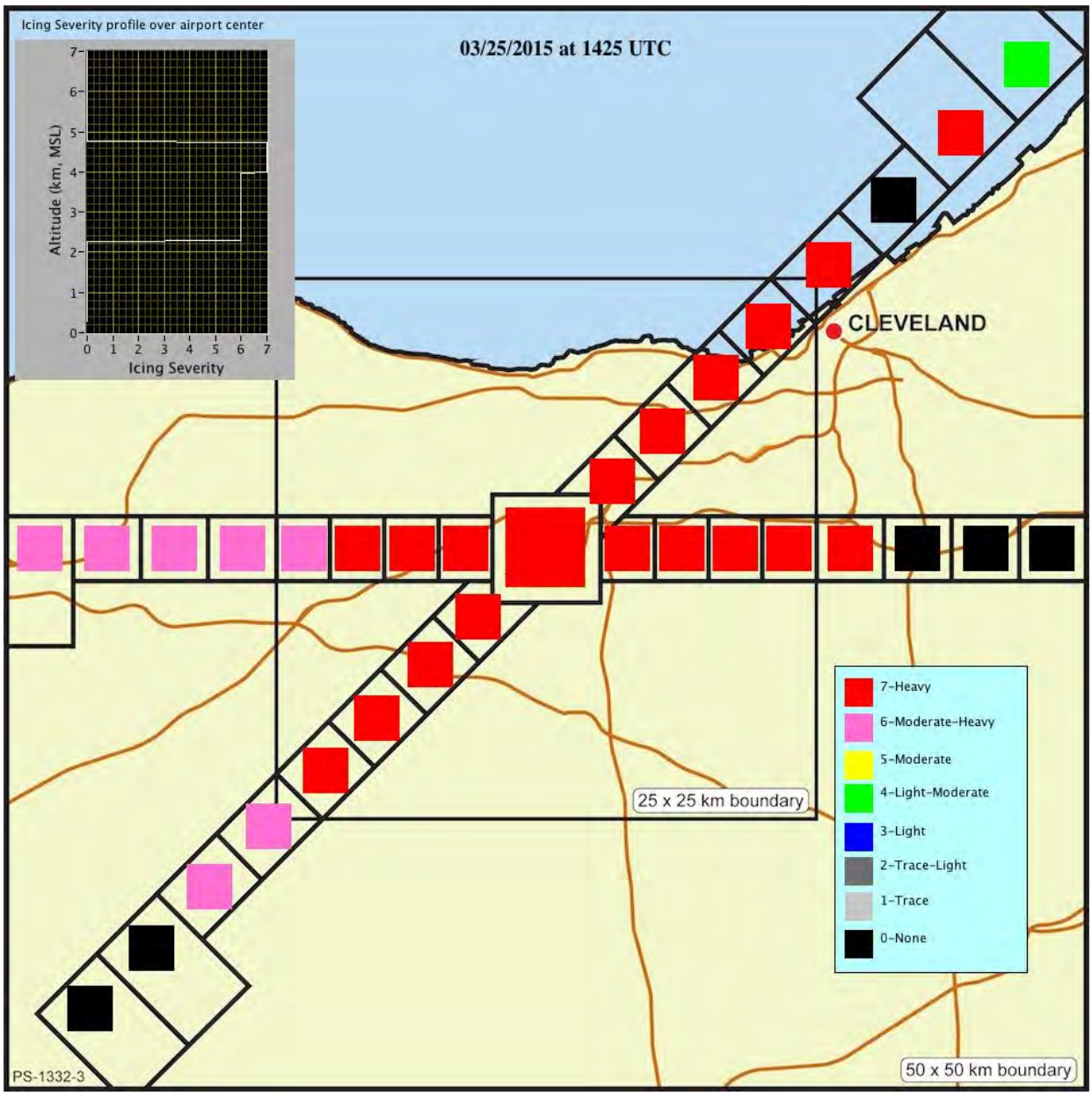

Figure 59.—NIRSS terminal area qualitative in-flight icing hazard classification from 14:25 UTC on March 25, 2015.

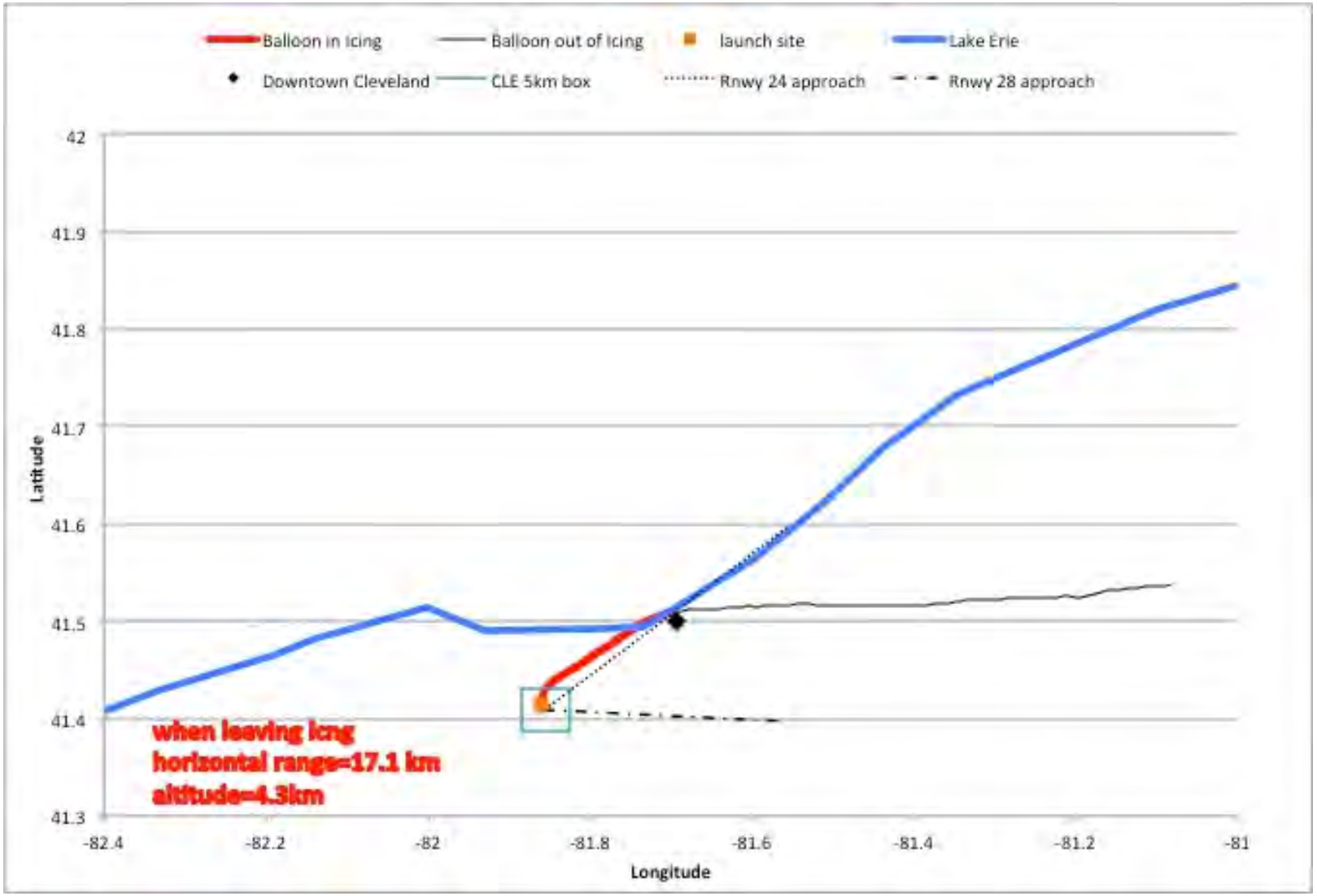

Figure 60.—Map of SLW-sensor trajectory (red) from 15:01 UTC on March 25, 2015.

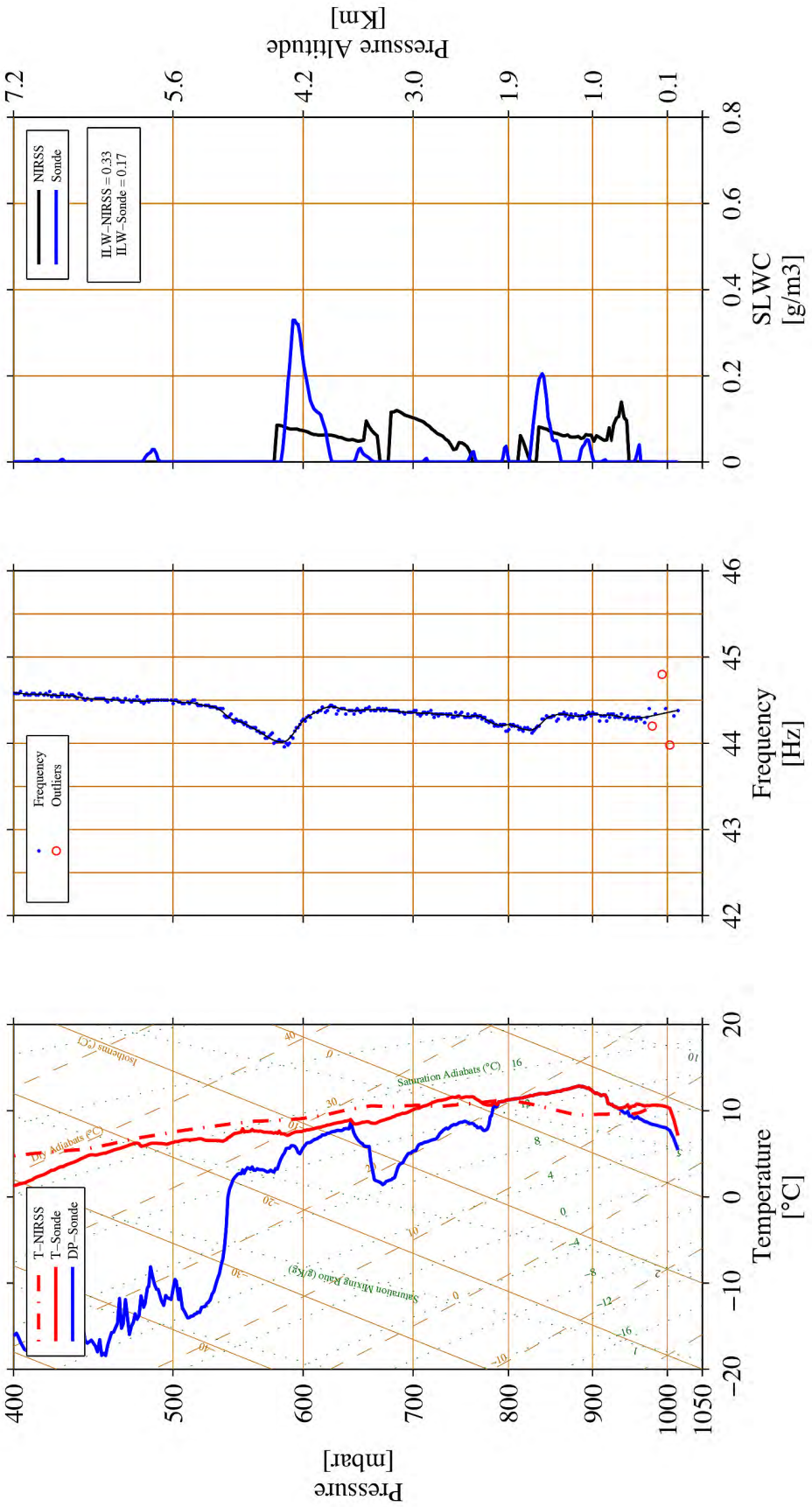

Figure 61.—Skew-T log P profile of SLW-sensor temperature (left, red line) and dewpoint temperature (left, blue line), SLW-sensor wire frequency (center, black line) and SLW-sensor LWC (right, blue line) with NIRSS LWC (right, black line) from 15:01 UTC on March 25, 2015.

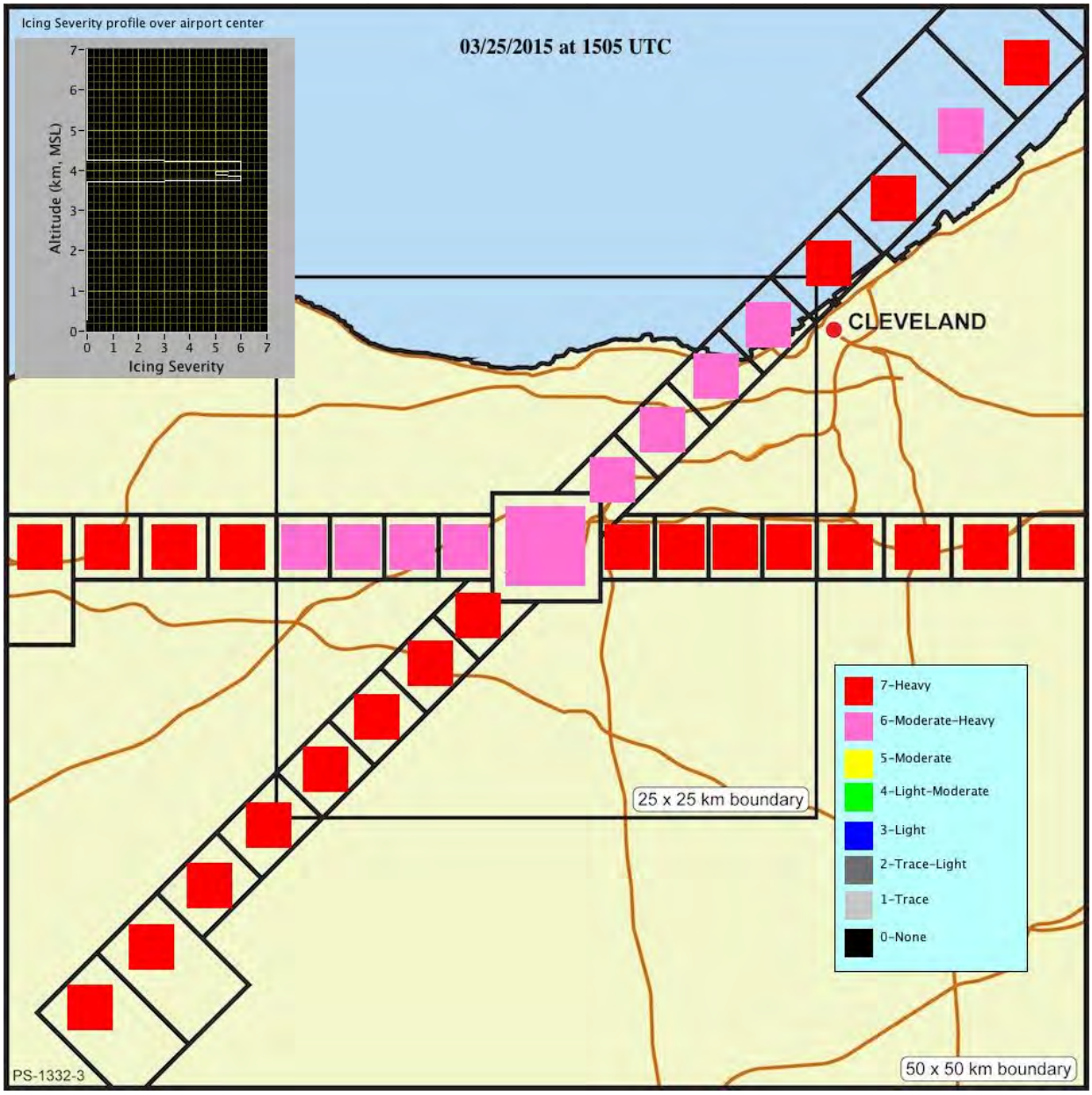

Figure 62.—NIRSS terminal area qualitative in-flight icing hazard classification from 15:05 UTC on March 25, 2015.

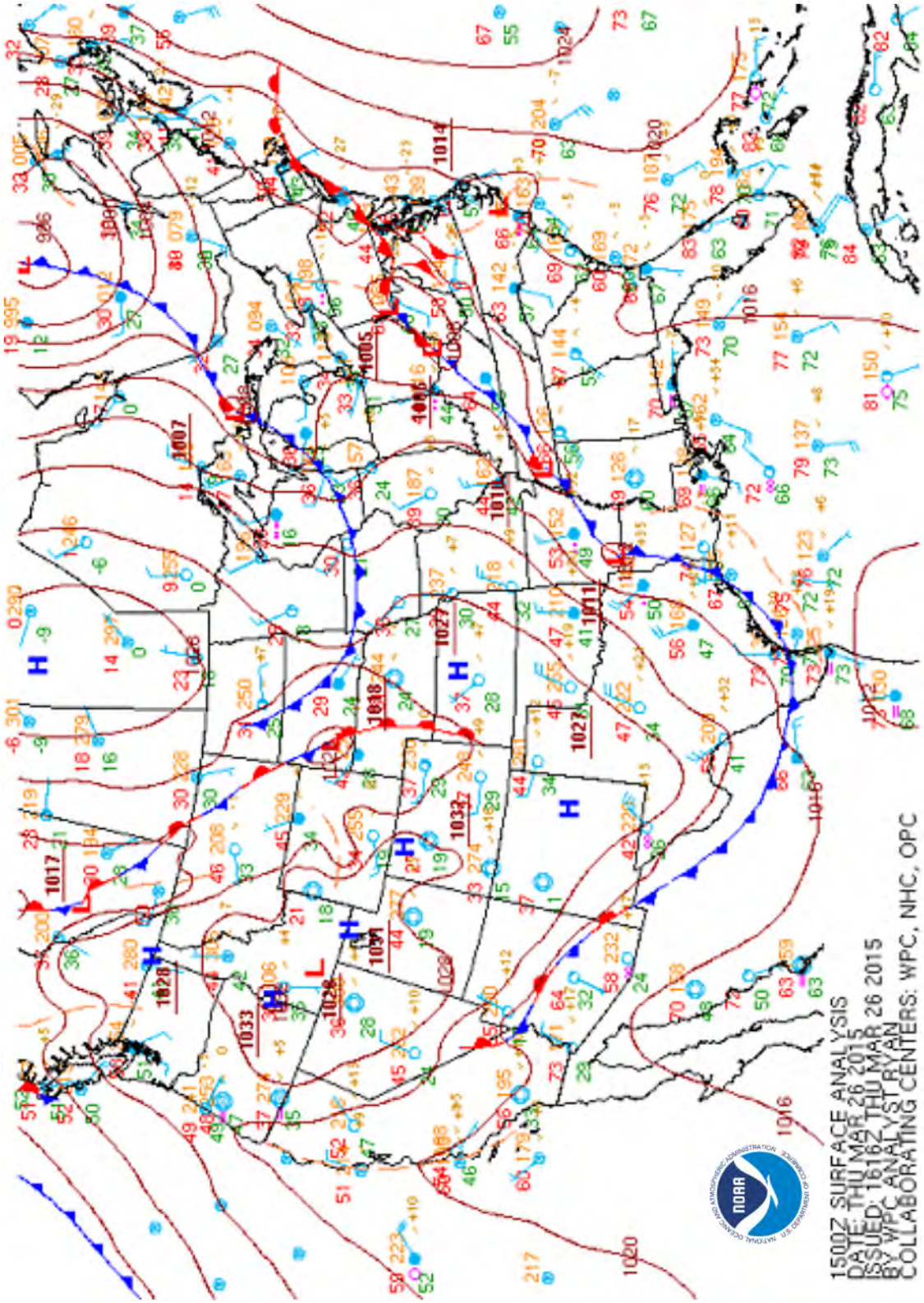

Figure 63.—Surface analysis chart from 15:00 UTC on March 26, 2015.

Figure 64.—Map of SLW-sensor trajectory (red) from 15:07 UTC on March 26, 2015.

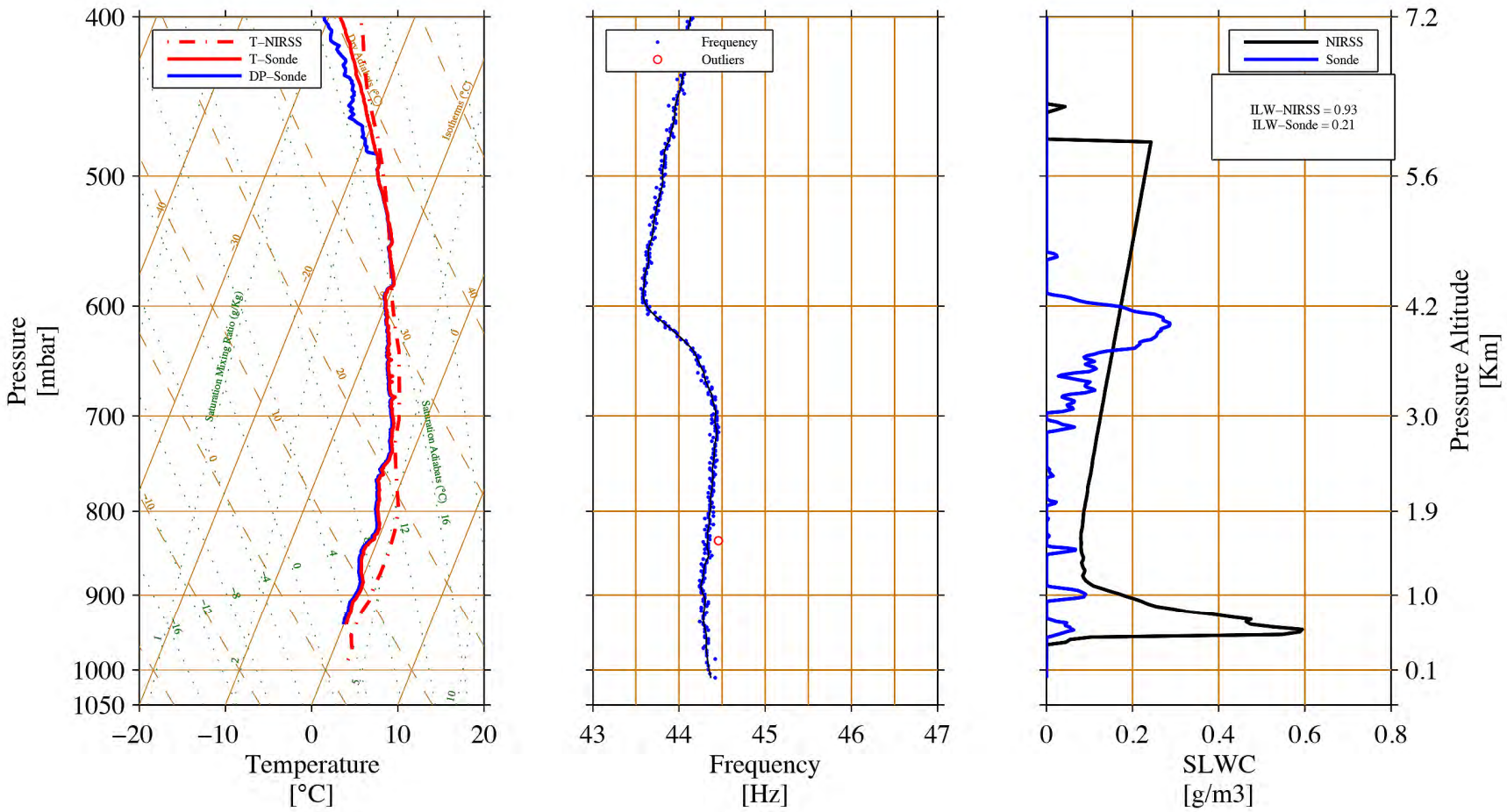

Figure 65.—Skew-T log P profile of SLW-sensor temperature (left, red line) and dewpoint temperature (left, blue line), SLW-sensor wire frequency (center, black line) and SLW-sensor LWC (right, blue line) with NIRSS LWC (right, black line) from 15:07 UTC on March 26, 2015.

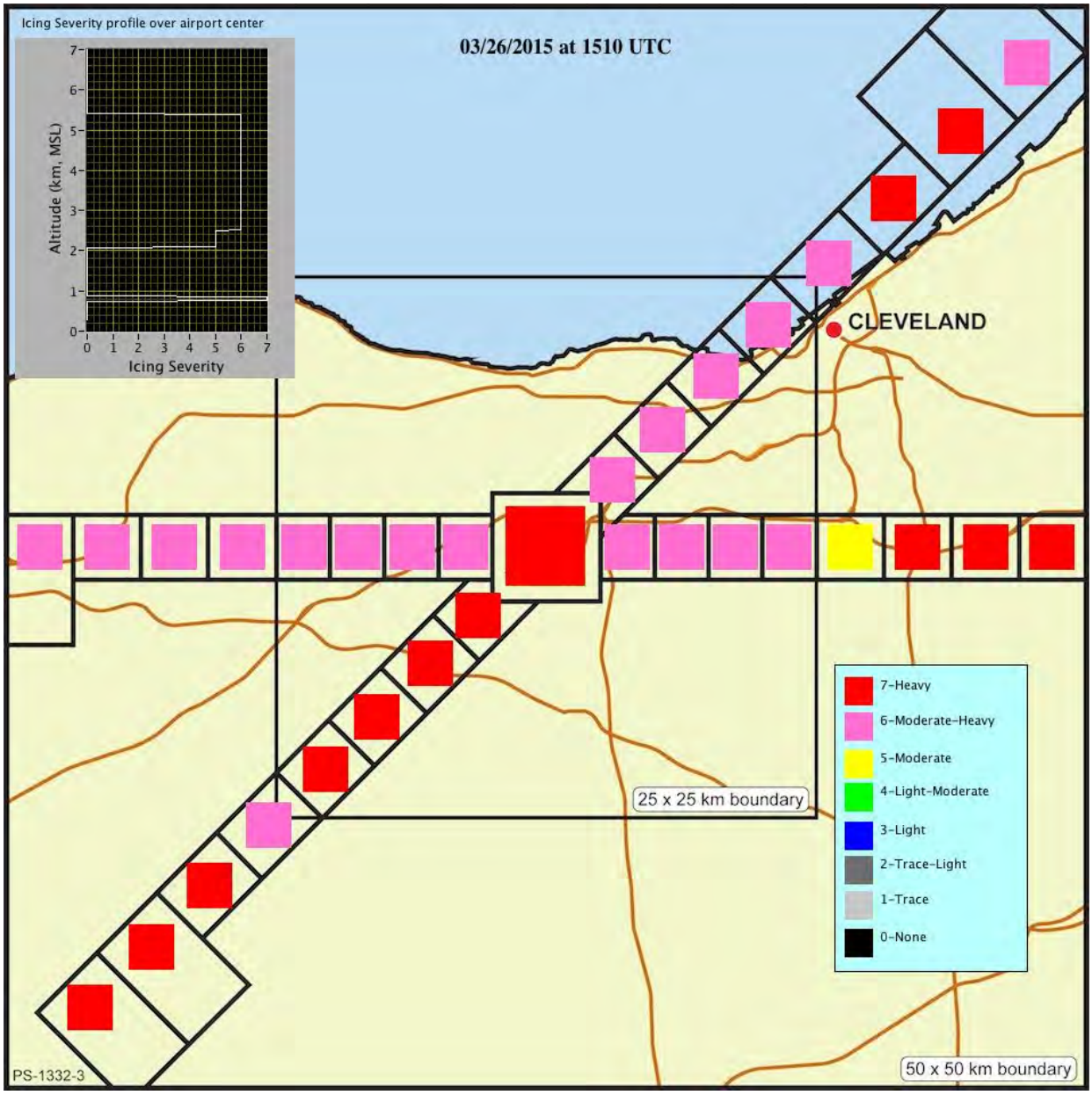

Figure 66.—NIRSS terminal area qualitative in-flight icing hazard classification from 15:10 UTC on March 26, 2015.

Figure 67.—Map of SLW-sensor trajectory (red) from 15:51 UTC on March 26, 2015.

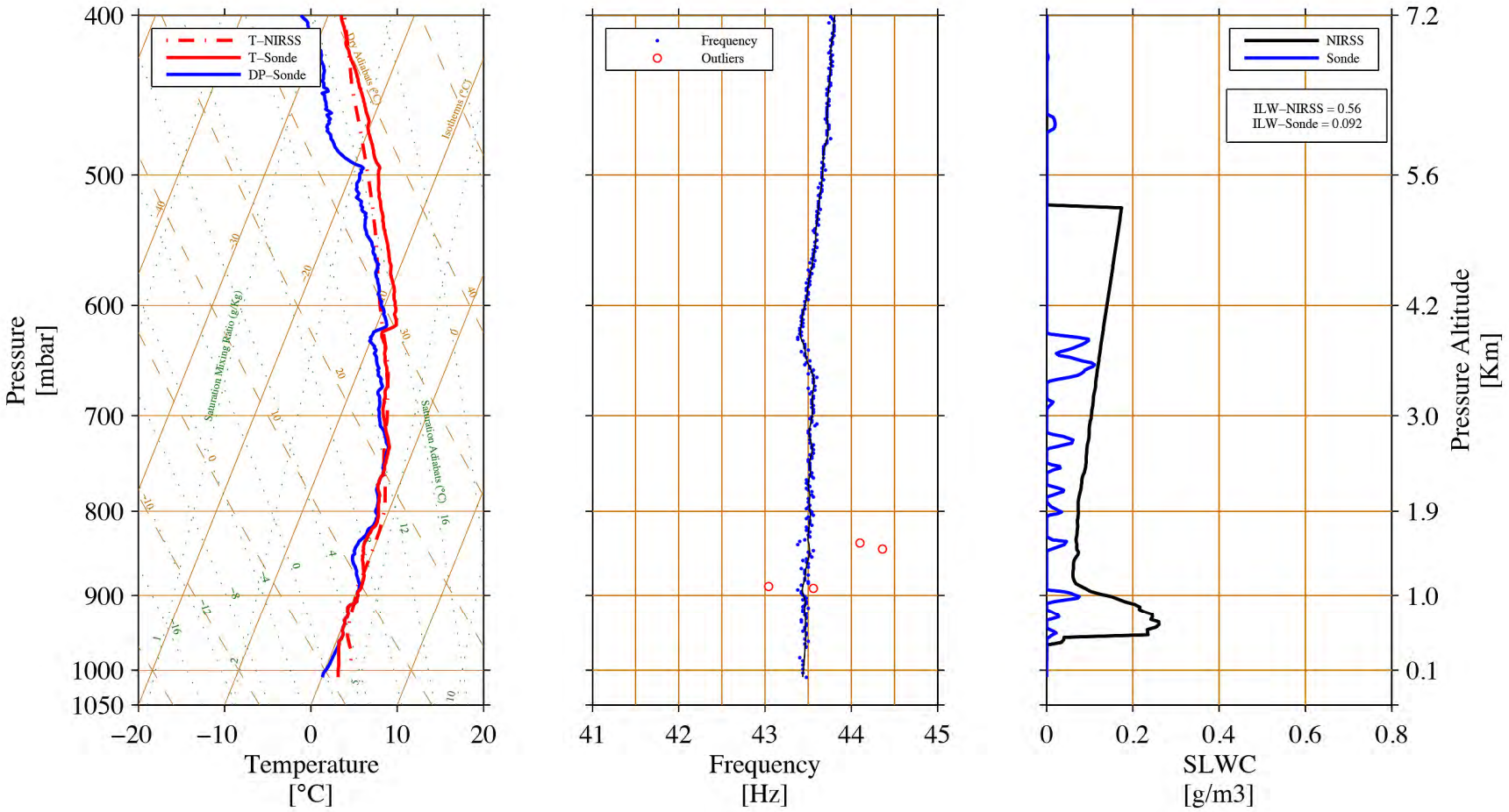

Figure 68.—Skew-T log P profile of SLW-sensor temperature (left, red line) and dewpoint temperature (left, blue line), SLW-sensor wire frequency (center, black line) and SLW-sensor LWC (right, blue line) with NIRSS LWC (right, black line) from 15:51 UTC on March 26, 2015.

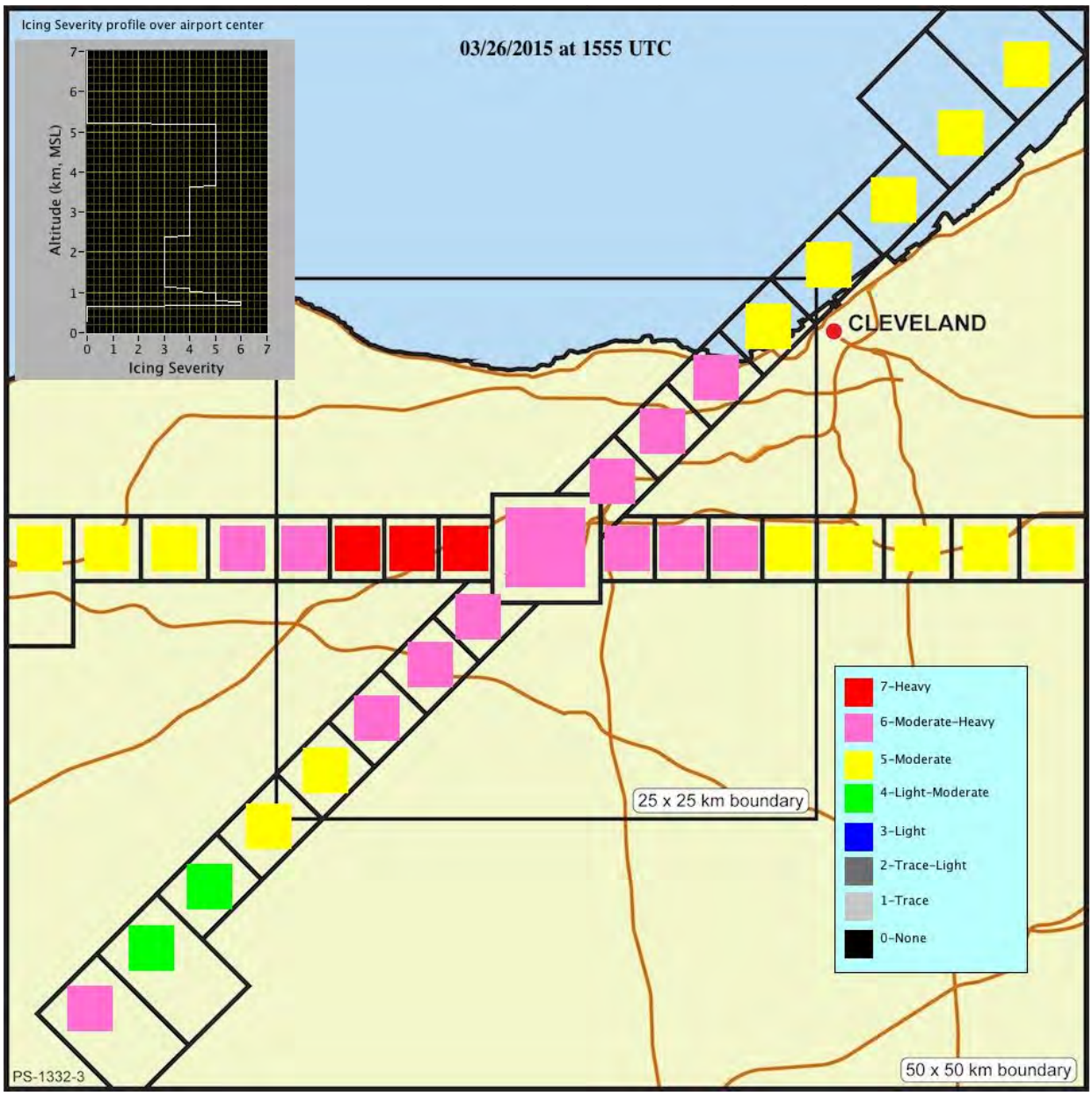

Figure 69.—NIRSS terminal area qualitative in-flight icing hazard classification from 15:55 UTC on March 26, 2015.

Figure 70.—Map of SLW-sensor trajectory (red) from 16:59 UTC on March 26, 2015.

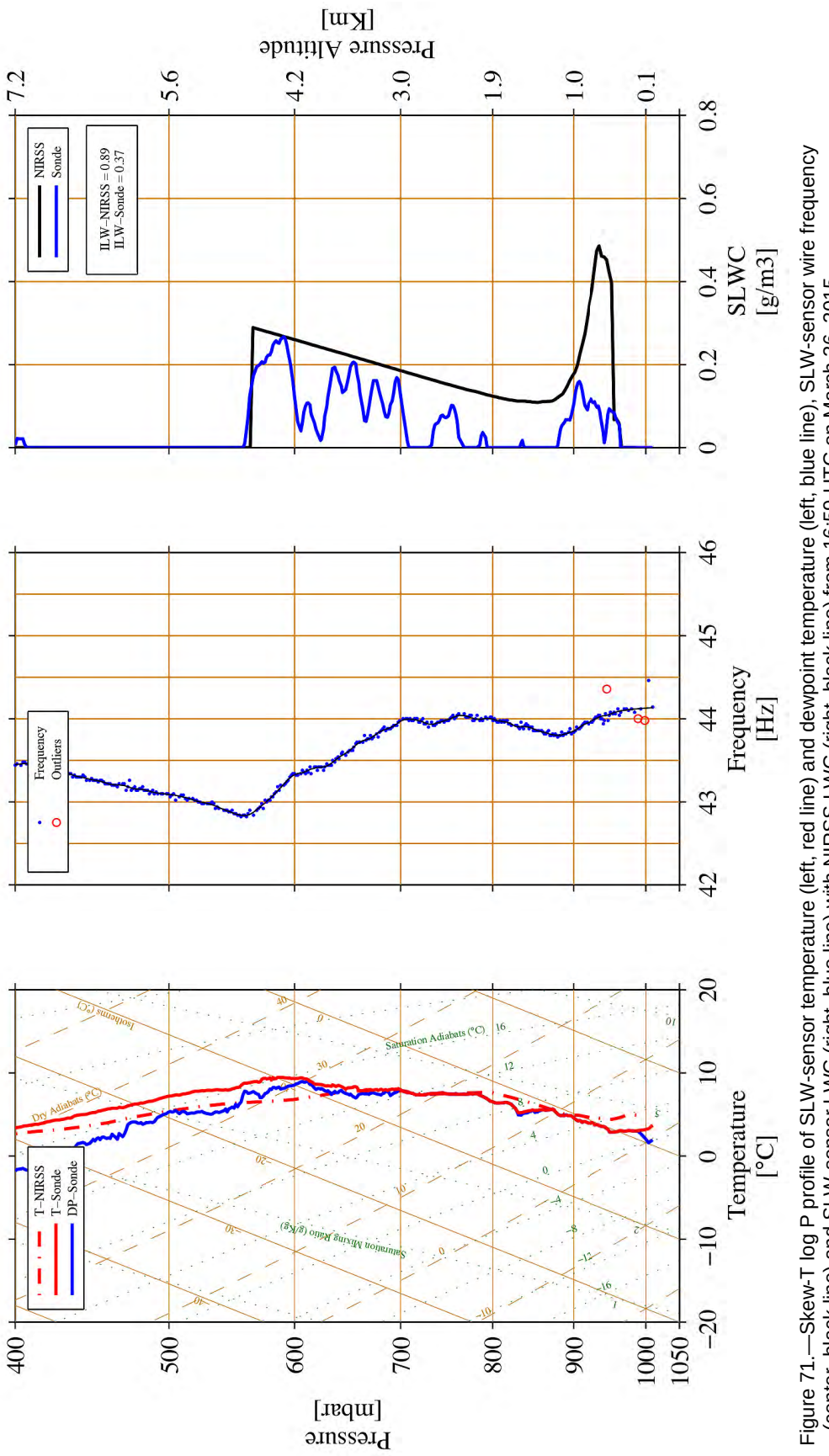

Figure 71.—Skew-T log P profile of SLW-sensor temperature (left, red line) and dewpoint temperature (left, blue line), SLW-sensor wire frequency (center, black line) and SLW-sensor LWC (right, blue line) with NIRSS LWC (right, black line) from 16:59 UTC on March 26, 2015.

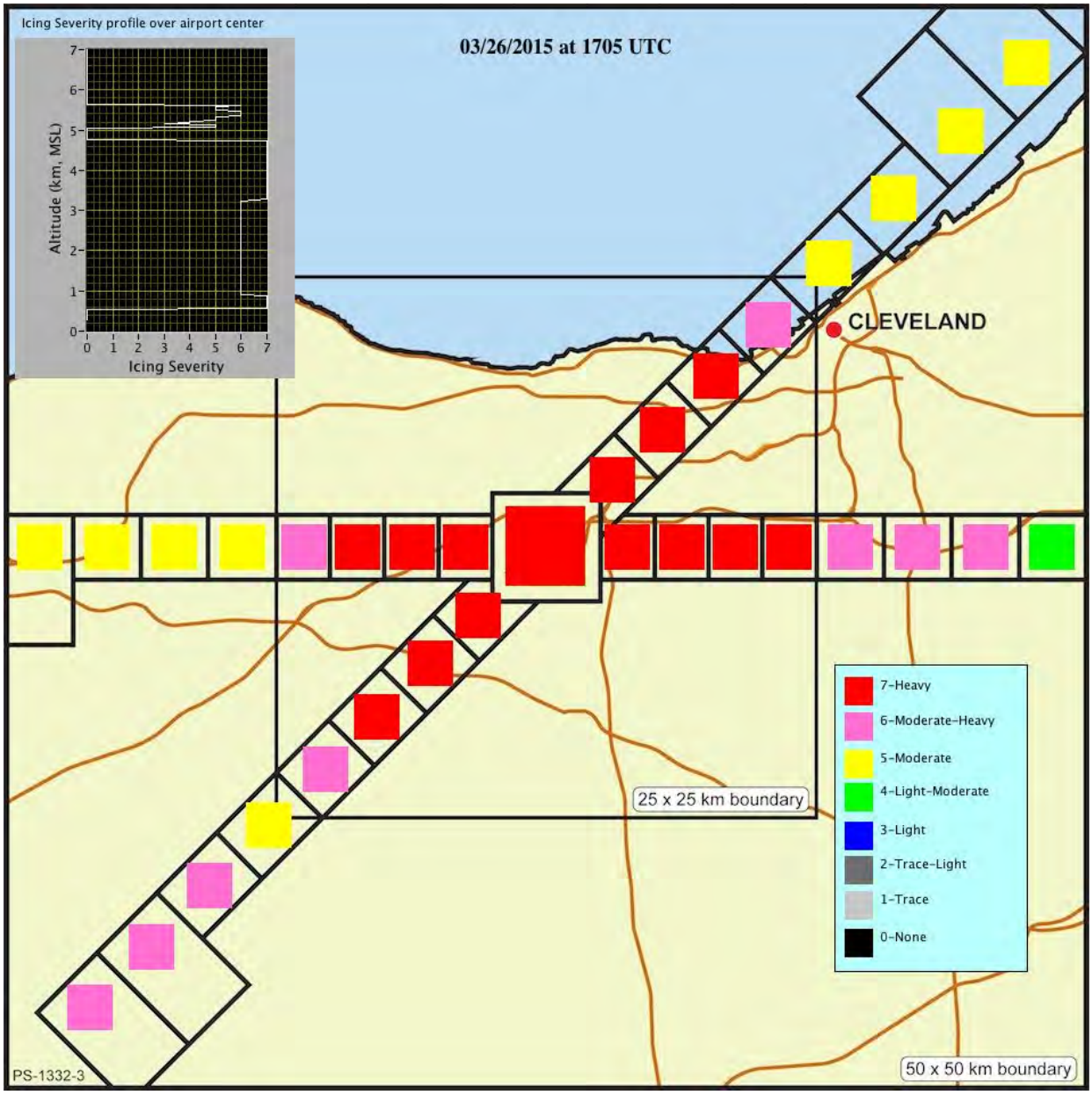

Figure 72.—NIRSS terminal area qualitative in-flight icing hazard classification from 17:05 UTC on March 26, 2015.

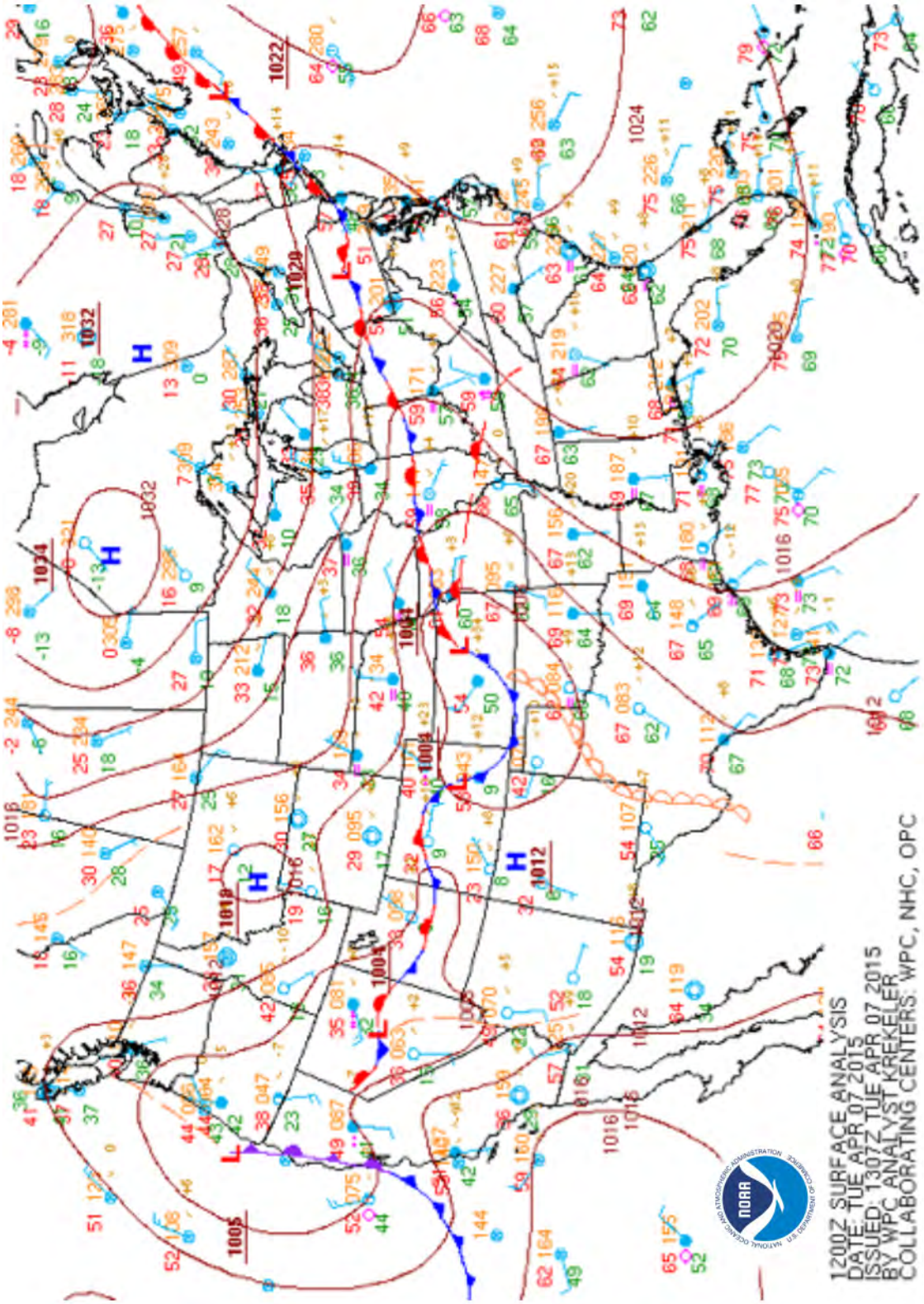

Figure 73.—Surface analysis chart from 12:00 UTC on April 7, 2015.

Figure 74.—Map of SLW-sensor trajectory (red) from 12:56 UTC on April 7, 2015.

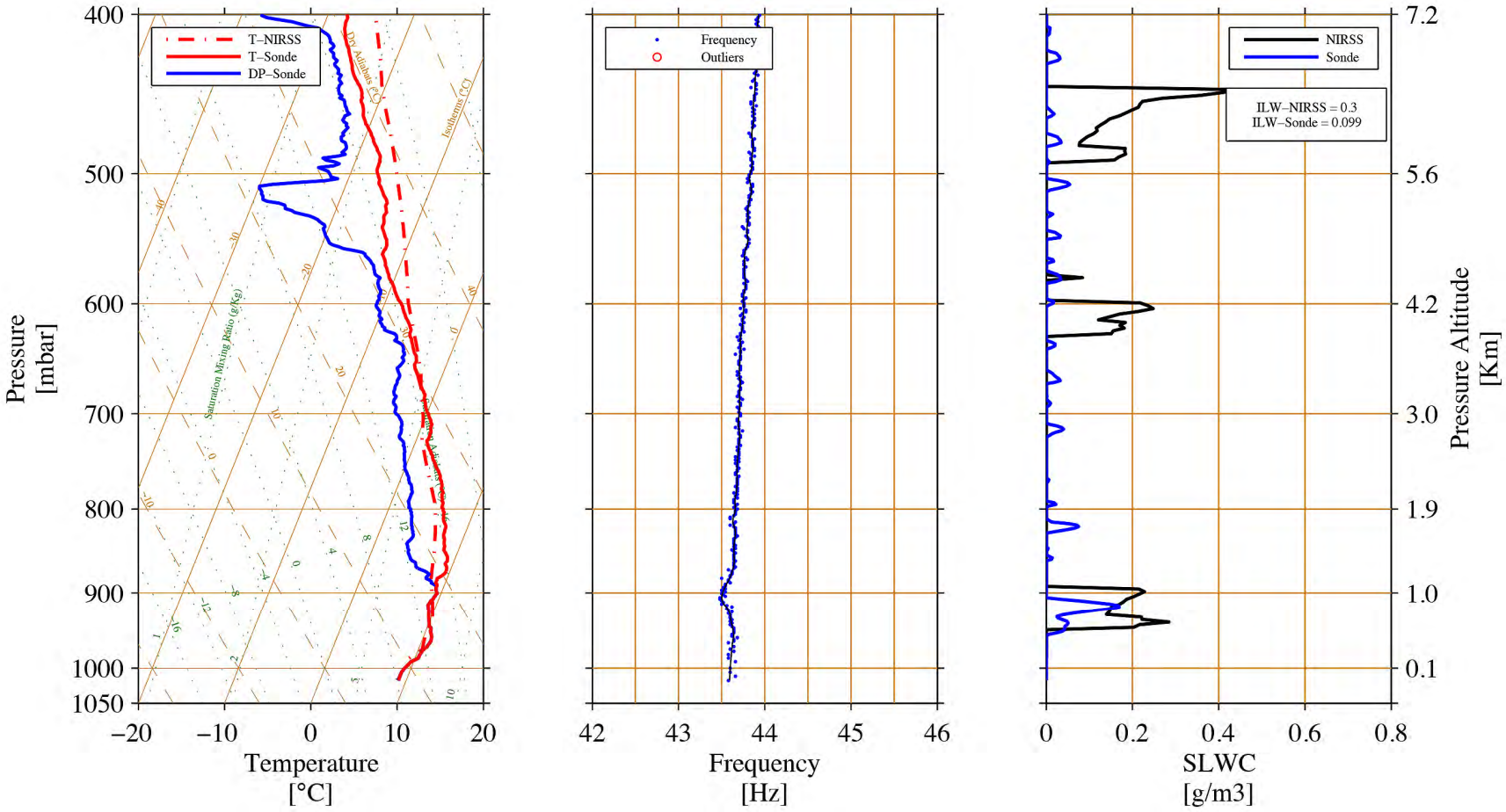

Figure 75.—Skew-T log P profile of SLW-sensor temperature (left, red line) and dewpoint temperature (left, blue line), SLW-sensor wire frequency (center, black line) and SLW-sensor LWC (right, blue line) with NIRSS LWC (right, black line) from 12:56 UTC on April 7, 2015.

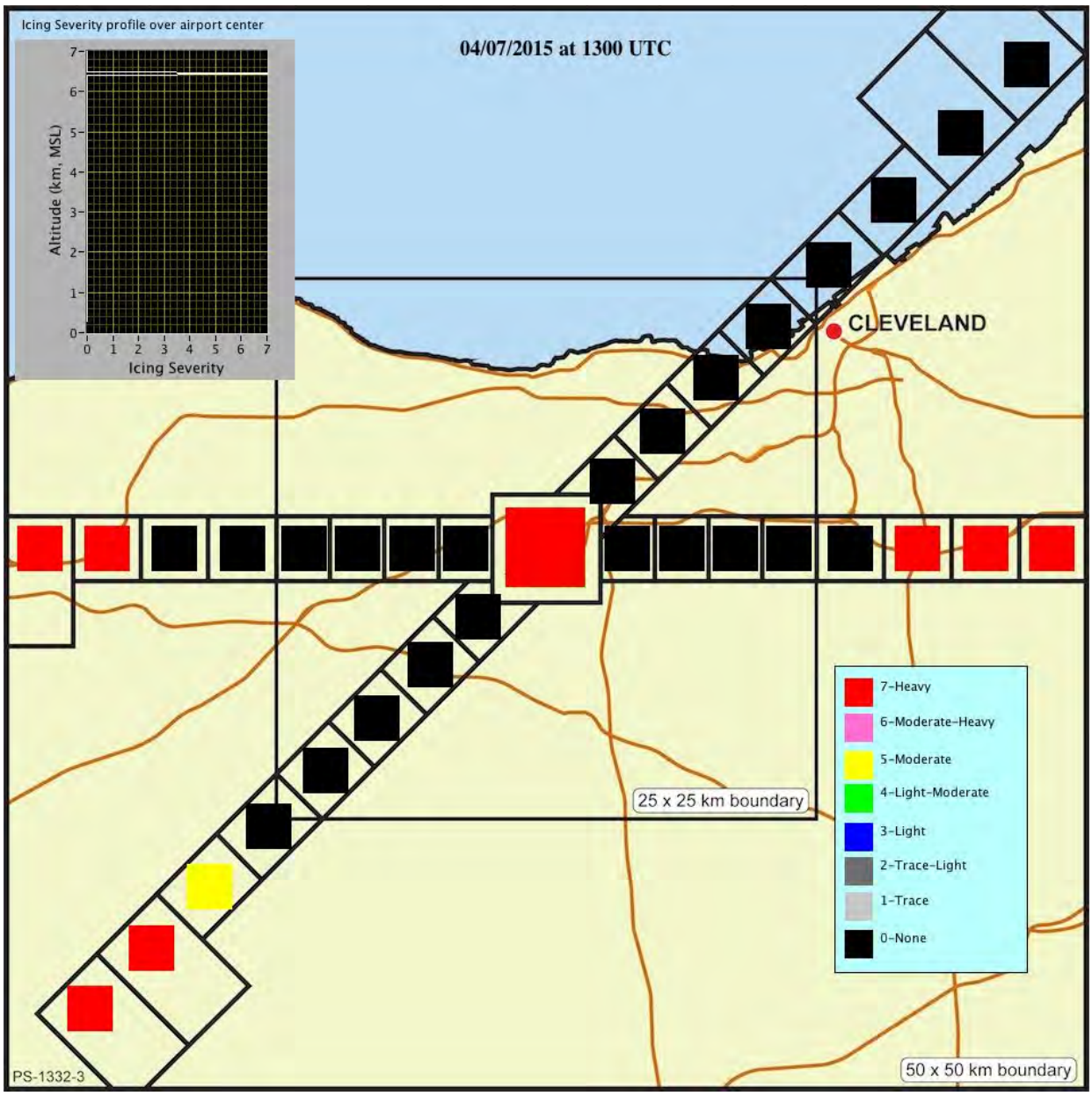

Figure 76.—NIRSS terminal area qualitative in-flight icing hazard classification from 13:00 UTC on April 7, 2015.

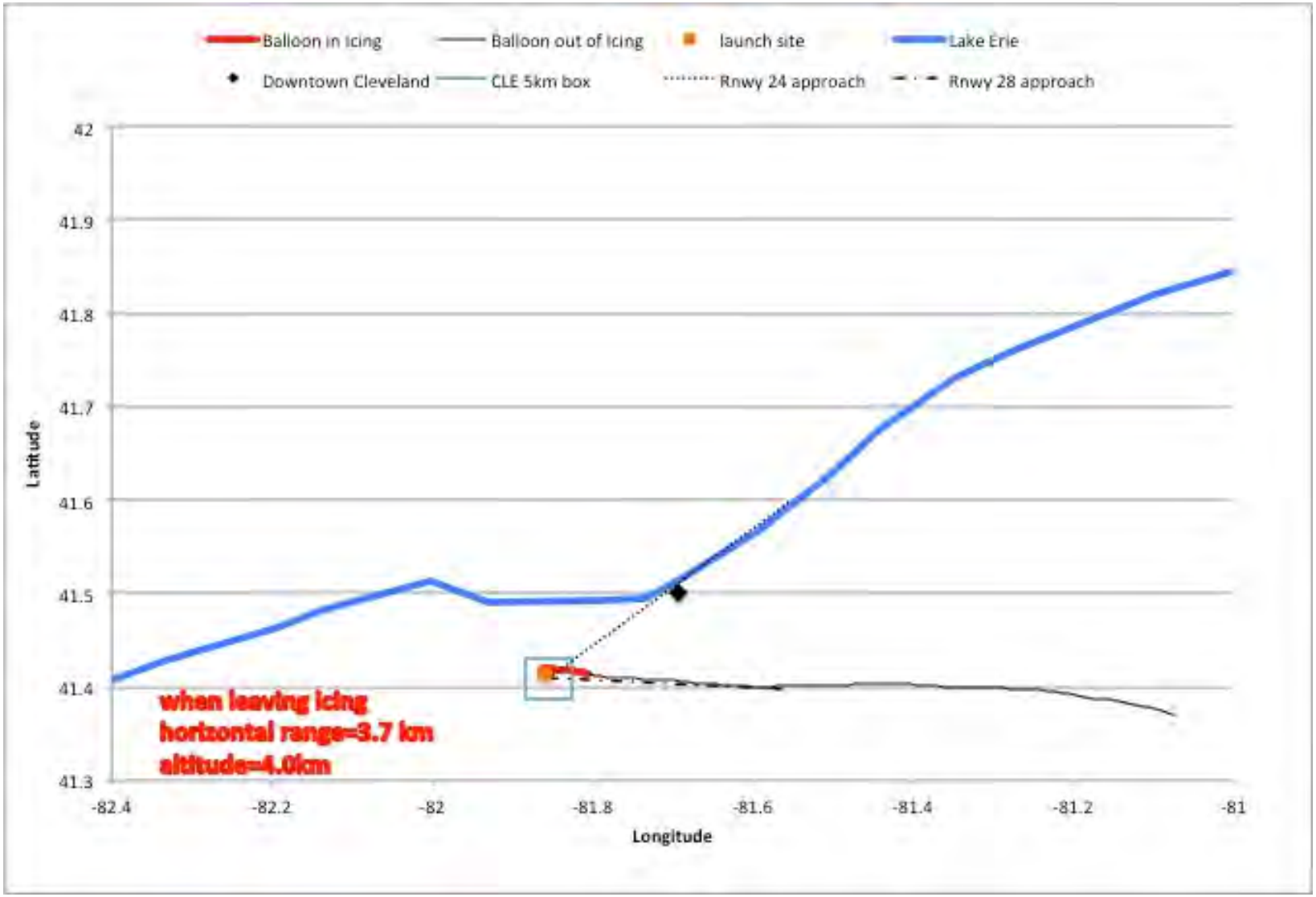

Figure 77.—Map of SLW-sensor trajectory (red) from 14:35 UTC on April 7, 2015.

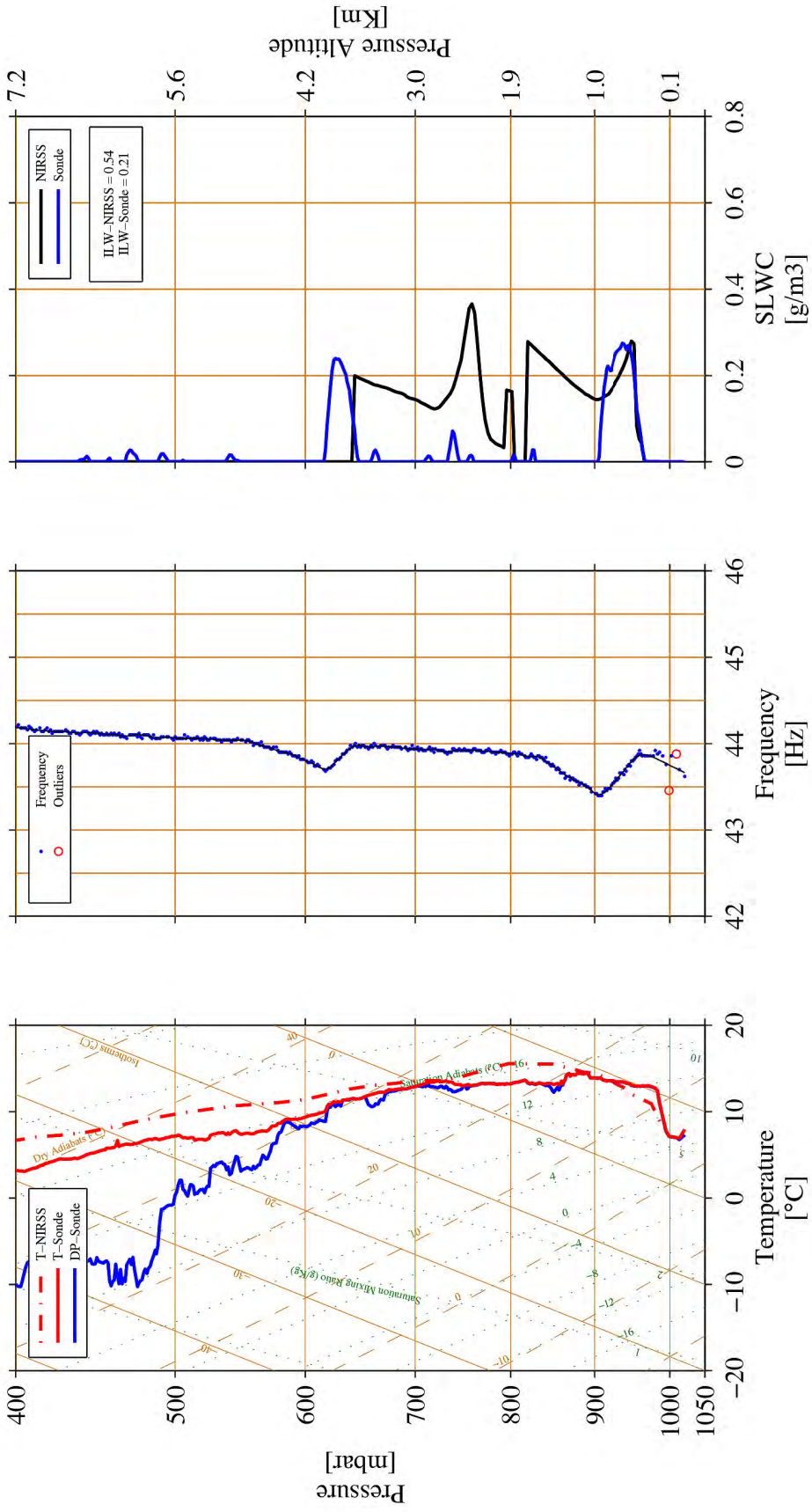

Figure 78.—Skew-T log P profile of SLW-sensor temperature (left, red line) and dewpoint temperature (left, blue line), SLW-sensor wire frequency (center, black line) and SLW-sensor LWC (right, blue line) with NIRSS LWC (right, black line) from 14:35 UTC on April 7, 2015.

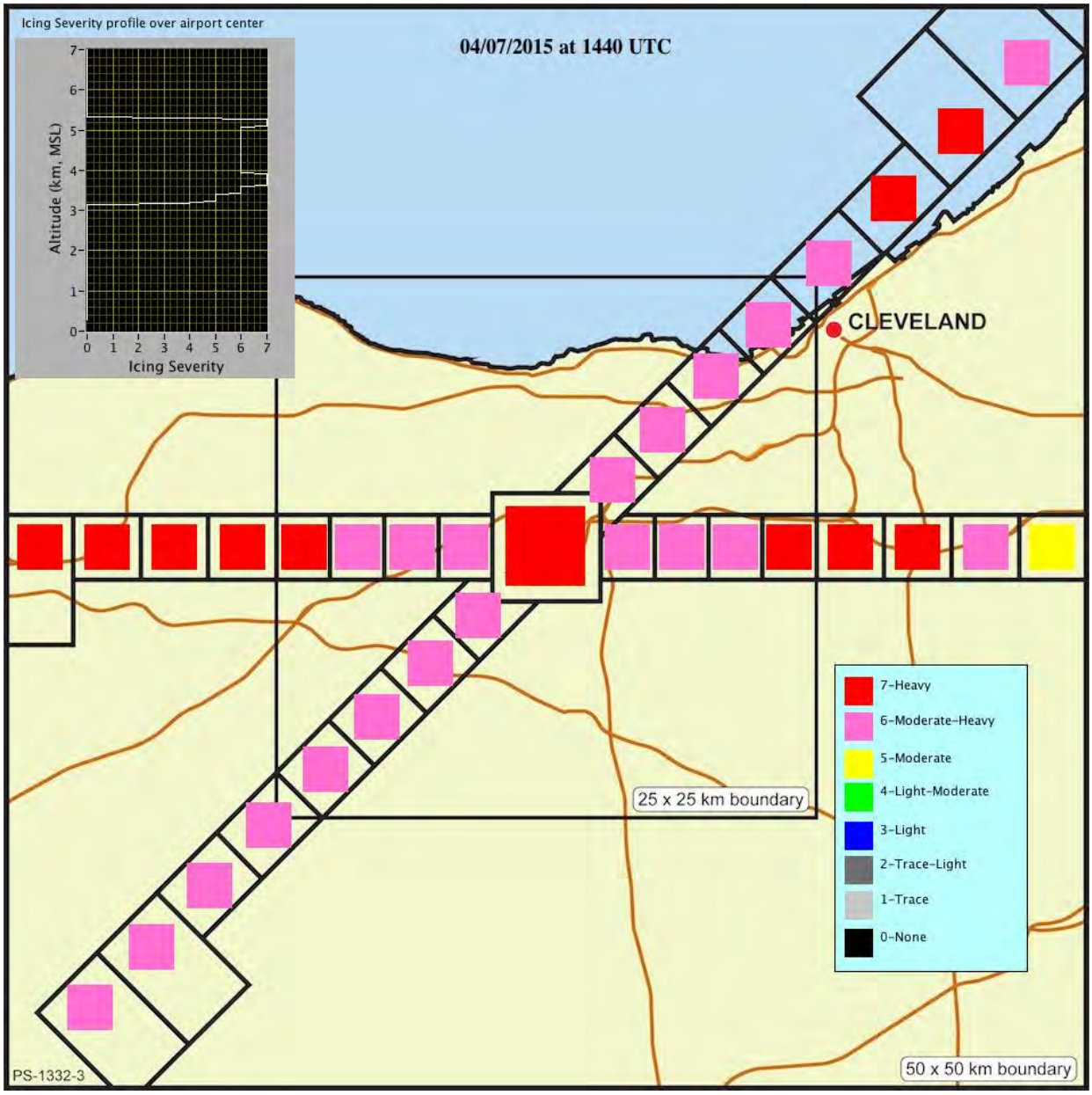

Figure 79.—NIRSS terminal area qualitative in-flight icing hazard classification from 14:40 UTC on April 7, 2015.

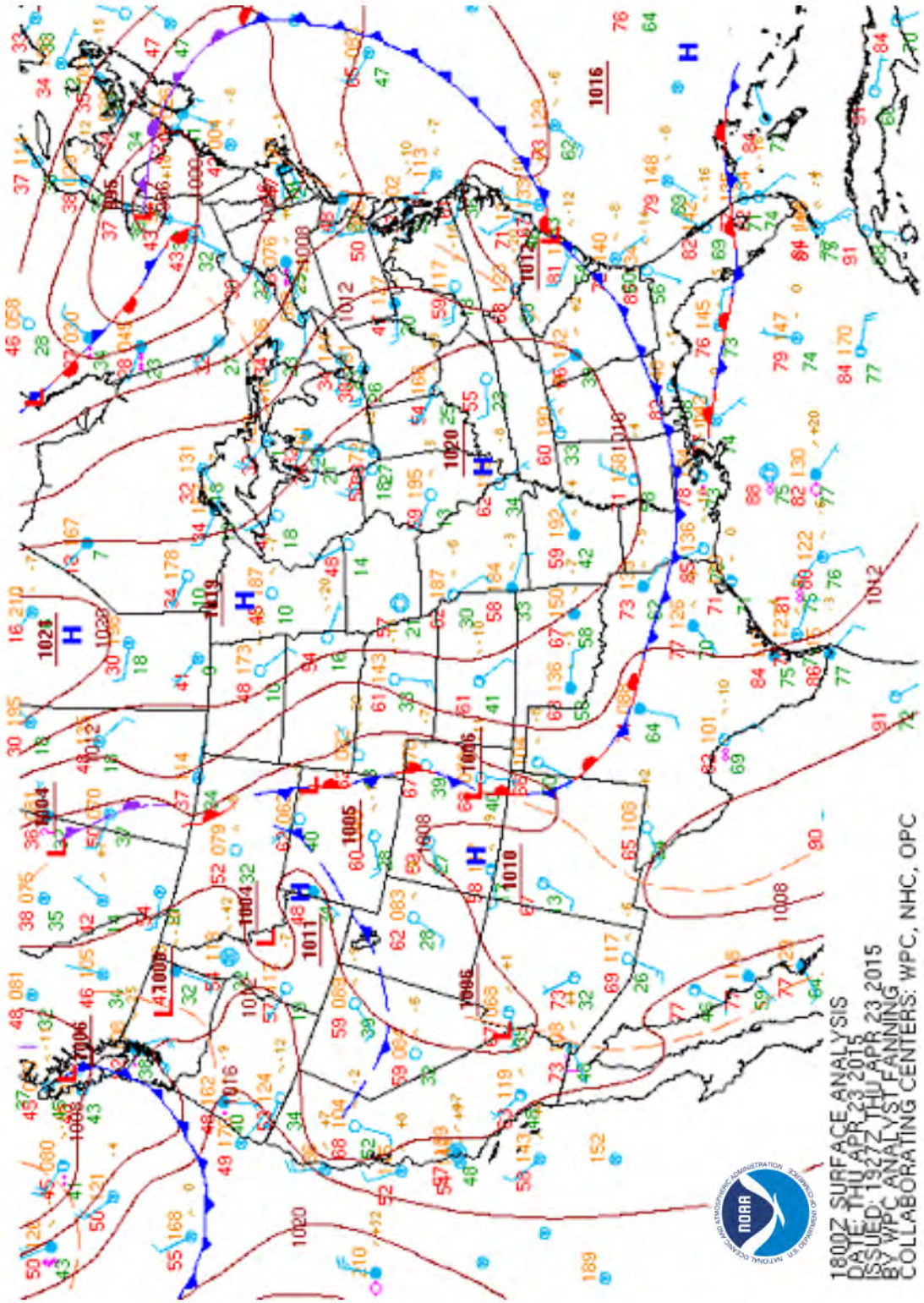

Figure 80.—Surface analysis chart from 18:00 UTC on April 23, 2015.

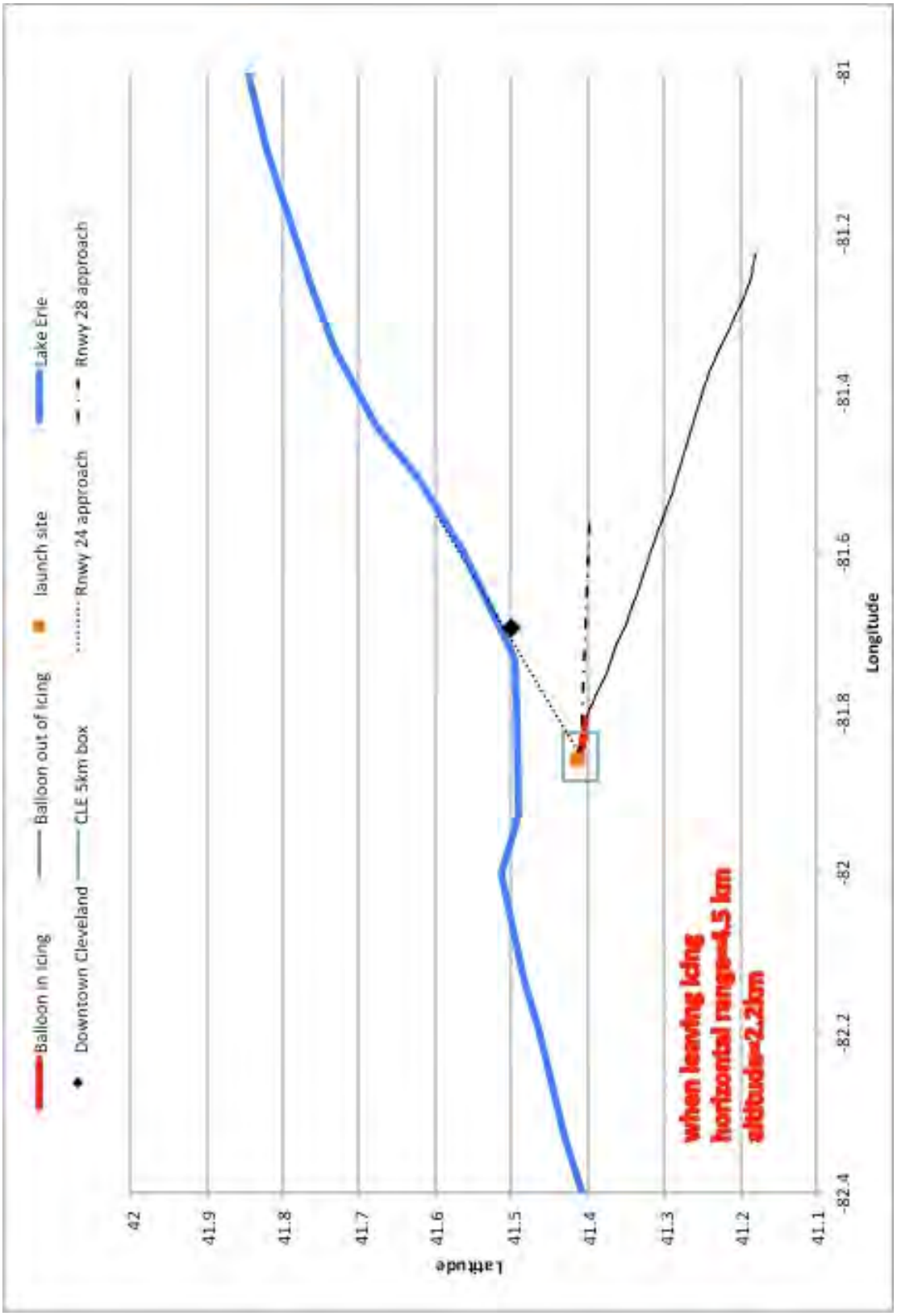

Figure 81.—Map of SLW-sensor trajectory (red) from 17:16 UTC on April 23, 2015.

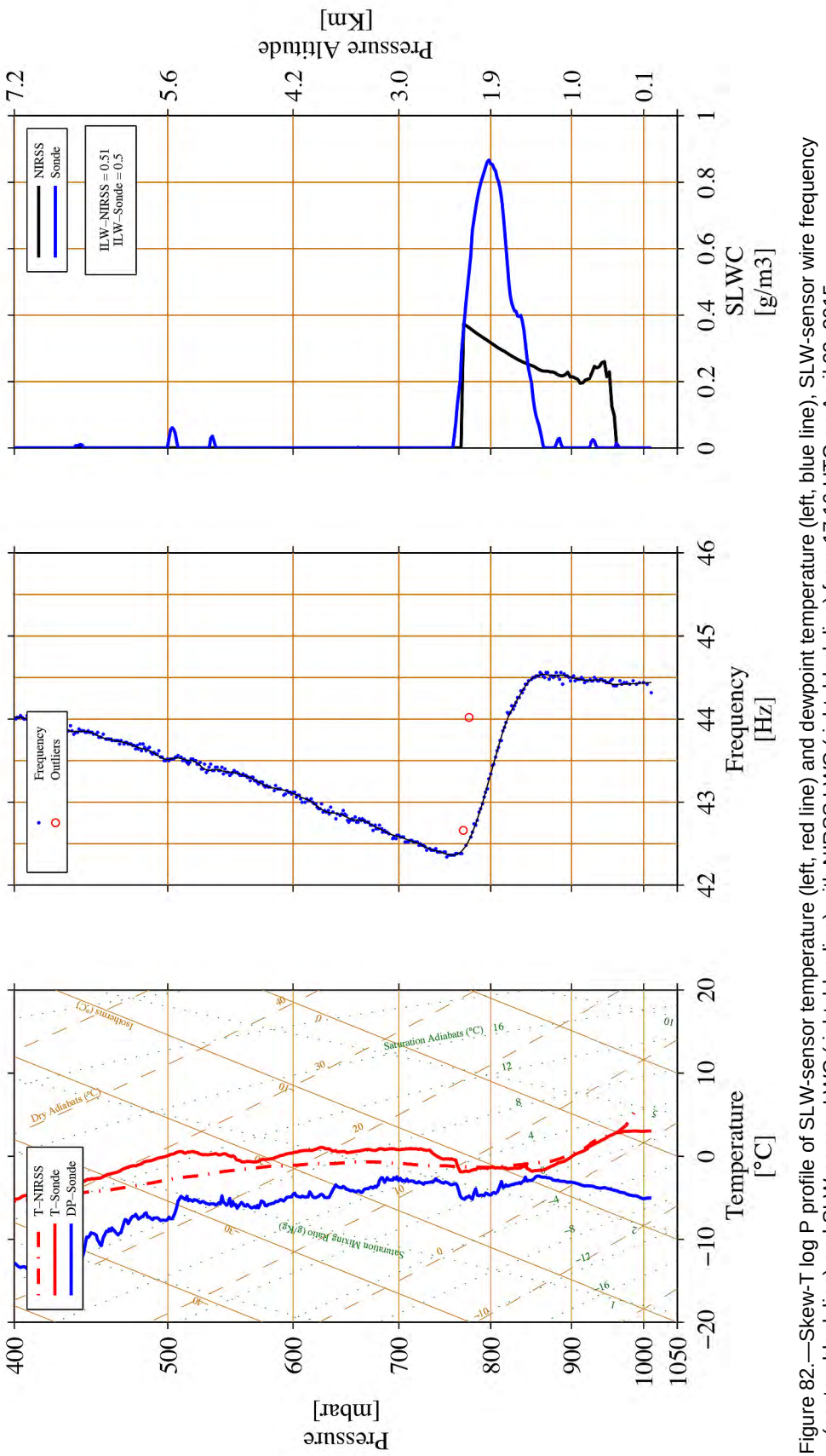

Figure 82.—Skew-T log P profile of SLW-sensor temperature (left, red line) and dewpoint temperature (left, blue line), SLW-sensor wire frequency (center, black line) and SLW-sensor LWC (right, blue line) with NIRSS LWC (right, black line) from 17:16 UTC on April 23, 2015.

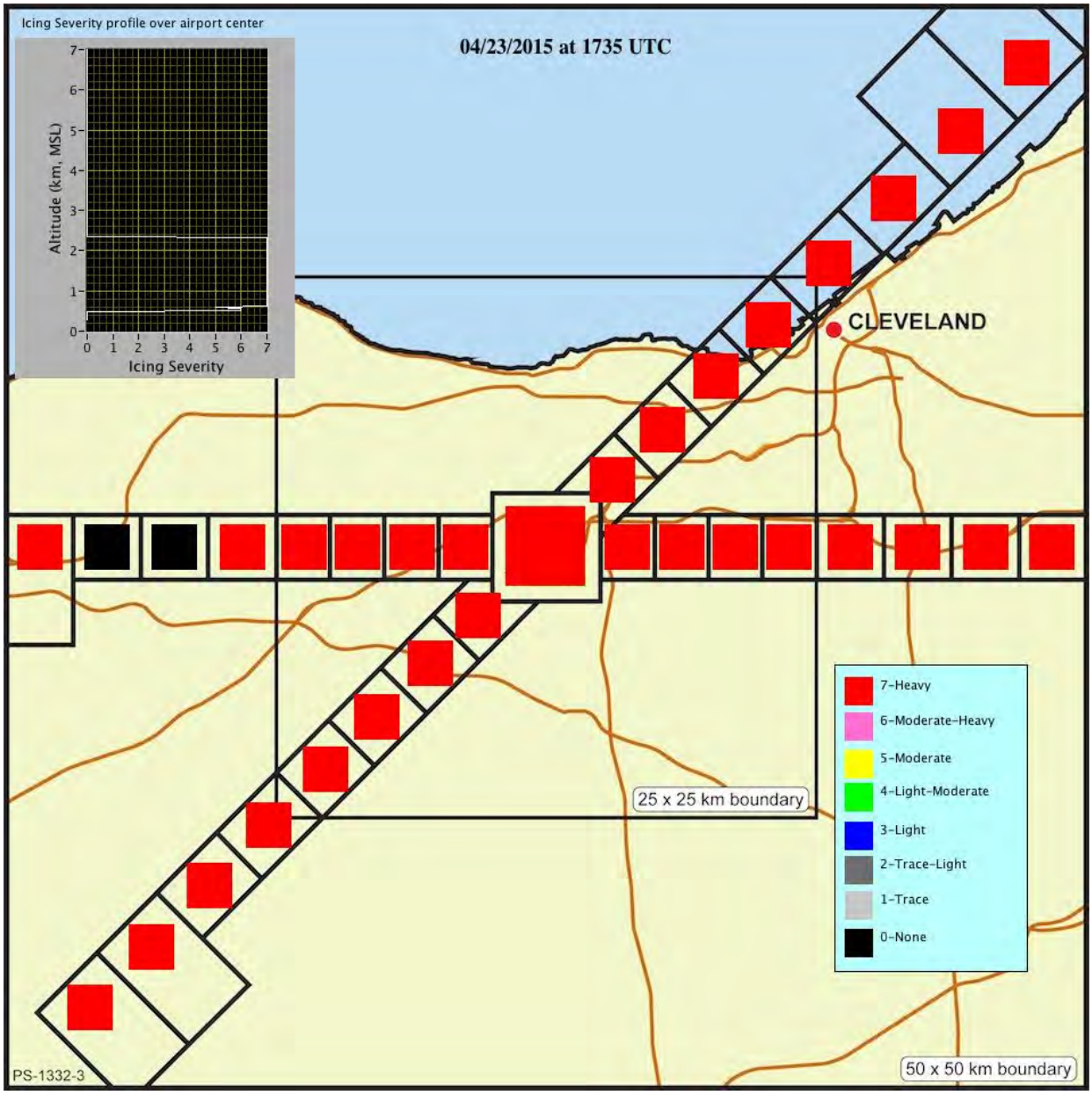

Figure 83.—NIRSS terminal area qualitative in-flight icing hazard classification from 17:33 UTC on April 23, 2015.

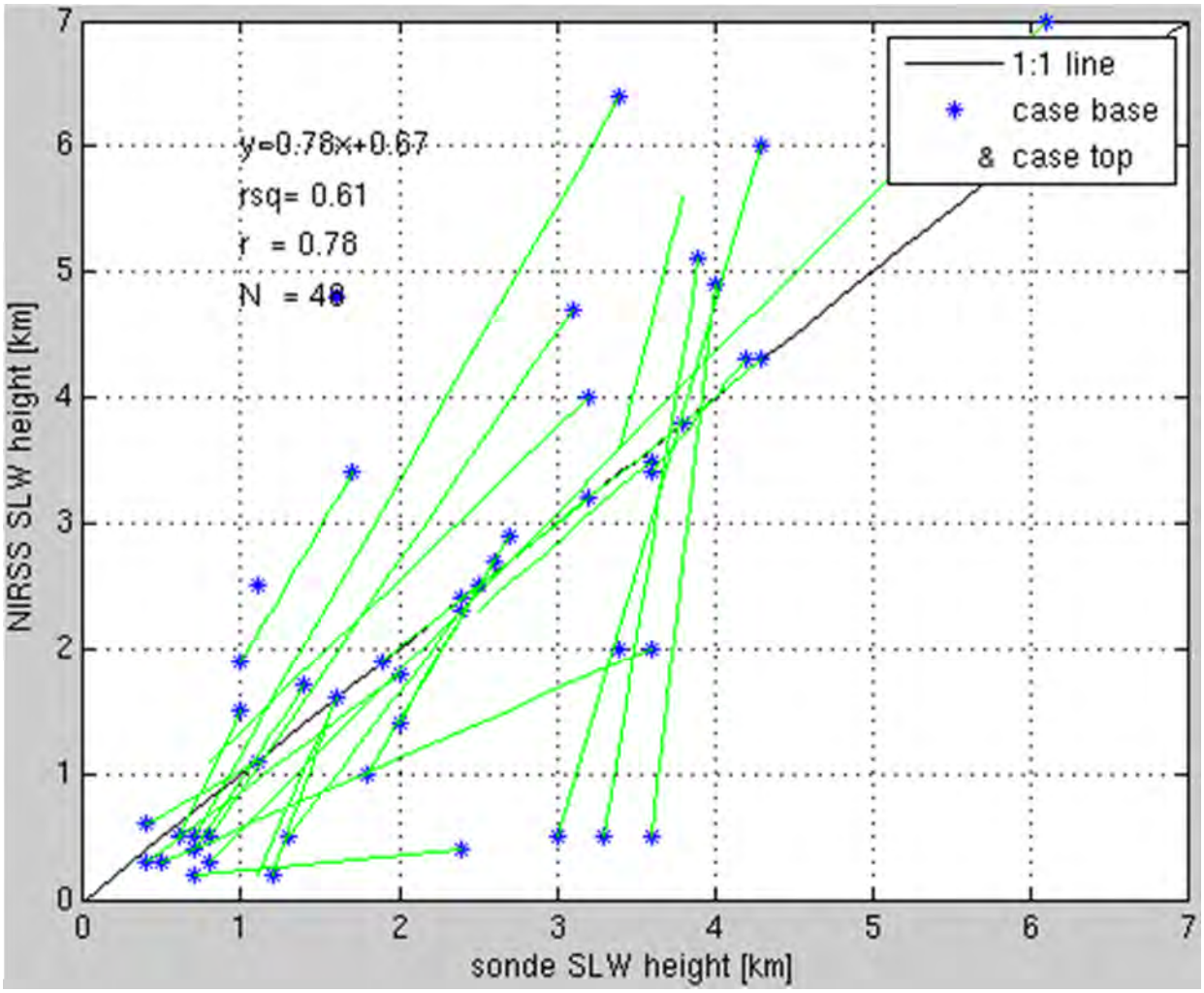

Figure 84.—Plot of base (blue star) and top (blue star) SLW heights ([km], connected by green line for each case) for SLW-sensor versus NIRSS. 1:1 line shown in black.